Proceedings of the STRESS-MAE Center Workshop on Structural Design Issues for Buildings in Moderate Risk Seismic Zones

Edited by Neil Hawkins
Mid-America Earthquake Center

UILU-ENG-98-2007

Proceedings of the STRESS-MAE Center Workshop on Structural Design Issues for Buildings In Moderate Risk Seismic Zones

Edited by

Neil M. Hawkins
University of Illinois at Urbana-Champaign
Department of Civil and Environmental Engineering
205 N. Mathews Avenue
Urbana, IL 61801

Technical Report MAE Center 98-001
NSF Master Contract Number CMS-97-01785 COOP

July 10, 1998

This workshop was conducted at the University of Illinois at Urbana-Champaign in February 1998.

MID-AMERICA EARTHQUAKE CENTER
UNIVERSITY OF ILLINOIS AT URBANA-CHAMPAIGN
NEWMARK LABORATORY, URBANA, IL 61801

PREFACE

The Mid-America Earthquake (MAE) Center is a research center headquartered at the University of Illinois at Urbana-Champaign (UIUC), Illinois, USA, for the purpose of reducing potential losses resulting from future earthquakes in Mid-America through improved evaluation of seismic hazards and development of cost-effective retrofit strategies. The MAE Center was established on October 1, 1997 when the UIUC was awarded one of three NSF earthquake engineering research centers. The activities of the MAE Center are focused around three themes: research, education, and outreach including international collaboration. The initial research program consists of coordinated activities on Essential Facilities, Transportation Networks, and Hazard Evaluation. Researchers are drawn from the seven partner institutions of the MAE Center: University of Illinois at Urbana-Champaign, Georgia Institute of Technology, University of Memphis, Massachusetts Institute of Technology, St. Louis University, Texas A & M, and Washington University at St. Louis. Partner institutions provide funding for center activities in excess of that provided by NSF.

The advanced STructure RESearch Station (STRESS) is a research center established at Hanyang University, Seoul, Korea for the purpose of developing advanced construction technologies for the 21st century. The principal activities of STRESS focus on developing advanced construction technologies for large structural systems, promoting international collaboration in the related research areas of strategic importance, transferring advanced construction technologies to local companies, training and re-educating construction engineers, and educating quality graduate students to prepare them as the future leaders of the Korean construction industry. The main thrusts of the research activities underway by STRESS are:

- Reinforced Concrete Structural Systems of Ultra High-Rise Buildings
- Steel and Hybrid Structural Systems
- Large Span Spatial Structures
- Structural Analysis of High-Rise Buildings
- Construction Automation

STRESS researchers are drawn from industries and universities throughout Korea. Funding for STRESS comes primarily from the Korea Science and

Engineering Foundation (KOSEF) which is an agency of the Korean government analogous to the US National Science Foundation (NSF).

A memorandum of agreement covering cooperative relations between the University of Illinois at Urbana-Champaign and Hanyang University, especially to develop academic and cultural exchanges, was signed in April 1994. That agreement specifically encourages joint research activities, participation in seminars and special short-term academic programs. In January 1997 an addendum to that agreement was signed between the Department of Civil Engineering at the University of Illinois at Urbana-Champaign and the STRESS Center with the specific objectives of conducting joint research activities and exchanging information and materials of mutual interest. With the establishment of the MAE Center, a similar memorandum of cooperation was signed between Director Daniel P. Abrams of the MAE Center and Director Li Hyung Lee of STRESS in January 1998.

These proceedings represent the first outcome of the agreement for cooperation between the MAE Center and STRESS and form part of the cooperation between the STRESS Center and the UIUC Department of Civil Engineering. This activity reflects those entities mutual interest in problems associated with the response of buildings to the low probability/high consequence infrequent earthquake event that is a concern both in Mid-America and Korea. The papers for this workshop were invited from selected researchers of the STRESS and MAE Centers. The observations, opinions, findings and conclusions presented in those papers are those of the individual participants and do not necessarily reflect those of STRESS, MAE Center, KOSEF or NSF.

Workshop on Structural Design Issues in Moderate Seismic Zones
February 24-25, 1998, Urbana, Illinois

TABLE OF CONTENTS

Workshop on Structural Design Issues for Moderate Seismic Zones
February 24-25, 1998, Urbana, Illinois

EFFECT OF HYSTERETIC MODEL ON DUCTILITY-BASED STRENGTH REDUCTION FACTOR

Sang Whan, Han
Professor, Dept. of Architectural Eng., Han Yang Univ., Seoul, Korea
Young Hun, Oh
Grad. Student, Dept. of Architectural Eng., Han Yang Univ., Seoul, Korea,
Li Hyung, Lee
Professor, Dept. of Architectural Eng., Han Yang Univ.Seoul, Korea

ABSTRACT

Current seismic design code is based on the assumption that structures designed according to the code behave inelastically during a severe earthquake ground motion (EQGM). For this reason, seismic design force calculated by current seismic code is prescribed to be much lower than the force level required for a structure to respond elastically during design level earthquake ground motion. Present procedures for calculating seismic design forces are based on the use of elastic spectra reduced by a strength reduction factor known as "response modification factor, R". This factor accounts for the inherent ductility, overstrength, redundancy, and damping of a structural system. This study considers only ductility for investigating R factor, which means that R factor is calibrated to attain the target ductility ratio (system ductility capacity). In this study this factor is called "ductility-based R factor, R_μ." The objective of this study is to investigate the effect of hysteretic models on R_μ factor. The considered hysteretic models are elasto-perfectly plastic, bi-linear, strength degradation, stiffness degradation, and pinching models. Statistical studies are also performed to investigate the effect of the parameters of each hysteretic model on R_μ factor. Based on the results of this parametric study the functional form of R_μ factor is established.

Key words: strength reduction factor, ductility ratio, hysteretic models

1 Introduction

In the commentary of the 1994 NEHRP provision strength reduction factor is defined as "an empirical response reduction factor intended to account for both damping and ductility inherent in the structural system at displacements great enough to surpass initial yield and approach the ultimate load displacement of the structural system." In US the strength reduction factor has been determined mainly based on engineering judgement and accumulated experiences from the past earthquakes rather than theoretical background. However, strength reduction factor has not been changed much since this factor was introduced in 1959 as a horizontal force factor (SEAOC Blue Book, 1959).

According to the report of ATC-19 and ATC-34 there are three major weaknesses of the R factor used in the current seismic design as follows :

1) It is not valid to assign the same value of R factor to the same type of structural system with different heights.
2) R factor does not account for the effects of ductility, damping, and overstrength explicitly.
3) The effect of the soil condition is not considered.

Considering above weaknesses it can be concluded that single value of R factor for a given structural system is not appropriate to account for ductility, damping, and overstrength inherent in the structural system.

Many researchers have evaluated R factor and pointed out the problems in current R factor. Uang and Bertero (1986) performed experimental study to evaluate the seismic performance and R factor of Concentric Braced Steel Frame (CBF). Whittaker (1987) and Foutch (1987) performed similar studies with Uang and Bertero (1986) for the different structural systems. They discussed the appropriateness of the R factor which is used in current seismic design code or provisions.

Riddell and Newmark (1979) performed the statistical studies for evaluating R_μ factor using 10 different earthquake ground motions recorded at the sites with rock or alluvium soil condition. They considered three different hysteretic models which are elasto-perfectly plastic, bilinear and stiffness degradation models. According to their studies elasto-prefectly plastic model gives conservative value of R factor.

Nassar and Krawikler (1991) established the functional format for R_μ factor with respect to the component parameters of bilinear model and dynamic properties of the system. Fifteen earthquake ground motions are used which are recorded at the western part of the US. Miranda (1991) performed similar studies with that of Nassar and Krawinkler (1991). He used more earthquake records and also consider the effect of the different soil conditions.

Osteraas and Krawinkler (1990) made the spectra of the overstrength factor for distributed moment frame, perimeter moment frame, and braced frame. However, they pointed out that "Overstrength varies with the structural type, building height, plan configuration, design code and a host of other factors." However, this study is valuable to show the process of the evaluation of overstrength factor for a structure at a given site constructed by local construction process.

This study is performed as a part of the project which is "Investigation on Strength Reduction Factor for wall-type apartment structure in Korea." It is difficult to determine R factor of the specific structural systems in low or moderate seismic zone based on engineering experiences from the past earthquakes since the occurrence of earthquakes is very rare in Korea. Thus, R factor needs to be investigated either theoretically or experimentally.

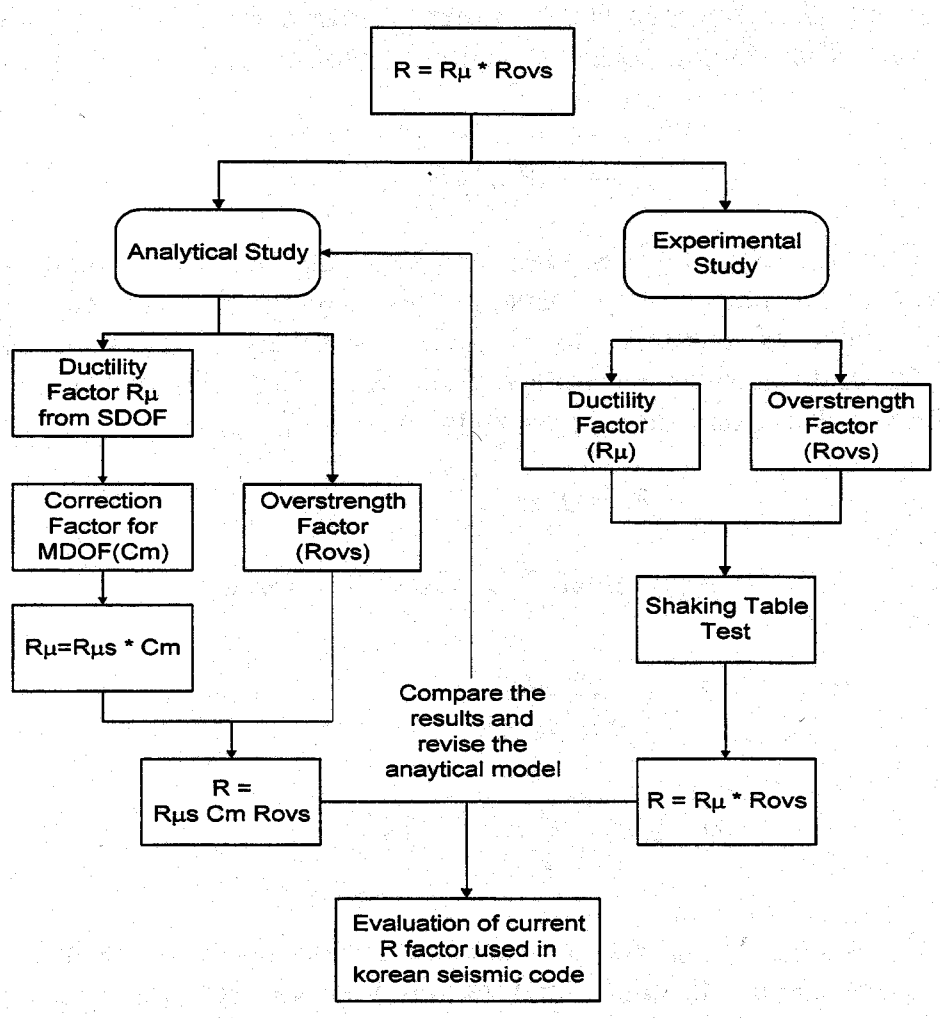

Figure 1 Overall Process of the Project

Figure 1 shows the overall process to evaluate the R factor of wall-type apartment structure in Korea. As a part of this project R_μ factor is investigated with the consideration of several different hysteretic models such as elasto-perfectly plastic model, bi-linear model, stiffness degradation model, pinching model and strength degradation model. The effect of each hysteretic model and its component parameters on the R factor is investigated. Also functional relationship between R_μ factor and component parameters of each hysteretic model is established by statistical analysis. For performing this statistical study 40 earthquake ground motions recorded at rock and stiff soil type (S_1) are used.

2 Basic Components of Strength Reduction Factor

According to the findings from other researchers (ATC-19, ATC-34) strength reduction factor can be splitted into several major factors as follows :

$$R = R_s R_\mu R_\xi R_r \tag{1}$$

where R_s, R_μ, R_ξ, and R_r are overstrength, ductility, damping, and redundancy factor respectively. Among these factors R_ξ can be neglected since the effect of damping to R factor is minor. Also it is hard to quantify R_r and consider separately from R_s. For this reason R_ξ, and R_r can be omitted from Eq. (1) as follows :

$$R = R_s R_\mu \tag{2}$$

R_s and R_μ can be represented by following formulas :

$$R_s = \frac{V_{\max}}{V_{design}} \tag{3}$$

$$R_\mu = \frac{V_{elastic}}{V_{\max}} \tag{4}$$

where V_{max}, V_{design}, $V_{elastic}$ are the maximum shear force (capacity), design required shear force (demand), and required elastic strength. Eq. (3) and (4) can be denoted as different form shown below :

$$V_{max} = R_s \; x \; V_{design} \tag{5}$$

$$V_{elastic} = R_{\mu} \; x \; V_{max} \tag{6}$$

$$V_{elastic} = R_{\mu} \; x \; Rs \; x \; V_{design} \tag{7}$$

3 Evaluation of Ductility-Based Strength Reduction Factor

Under a given earthquake ground motion the inelastic deformation generally increases as the yield strength level of a structure becomes lower. It requires iterative process to find the yield strength of a SDOF system which attains the target ductility ratio. After obtaining F_y for a given ductility it is easy to calculate R using following equation.

$$R_{\mu} = \frac{F_{y(\mu=1)}}{F_{y(\mu=\mu_t)}} \tag{8}$$

where $F_{y(\mu=1)}$ is yield strength of a structure to attain target ductility ratio of 1 and $F_{y(\mu=\mu t)}$ is the yield strength of a structure to attain the target ductility for a given earthquake ground motion.

This process can be repeated for a system with different natural period. Based on the results it is possible to draw the R_{μ} spectra with respect to natural period for a given structure. If many earthquake records are considered the process can be repeated to obtain the mean spectra or mean+σ spectra. In Figure 2 $F_{y(\mu=1)}$ and $F_{y(\mu=\mu t)}$ are shown. The overall procedure for calibrating R_{μ} factor is shown in Figure 3. Ductility ratio, μ can be defined as following equation :

$$\mu = \frac{\max . |u(t)|}{u_y} \tag{9}$$

For a structure with very short period (T $\rightarrow$ 0) F_y for any target ductility approaches elastic strength, $F_{y(\mu=1)}$. Conversely, if the natural period of the system goes infinity (T$\rightarrow\infty$) the maximum displacement of the system becomes the ground displacement irrespective to the yield force level.

In order to evaluate the yield strength of a SDOF system for a given target ductility ratio and a given earthquake ground motion the following equation of motion is used.

$$m\ddot{u}(t) + c\dot{u}(t) + F(t) = -m\ddot{u}_g(t) \tag{10}$$

where m, c and, $F(t)$ are mass, damping factor, and restoring force respectively. And u(t) and $u_g(t)$ are relative displacement and ground displacement.

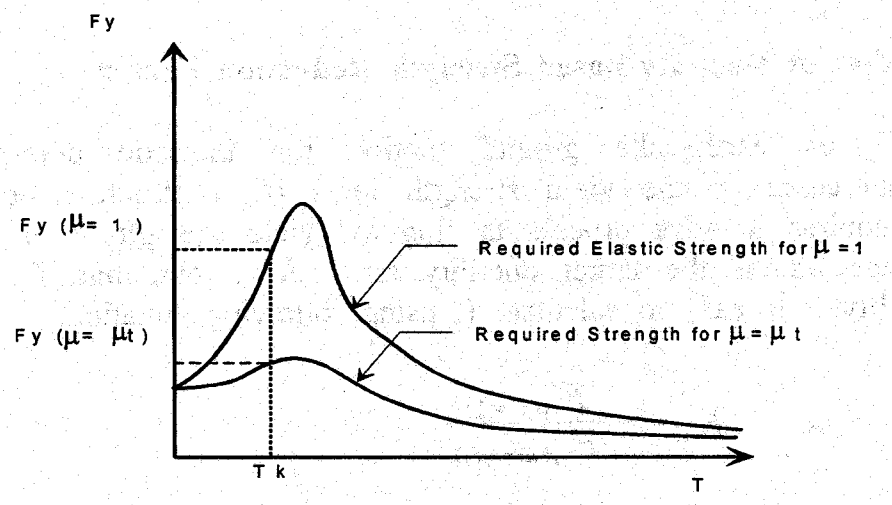

Fig. 2. Yield strength for a given target ductility ratio vs. natural period, T

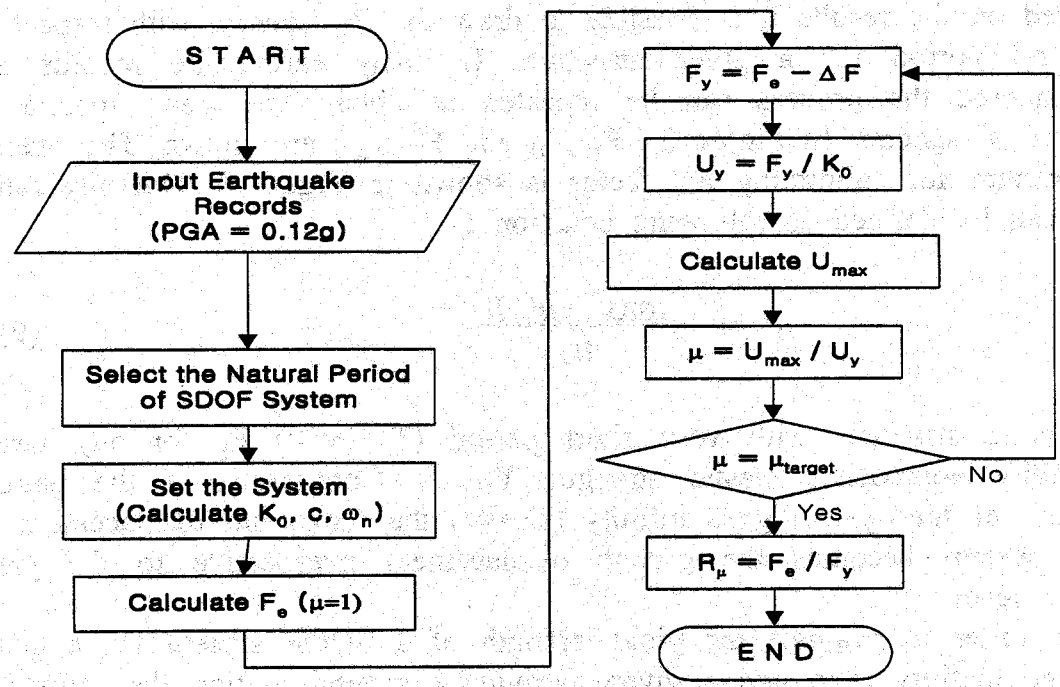

Fig. 3. Overall Procedure for Calibrating R μ factor

4 Hysteretic Models Used in this Study

In this study five different hysteretic models are considered which are elasto-perfectly plastic model, bi-linear model, strength degradation model, and stiffness degradation model. These models are shown in Figure 4. Among these models the elasto-perfectly plastic model is used as a basis model. R_μ factors obtained using the other models are compared with that of the basis model. Each model has key parameters which is shown in Table 1. The detail description of hysteretic models are in the study by Kunnath et al (1990).

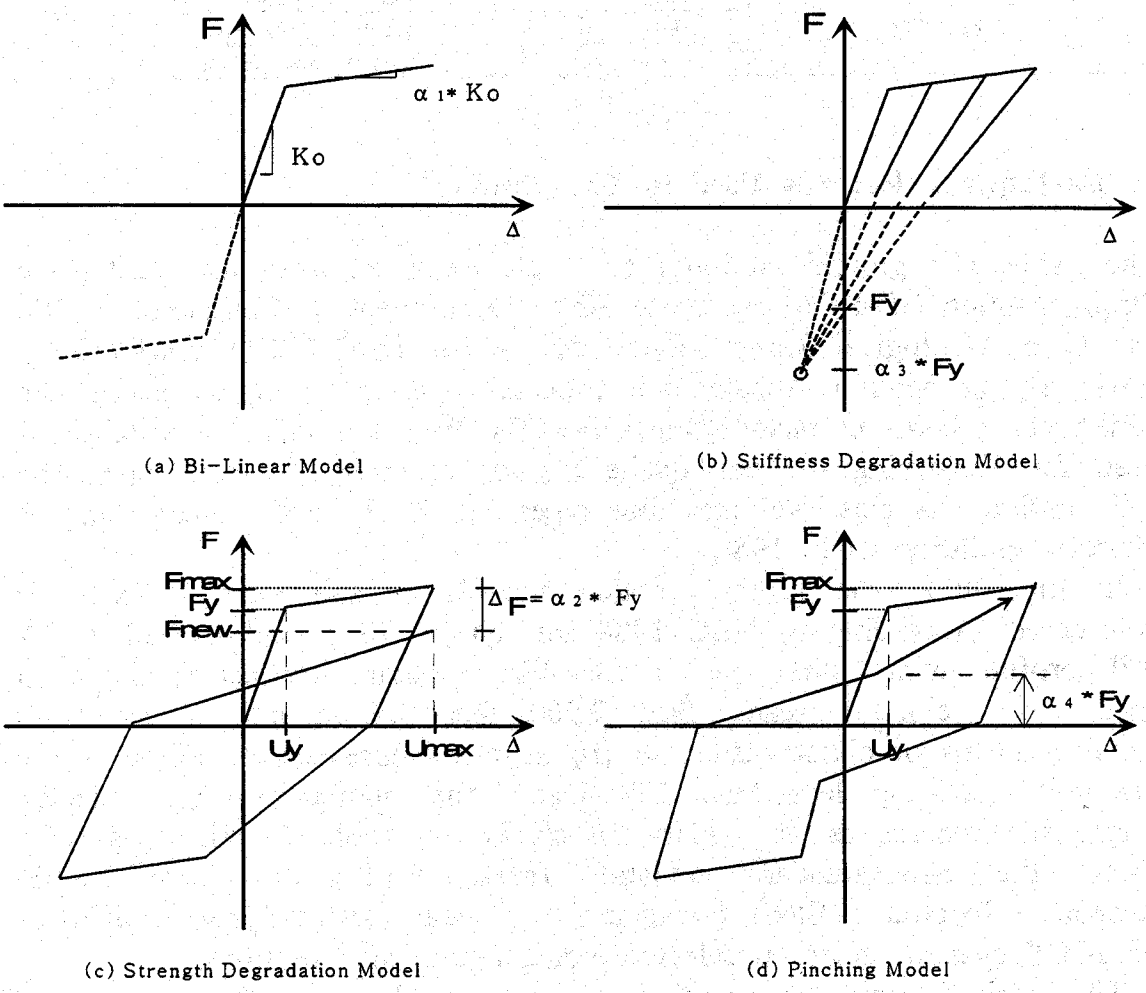

(a) Bi-Linear Model

(b) Stiffness Degradation Model

(c) Strength Degradation Model

(d) Pinching Model

Fig. 4. Hysteretic Models

Table 1. Key parameters of Hysteretic Models

Hysteretic Model	Parameters	Effect
Elasto-Perfectly Plastic	ko	Initial Stiffness
	Uy	yield displacement
Bi-linear	ko	Initial Stiffness
	Uy	yield displacement
	α_1	second slope
Strength degradation	ko	Initial Stiffness
	Uy	yield displacement
	α_2	Strength degradation
Stiffness degradation	ko	Initial Stiffness
	Uy	yield displacement
	α_3	Stiffness degradation
Pinching	ko	Initial Stiffness
	Uy	yield displacement
	α_4	Pinchimg degradation

5 Earthquake Records Used in This Study

The earthquake ground motion records are extracted from the Earthquake Strong Motion CD-ROM by Unite States Department of Commerce (1996) and U. S. Geological Survey digital data series, DDS-7, CD-ROM (1992). Basic Strong Motion Acceleration Processing is used for correcting the earthquake records extracted from CD-ROM. Also the software SMCAT is used for classifying the earthquake records according to soil type. The soil condition is classified into four types S_1, S_2, S_3, and S_4 according to Uniform Building Code 1988.

In this study the ground motion records at soil type 1 (S_1) are considered. According to UBC 1988 soil type 1 (S1) is described as "A soil profile with either (a) a rock-like material characterized by a shear-wave velocity greater than 2,500 feet per second or by other suitable means of classification, or (b) Stiff or dense soil condition where the soil depth is less than 200 feet." The number of the selected earthquake records is 40 which are shown in Table 2. Also Figure 5 shows the mean+standard deviation (mean + 1s) of Linear Elastic Response Spectral (LERS) obtained from linear elastic dynamic analysis of SDOF system under 40 selected earthquake ground motions.

The Peak Ground Accelerations (PGA) of all earthquake records are normalized to 0.12g which is used as a seismic zone factor at Seoul area in Korea to calculate the statistical values. Figure 5 also shows the Linear Elastic Design Spectra (LEDRS) in NEHRP provision (1994) in order to compare to statistical values of LERS.

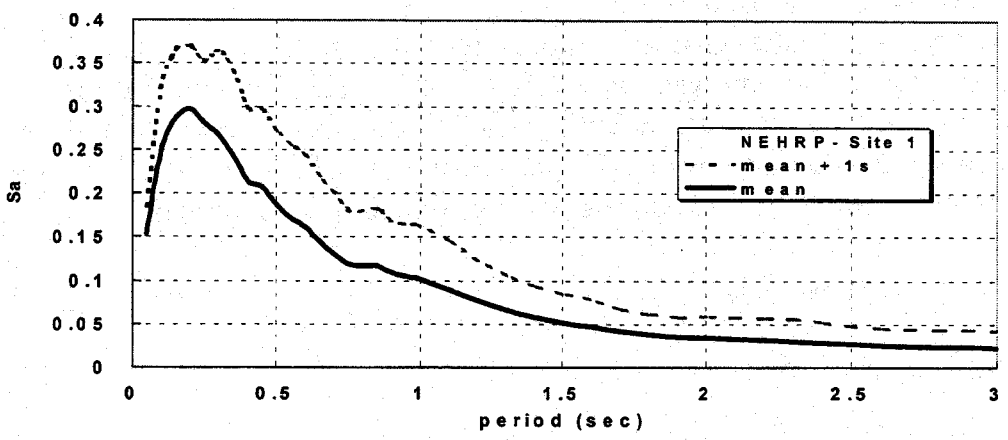

Fig. 5. Linear Elastic Spectrum vs. NEHRP Spectra for S_1

6 Statistical Studies for Ductility-Based R Factor, R_μ

This study investigates the effect of the parameters of each hystertic model and response on R_μ factor using statistical study. Based on this statistical study the functional format is established as follows :

$$R_\mu = f(T, \mu, \alpha_1, \alpha_2, \alpha_3, \alpha_4) \qquad (11)$$

It is assumed that Eq.(11) can be rewritten as follows :

$$R_\mu = R(T, \mu) \times C_{\alpha 1} \times C_{\alpha 2} \times C_{\alpha 3} \times C_{\alpha 4} \qquad (12)$$

where $R(T, \mu)$ is the functional format of R_μ factor of elasto-perfectly plastic model which is the basis model in this study. $C_{\alpha 1}$, $C_{\alpha 2}$, $C_{\alpha 3}$, and $C_{\alpha 4}$ are correction factor accounting the effect of bilinear (α_1), strength degradation (α_2), and stiffness degradation(α_3) to obtain R_μ factor of any arbitrary hysteretic model using elasto-perfectly plastic model. In Eq. (12) the effect of each model is assumed to be treated to be independently. The correction factors are determined by regression analysis.

6.1 The Ductility Based R factor of Elasto-Perfectly Plastic Models

In order to establish the functional form of $R\mu$ factor with respect to dynamic properties and system responses, regression analysis is performed. The 19,200 of nonlinear dynamic analysis is performed for following permutations :

1) Target ductility ratios of 1, 2, 3, 4, 5, 6, 8, and 10 (8)
2) Sixty discrete natural periods of SDOF systems from 0.05

second to 3.0 second (60)

3) Fourty earthquake ground motions recorder at S_1 site (40)

Two stage regression analysis is carried out in 2D domain. In the first stage the function for R_μ vs. natural period of SDOF is regressed for the discrete values of ductility ratio (7) and then the effect of ductility ratio is evaluated at the second stage. Following function is obtained :

$$R_\mu = a_0 (1-\exp(-b_0 T_n)) \quad (13)$$

$$a_0=0.9921 \ \mu + 0.1532 \quad (14)$$

$$b_0=23.686 \ \mu^{-0.8313} \quad (15)$$

where T_n is the natural period and μ is ductility ratio. Figure 6 shows the fitness of the regressed function of R_μ factor. In this figure solid line shows the values obtained from regressed function and dashed line shows the mean values of R_μ factor obtained using nonlinear dynamic analysis. Figures 7 and 8 show the fitness of Eq.(14) and (15). Also Figure 9 compares the regressed function of model R_μ factor by this study (Han and Oh), Nassar and Krawikler (1991), and Miranda (1992).

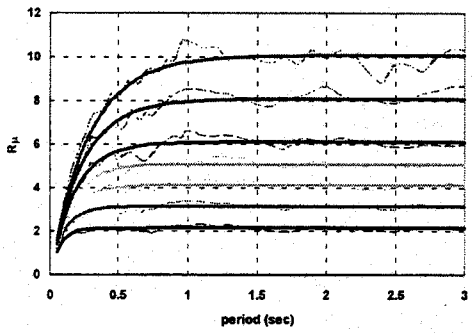

Fig. 6. Fitness of Regressed R_μ factor

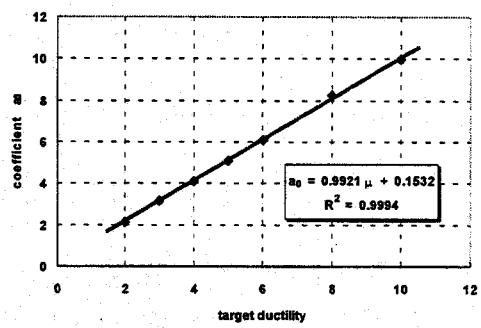

Fig. 7. Fitness of Coefficient a_0

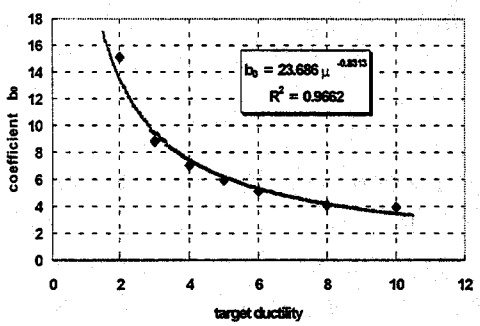

Fig. 8. Fitness of Coefficient b_0

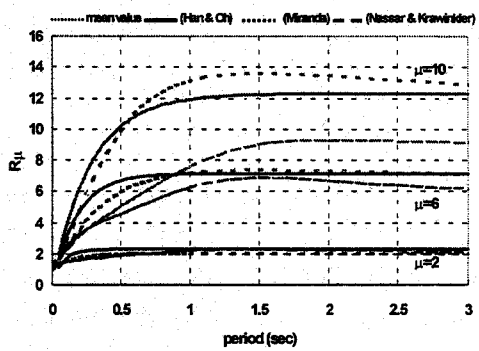

Fig. 9. Comparison of R_μ Functions

Table 2 List of Earthquake Records for S_1

No.	Event Name	Station Name	Event Date	M	Component	PGA (cm/s^2)	PGV (cm/s)	PGD (cm)
S1-1	Offshore Eureka	Cape Mendocino	1994.9.1	7.2	90	23.3	-2.4	1.5
S1-2	Western Washington	Olympia, Washington Highway Test Lab	1949.4.13	7.1	356	-177.8	-17.8	3.7
S1-3	Western Washington	Olympia, Washington Highway Test Lab	1949.4.13	7.0	86	274.6	17.0	*
S1-4	Whittier	Pacoima - Kagel Canyon	1987.10.1	6.1	90	154.9	7.7	1.0
S1-5	Iwate Prefecture	Miyako Harbor Works, Ground	1970.4.1	5.8	NS	-189.7	-4.4	-0.3
S1-6	Iwate Prefecture	Miyako Harbor Works, Ground	1970.4.1	5.8	EW	161.8	3.3	-0.3
S1-7	Michoacan, Mexico City	Calete De Campo	1985.9.19	8.1	N90E	137.8	-12.6	3.2
S1-8	San Fernando	Lake Hughes, Array Station 4, CAL.	1971.2.9	6.5	S69E	168.2	5.7	1.2
S1-9	San Fernando	Lake Hughes, Array Station 4, CAL.	1971.2.9	6.5	S21W	-143.5	-8.6	1.7
S1-10	Humbolt County	Petrolia, California, Cape Mendocino	1975.6.7	5.3	S60E	-198.7	5.9	0.6
S1-11	Humbolt County	Petrolia, California, Cape Mendocino	1975.6.7	5.3	N30E	103.0	-3.3	0.4
S1-12	Kern County	Taft Lincoln School Tunnel	1952.7.21	7.7	21	152.7	15.7	*
S1-13	Kern County	Taft Lincoln School Tunnel	1952.7.21	7.7	111	175.9	17.7	*
S1-14	Puget Sound	Olympia, Washington Hwy Test Lab	1965.4.29	6.5	176	194.3	12.7	*
S1-15	Long Beach	Public Utilities Building	1933.3.10	6.3	180	192.7	29.3	*
S1-16	Long Beach	Public Utilities Building	1933.3.10	6.3	270	156.0	15.8	*
S1-17	Imperial Valley	Holtville P.O.	1979.10.15	6.6	225	246.2	44.0	*
S1-18	Imperial Valley	Calexico Fire Station	1979.10.15	6.6	225	269.6	18.2	*
S1-19	Coalinga	Parkfield Zone 16	1983.5.2	6.5	0	178.7	14.7	*
S1-20	Adak,Alaska,Us	Naval Base	1971.5.1	6.8	North	85.38	-3.22	1.40
S1-21	Alaska Subduction	Cordova, Mt. Eccles School	1964.7.5	5.2	N196E	34.20	3.48	0.51
S1-22	Alaska Subduction	Chernabura Island	1983.2.14	6.3	N070E	46.90	3.11	0.34
S1-23	Alaska Subduction	Chernabura Island	1983.2.14	6.3	N070E	16.70	1.05	0.30
S1-24	Dursunbey	Dursunbey Kandilli Gozlem Istasyonu	1979.7.18	5.2	NS	233.77	*	*
S1-25	Imperial Valley Main Shock	Cerro Prieto	1979.10.15	6.6	135	163.20	*	*
S1-26	Loma Prieta	Anderson Dam, Lest Abutment	1989.10.18	7.1	250	59.70	12.13	3.77
S1-27	Mammoth Lakes	Long Valley Dam Left Abutment	1980.5.25	6.1	90	-75.45	7.12	-3.37
S1-28	Mammoth Lakes	Long Valley Dam (Right Crest)	1980.5.25	6.1	90	-147.72	13.06	-3.89
S1-29	Mexicali Valley	Cerro Prieto	1979.10.10	4.1	S33E	-42.00	*	*
S1-30	Miyagi Prefecture	Ofunato Harbor, Jetty	1978.6.12	6.3	E41S	-222.1	14.10	-5.10
S1-31	Miyagi Prefecture	Ofunato Harbor, Jetty	1978.6.12	6.3	N41E	-206.70	-12.8	-2.20
S1-32	Morgan Hill	Gilroy - Gavilan College	1984.4.24	6.2	67	94.98	-3.39	0.47
S1-33	New Ireland	Bato Bridge, Papua New Guinea	1983.3.18	7.7	270	31.60	4.12	1.92
S1-34	San Fernando	800 W. First Street, 1st Floor, Los Angeles, Cal.	1971.2.9	6.5	N53W	138.02	19.36	9.99
S1-35	San Salvador	Hotel Sheraton	1986.10.10	5.4	0	213.90	-17.67	-4.55
S1-36	San Salvador	Hotel Sheraton	1986.10.10	5.4	270	295.62	26.34	4.36
S1-37	Sitka,Alaska	Sitka Observatory	1972.7.30	*	North	-70.11	10.79	9.86
S1-38	WestMorland	Superstition Mountain, California	1981.4.26	5.6	135	-102.47	-7.67	-2.03
S1-39	Whittier Narrows	Garvey Reservoir - Control Building	1987.10.1	5.9	330	468.20	19.78	2.21
S1-40	Whittier Narrows	Los Angeles, Griffith Park Observatory	1987.10.1	5.9	270	133.80	7.54	0.96

6.2 The Effect of the Second Slope of Bi-linear Model

In Figure 10 mean of R_μ factor with respect to the second slope of bi-linear model is shown. As the second slope increases the larger R_μ factor is obtained. Based on this fact following functional form of correction factor $C_{\alpha 1}$ is obtained using two stage regression analysis. At

the first stage correction factor $C_{\alpha 1}$ vs. α_1 is regressed for the discrete values of target ductility ratio and then effect of the target ductility ratio is evaluated at the second stage. For this regression analysis the total number of 115,200 nonliear dynamic analyses are performed for the number of permutions described in 6.1 with 6 different second slopes (α_1 = 0, 2, 5, 7, 10 and 15 %). Following regressed function is obtained.

$$C\alpha 1 = 1.0 + a1\,\alpha 1 + b1\,\alpha 12 \quad (19)$$

$$a1 = 2.0729\ \mathrm{Ln}(\mu) - 0.2802 \quad (20)$$

$$b1 = -10.548\ \mathrm{Ln}(\mu) + 5.2074 \quad (21)$$

Figure 11 shows the fitness of $R\mu$ factor which accounts for the second slope effects to the mean value of $R\mu$ factors. In this figure solid line denotes the regressed function and dashed line denotes the mean values obtained from nonlinear dynamic analysis of SDOF system.

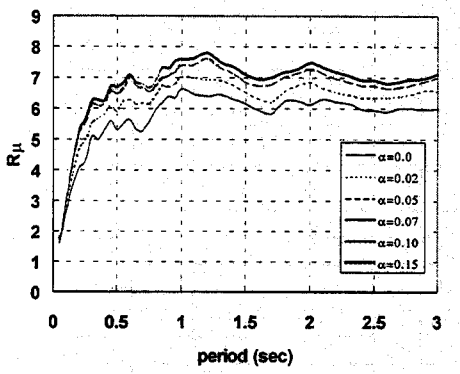

Fig. 10. Effect of the 2nd slope on $R\mu$ factor

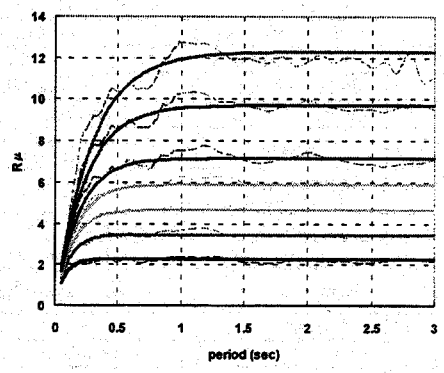

Fig. 11. Fitness of $R\mu$ factor(α=7%)

6.3 The Effect of the Strength Degradation and Stiffness Degradation Model

In order to estimate the correction factors, $C_{\alpha 2}$, and $C_{\alpha 3}$ statistical analyses need to be performed. However, this study does not propose these correction factors since the results have not been obtained completely yet. However based on 5 earthquake ground motions selected arbitrarily from Table 1 Figure 12 and 13 can be drawn. For this figure 4 different values of strength reduction factors and stiffness degradation are used. These figures show the dependancy of R_μ factor on the level of strength degradation and stiffness degradation.

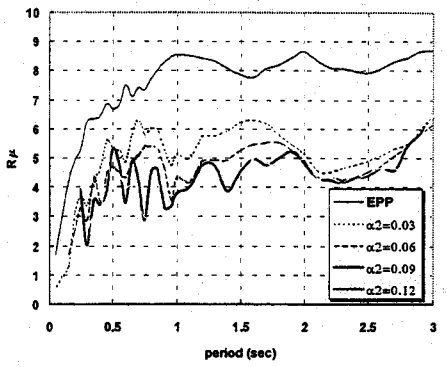

Fig. 12. Effect of Strength Degradation

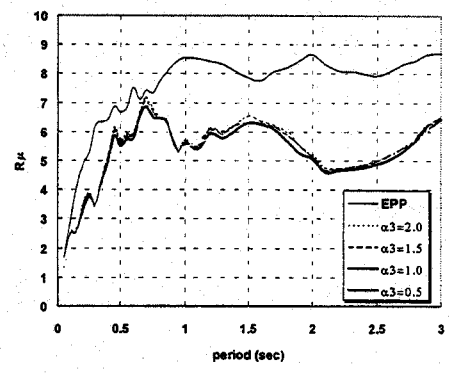

Fig. 13. Effect of Stiffness Degradation

7 Conclusion

The main purpose of this study was to evaluate the ductility-based strength reduction factor which accounts for the characteristic of different hysteretic models. In this study soil type, S_1 was only considered. The statistical analysis was performed for proposing the functional form of R_μ factor with respect to the system parameters and component parameters of each hysteretic model using 40 earthquake ground motions recorded at S_1 site. Following conclusion can be drawn from the results of this study.

1. The R_μ factor for elasto-perfectly plastic model is the function with respect to natural period and target ductility ratio.

2. From Figure 9 the regression formula of R_μ factor proposed by Nassar and Krawinkler (1991) overestimates the factor and that by Miranda (1992) underestimates this factor for S_1 site.

3. The second slope of bilinear model affects the R_μ factor. From the figure 11 it is concluded that R_μ factor becomes higher as the value of second slope increases.

4. Regressed formula for R_μ factor of bilinear model fit the real R_μ which is shown in Figure 10.

5. Figure 12 and 13 show that the strength and stiffness

degradation give the strong effect.

6. It is concluded that smaller $R\mu$ factor is obtained as strength degradation factor and stiffness degradation factor become larger.

Acknowledgement

It is acknowledged that the STRESS center supports this research.

References

1. Architectural Institute of Korea (1987), Development of Seismic Design Provision.
2. Ministry of Construction (1997), Provisions for Design Loads and Com mentary.
3. H. Krawinkler (1995), "New Trends in Seismic Design Methodology" , Proceedings of Tenth European Conference on Earthquake Engineering, Duma, pp. 821-830.
4. Building Seismic Safety Council (1992), NEHRP Recommended Provisions for the Development of Seismic Regulation for New Buildings, Part 1 and 2, Provisions and Commentary, FEMA.
5. J. D. Osteraas and H. Krawinkler (1990), "Strength and Ductility Considerations in Seismic Design", John A. Blume Earthquake Engineering Center, Report No. 90, Stanford University, California.
6. Christopher Rojahn (1988), "An Investigation of Structural Response Modification Factors" , Proceedings of 9th World Conference on Earthquake Engineering, Vol. 5, Tokyo-Kyoto, Japan, pp. 1087-1092.
7. ATC, Tentative Provisions for the Development of Seismic Regulations for Buildings, Applied Technology Council Report ATC 3- 06, 2nd Printing, Palo Alto, California, 1984.
8. ATC, An Evaluation of a Response Spectrum Approach to the Seismic Design of Buildings, Applied Technology Council Report ATC-2, Redwood City, California, 1974.
9. ATC, A Critical Review of Current Approaches to Earthquake-Resistant Design, Applied Technology Council Report ATC-34 (not published), Redwood City, California.
10. ATC, Structural Response Modification Factors, Applied Technology Council Report ATC-19, Redwood City, California, 1995.
11. SEAOC, Performance Based Seismic Engineering of Buildings, Vision 2000 Committee, Structural Engineering Association of California,

Sacramento, California, 1995.
12. BSSC, NEHRP Recommended Provisions for Seismic Regulations for New Buildings, Building Seismic Safety Council, National Hazard Reduction Program Report, Washington, D.C.,1994.
13. Foutch, D.A. et al., "Seismic Testing of Full Scale Steel Building-Part I," Journal of Structural Engineering, American Society of Civil Engineering, Vol 113, No. 11, pp. 2111-2129, November 1987.
14. ICBO, Uniform Building Code, International Conference on Building Officials, Whittier, California, 1994.
15. Uang, C.M., and Bertero, V.V., Earthquake Simulation Tests and Associated Studies of a 0.3 Scale Model of a Six Story Concentrically Braced Steel Structure, EERC, UCB/EERC-86/10, University of California at Berkeley, California, 1986.
16. Whittaker et al., Earthquake Simulation Tests and Associated Studies of a 0.3 Scale Model of a Six Story Eccentrically Braced Steel Structure, EERC, UCB/EERC-87/02, University of California at Berkeley, California, 1987.
17. Sashi K. Kunnath, Andrei M. Reinhorn, and Young J. Park, "Analytical Modeling of Inelastic Seismic Response of R/C Structures," Journal of Structural Engineering, pp 996-1017, April, 1990.

Workshop on Structural Design Issues for Moderate Seismic Zones
February 24-25,1998, Urbana, Illinois

LIMITING DRIFT AND ENERGY DISSIPATION RATIOS FOR EARTHQUAKE LOADING OF SHEAR WALLS

Soo-Yeon Seo[1], N. M. Hawkins[2], Li-Hyung Lee[3]
1) Visting Scholar, University of Illinois at Urbana-Champaign, USA
2) Professor, University of Illinois at Urbana-Champaign, USA
3) Professor, Hanyang University, Seoul, Korea

Abstract
This paper proposes criteria for acceptable limiting drift and energy dissipation ratios for reinforced concrete shear walls, with the objective of providing the background information necessary to develop building code provisions that can be used to qualify shear walls whose characteristics differ from those of walls conforming to the prescritive requirements of codes such as ACI Code 318-95. Limiting drift and energy dissipation ratios were examined for tests on shear walls having ductile type failures. Test data were analyzed and compared to results for a suggested acceptance criteria that involves a limiting drift that is a function of aspect ratio and a limiting energy dissipation ratio that is a function of displacement ductility and damping.

Key words: Acceptance criteria, Limiting drift, Energy dissipation ratio, Shear walls.

1 Introduction

Structural walls are very effective elements for resisting earthquake loads. Extensive experimental and analytical research have been conducted aimed at determining the factors controlling the behavior of structural walls and verifying procedures as to how to design them effectively. The need to specify guidelines or criteria for acceptance of walls based on structural

testing has been raised by many researchers (Bertero, 1991). Such guidelines would allow more direct comparisons between test results from different laboratories and provide more reliable information from which to develop design rules. The importance of such guidelines is apparent from the following finding on strucutral wall testing that was reached in a 1997 NSF sponsored workshop: "It is difficult to make valid comparisons of available ductility values reported by different researchers because they are often based on different response parameters or on yielding values determined using definitions that are different or unexplained or both".

Recently, a Provisional Standard for acceptance criteria (ACI 1998), based on the experimental evidence and analysis, has been developed that establishes dependable and predictable strength, drift capacity and relative energy dissipation requirements for strong column/weak beam moment frames in the regions of high seismic risk. This Provisional Standard envisages that precast and/or prestressed concrete moment frames satisfying its requirements also satisfy the requirements of 21.2.1.5 of ACI 318-95 and have strength and toughness equal to or exceeding those provided by conventional monolithic reinforced concrete frames satisfying the requirements of 21.2 through 21.6 of ACI 318-95. The Provisional Standard specifies, in addition to acceptance criteria, procedures for design of the modules required for the validation testing of a generic type of frame, the number and type of test modules required, test methods and test report content. A specific limiting drift ratio for the test modules and a corresponding limiting relative energy dissipation ratio are specified.

In a manner similar to that for frames, it is desirable that acceptance criteria, that meet the requirements of 21.2.1.5 of ACI 318-95 also be developed for structural walls. The objective of this paper is to initiate the development of such criteria by proposing limiting drift and energy dissipation ratios for structural walls based on examination and analysis of available test data.

2 General Behavior of Shear Walls

Shear walls contribute to the resistance to overturning moments, strong shear forces, and story drift. Also as infill panels they can be used to partially improve the stiffness and strength of building. Shear walls must resist not only vertical loads but also horizontal loads from wind forces as well as earthquakes forces. Those functional requirements generally result in structural requirements as follows (Paulay, 1992) :

a) Adequate stiffness so that during moderate seismic disturbances complete protection against damage, and particularly damage to non-structural components, is assured.
b) Adequate strength so that an elastic response to seismic

distrurbances does not result in more than superficial structural damage.

c) Adequate structural ductility and capability to dissipate energy for the case where the largest disturbance to be expected in the region occurs.

Shear wall behavior can be classified as either flexural or shear behavior. Walls with a height-to-length ratios greater than about 2.0, such as those likely in multistory building, behave like vertical cantilever beams. Their response is governed by flexural criteria. Short or squat walls resist horizontal forces in their plane by primarily by truss mechanisms, with the concrete providing the diagonal compressive struts and the steel reinforcement providing equilibrating vertical and horizontal ties.

Most cantilever walls can be treated as ordinary reinforced concrete beam-columns. Lateral forces are introduced by means of series of point loads through the floors acting as diaphragms. In such walls, it is relatively easy to ensure that when required, a plastic hinge at the base can develop with adequate plastic rotational capacity.

In low-rise buildings, or in the lower stories of medium-to high rise buildings, the response of the types of walls used is different. The walls are characterized by small height-to-length ratios, h_w/l_w. The potential strengths may be large in compression with the lateral forces, even when code specified minimum amounts of vertical reinforcement are used. Because of the small height, relatively large shearing forces must be generated to develop the flexural strength at the base. Therefore, the inelastic behavior of such walls is dominated by the shear response of the wall.

Shear walls are typically stiff, and can therefore prevent the large deformations that are a problem for attached nonstructural components. However, under sufficient lateral seismic excitation, shear walls can fail by a variety of mechanisms, resulting in significant lateral displacements and loss in stiffness and strength. The behavior of shear walls depends on the various sectional properities of the wall, such as aspect ratio, sectional shape, axial force, reinforcement details, etc. The displacement is less sensitive to the shapes and reinforcement details of the boundary elements, if any, than the strength of shear walls. Further, research results (Bertero, 1985) show that the displacements of frame structures with walls are very similiar to those of the same structure with shear walls only.

3 Limiting Drifts

3.1 Existing earthquake design code limits

1) NEHRP 94. Allowable story drift for shear walls depends on the seismic hazard exposure group (SHEG) for the building as folows:

Seismic Hazard Exposure I ------> 2.0 (%)
Seismic Hazard Exposure II ------> 1.5 (%)
Seismic Hazard Exposure III ------> 1.0 (%)

Values are the same for frame and wall structures. However, for a very rigid shear structure with rigid diaphragms whose lateral deflections cannot be reasonably estimated, there is the requirement that:

Structural separations < 1.25 (%) for heights above 20ft

2) ATC 3-06 (1978)
   Recommended value for "Essential Facilities" (SHEG III) : 1.0 (%)
   Recommended value for SHEG I and SHEG II : 1.5 (%)
   Recommended value for SHEG I
   ("Structures of Ordinary Importance") when height is
   less than 3 stories and no brittle-type finishes : 2.0 (%)
3) Mexico DF (1987)
   Value depends in whether or not the nonstructural
   components can be damaged : 0.6 or 1.2 (%)
4) BRI (Japan)
   In practice, no code limit is specified : 1.0 (%)
5) NZS (New Zealand, 1984)
   Maximum interstory drift index : 1.0 (%)

Limiting drifts have been classified for two states, the serviceability level and ultimate safety level, by Bertero (1991). At the service level, current seismic codes give maximum values in the range of 0.06% - 0.6%. The limiting drift at the service level is not the concern in this paper. The foregoing values for each code are ultimate limits. Bertero (1991) reports that the usual variations in interstory drifts for strucutres designed to present seismic codes are in the range of 1 to 3% and vary with the type of structure and its function.

3.2 Required limit drifts

The process adopted in the ACI provisional standard for acceptance criteria for frame structures (1996) is used here to suggest a required limit drift for the characteristics of the shear walls which codified in UBC code (1994) and NEHRP provision (1994) as a structural system.

The story drift limitations specified in UBC 1628.8 isare

$T < 0.7$ sec, $\delta = (0.04/R_w)\,H$ or $0.005H$
$T > 0.7$ sec, $\delta = (0.03/R_w)\,H$ or $0.004H$

Where T = fundmental period; R_w = numerical coefficient equal to 12 for special moment-resisting frames of a moment resisting frame system

(MRFS), 6 for shear walls of a bearing wall system (BWS), and 8 for shear walls of a building frame system (BFS); and H = height of structure.

The deformation compatibility requirement of UBC 1631.24 is $3(R_w/8) \times$ calculated drift. However, Uang (1993) has suggested that the upper bound for expected drifts is not (3/8) R_w but 1.0 R_w for frame structures. Further, (Veletsos, 1960), the drift of an inelastic structure is about that of an elastic structure with same initial period. Table 1 shows corresponding limiting drifts for three different structural forms specified in UBC 1994.

Table 1. Drift ratio according to UBC 1994

	R_w	δ	$3/8R_w\,\delta$ (%)	$1.0R_w\,\delta$ (%)	Suggested Value*
MRFS	12	0.00333H	1.5	4.0	3.5
Shear walls of BWS	6	0.005H	1.125	3.0	To be suggested
Shear walls of BFS	8	0.005H	1.5	4.0	To be suggested

* Suggested value for structural form for acceptance testing

It is difficult for a conventional moment frame, designed to UBC 1994, to achieve a drift of 4% without failure. Further, at that value, nonstructural damage is very high. Therefore a value of 3.5% was suggested as the limiting drift ratio for SMRF (ACI, 1996). Even though values of 3% for shear walls of BWS and 4% for shear walls of BFS are listed in Table 1, those values are unachieveable for shear walls with low aspect ratios. It is not easy to specify an acceptable limiting drift ratio for shear walls, because drifts are very senstive to the sectional characteristics of the wall.

3.3 Limiting drift based on analysis of test results

Duffey (1993) reviewed experimental data for squat shear walls with aspect ratios between 0.24 and 1.07 and , based on statistical analyses, suggested the limiting drifts shown in Table 2 and Fig.1. Limiting drifts are shown as the function of the fraction of the post-peak ultimate load. For either frames or walls the limiting strength, for stability reasons, is customarily taken as the strength when the load has decreased to 80 or to 85% of the peak load (Park, 1989 and ACI, 1996). Table 2 and Fig.2 show that limiting drifts for that condition are between 1.12% and 1.24%.

Duffey (1993) also analyzed specific test results to determine limiting drift values. His data are again analyzed here with data where drifts were controlled artificially to 1.0% excluded and with other test data appended. Table 3 lists the data analyzed in this paper. Results for 178 walls with aspect ratios between 0.25 and 3.53 are used.

Table 2. Drifts Variation with Post-Peak Load (Duffey, 1993)

Fraction of Peak Load (%)	Drift (%)
100	0.72
90	1.00
80	1.24
70	1.48
60	1.64
50	1.84

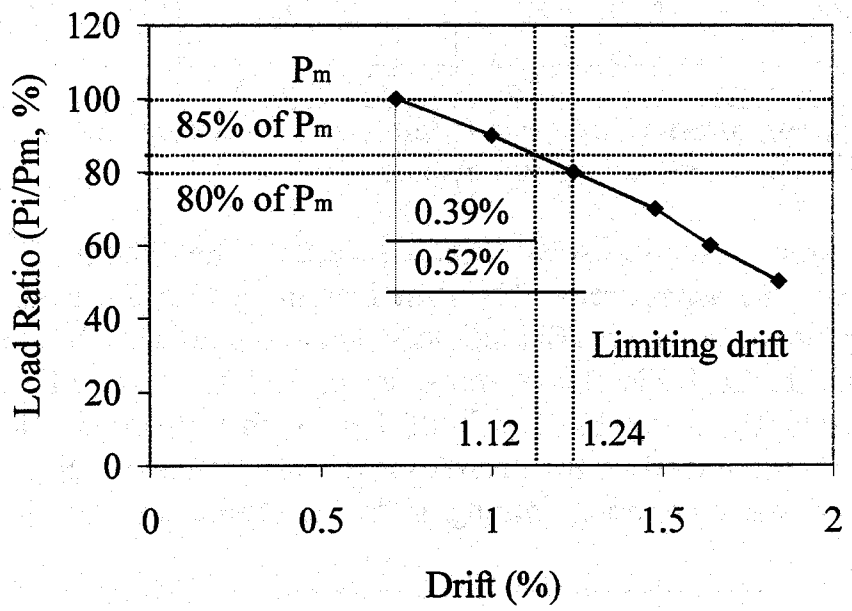

Fig. 1 Drift variation with post-peak load

Table 3 List of data

Researcher	Year	Number	Aspect Ratio	Loading*
Wiradinata	1986	4	0.25, 2.5	C
Saatcioglu	1991	8	0.25, 0.5	C
Shiga	1976	14	0.68	C
Endo	1982	20	1	C
Paulay	1982	3	0.5	C
Alexander	1973	2	0.75	C
Barda	1972	11	0.24, 0.51, 1.07	C, M
Benjamin	1954	19	0.32, 0.50, 0.58	M
Williams	1952	17	0.32, 0.50, 0.58,	M

			0.69, 0.71, 1.25	
Cervenka	1971	3	1.0	M
Corley	1981	19	2.69, 3.53	C, M
Elnashai	1990	16	2.0	C
Flonato	1976	4	2.40, 2.69	C
Lefas	1990	13	1.0, 2.0	M
Yamada	1974	7	.44	M
Maier	1985	11	1.22	C, M^{++}
Hiraishi	1988	4	1.7	C
Bertero	1975	2	1.28	C, M
Bertero	1979	2	1.28	C,M
Morgan	1986	1	2.78	C
Total		178	0.25 ~ 3.53	

* Loading patern (C : Cyclic loading, M : Monotonic loading, M^{++} : Some reloading, not cyclic)

Fig. 2 shows the statistical analysis result. The limiting drift varies linearly with the aspect ratio. The drift increment between peak load and the failure load, equal to 80% of peak load, should also be considered, because drifts in Table 3 are those at peak load. That effect can be approximated by using the result of Fig. 1 that post-peak load drifts increase almost linearly with decreasing post-peak loads. Eq. (1) is the resultant expression relating limiting drifts and aspect ratio for shear walls.

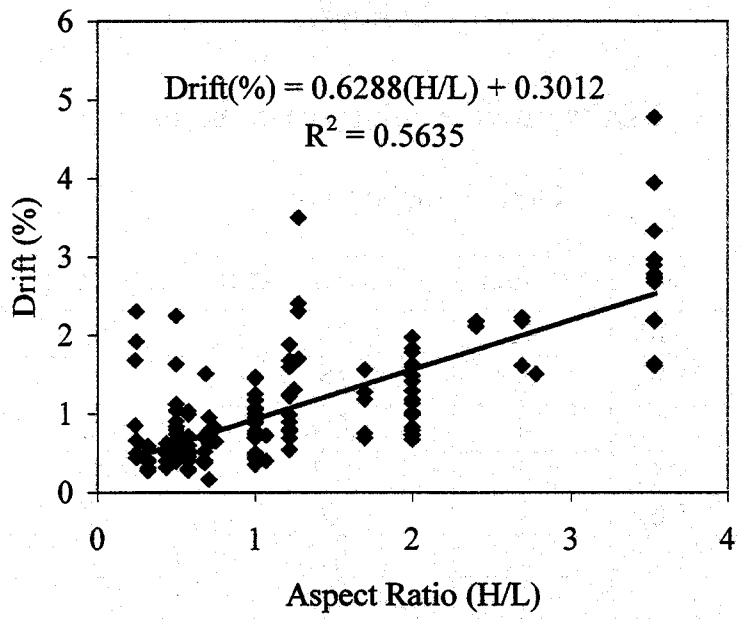

Fig. 2 Drift – aspect ratio relation

$$Drift(\%) = 0.6288\left(\frac{H}{L}\right) + 0.8212 \quad (1)$$

3.4 Simple method for calculating maximum drift

A procedure for relating displacements to local inelastic demands can be based on the model of Fig. 3. Elastic curvatures vary over the wall height in proportion to wall moment. For inelastic response, the maximum elastic curvature is equal to the yield curvature ϕ_y, which is the curvature at first yield of the wall boundary reinforcement. Inelastic curvatures up to the maximim curvature accumulate at the base of the wall along a height l_p resulting in a plastic hinge rotation θ_p.

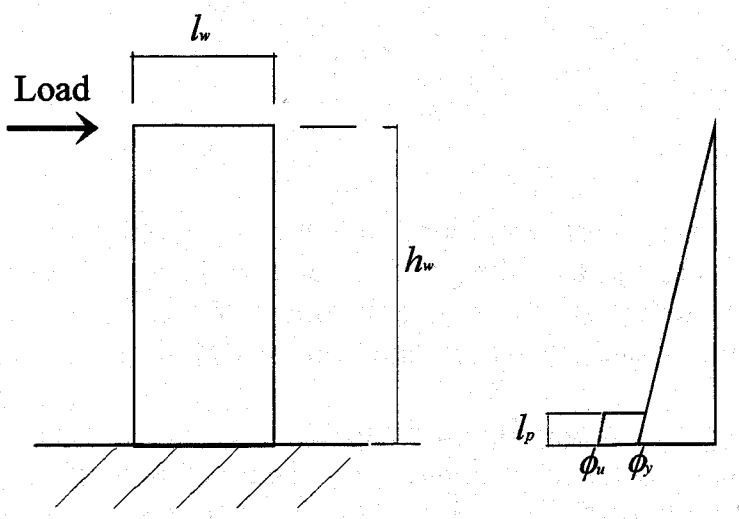

Fig. 3 Curvature of cantilever shear wall

The displacement at the top of the wall can be approximated by Eq. (2).

$$\delta_u = \delta_y + \theta_p h_w \quad (2)$$

$$= \left(\frac{\phi_y h_w^{\,2}}{3}\right) + \left(\phi_u - \phi_y\right) l_p h_w \quad (3)$$

The length of the plastic hinge zone and the yield curvature can be expressed as a function of the wall length.

$$l_p = \alpha\, l_w \quad \phi_y = \frac{\beta}{l_w}$$

$$\frac{\delta_u}{h_w} = \frac{\beta}{3}\frac{h_w}{l_w} + \left(\phi_u - \frac{\beta}{l_w}\right)\alpha\; l_w \quad (4)$$

From Fig. 3, the curvature ductility is

$$\mu_\phi = \frac{\phi_\mu}{\phi_y} = \frac{h_w{}^2(\mu_\delta - 1)}{3 l_p h_w} \tag{5}$$

$$\therefore \phi_u = \frac{\beta(\mu_\delta - 1)}{3\alpha h_w}\left(\frac{h_w}{l_w}\right)^2 + \frac{\beta}{l_w} \tag{6}$$

$$\frac{\delta_u}{h_w} = \frac{\beta}{3}\left(\frac{h_w}{l_w}\right) + \left[\phi_u - \frac{\beta}{l_w}\right]\alpha l_w \tag{7}$$

$$= \frac{\beta\mu_\delta}{3}\left(\frac{h_w}{l_w}\right) \tag{8}$$

Where, δ_u = displacement at ultimate load, δ_y = yield displacement, θ_p = plastic deflection angle, h_w = height of structure, ϕ_y = yield curvature, ϕ_u = curvature at ultimate load, l_p = plastic hinge length, μ_δ = displacement ductility at ultimate load, μ_ϕ = curvature ductility at ultimate load.

Eq. (8) involves both ductility and aspect ratio. However, the drift, δ_u/h_w of Eq. (8) is the value at the ultimate load. That value needs to include the additional post-peak drift. From Fig. 1 it can be seen that drift is 0.52% so that Eq. (8) becomes :

$$\frac{\delta_m}{h_w} = \frac{\beta\mu_\delta}{3}\left(\frac{h_w}{l_w}\right) + \frac{1}{192} \tag{9}$$

In Eq. (9) α is a coefficient that defines the plastic hinge length. Its value depends on the depth of section and typically ranges between 0.3 and 0.8. For simplicity its value can be taken as 0.5 (Wallace, 1992). The other factor, β, defines the relation between yield curvature ϕ_y and depth of section. Its value increases with increasing steel ratio and axial load, and is not easy to approximate. For design purposes, a value of 0.0025 is suggested (Wallace, 1992). Shown in Fig. 4 is the resultant variation in drift with aspect ratio and ductility demand calculated from Eq. (9)

The commentary to NZS 4203 (1992) defines an approximate criterion for the limiting displacement of shear wall structures such that the building as a whole can sustain four cycles of loading with a ductility ratio $\mu = 8$ without the base shear decreasing by more than 20 percent. Even though

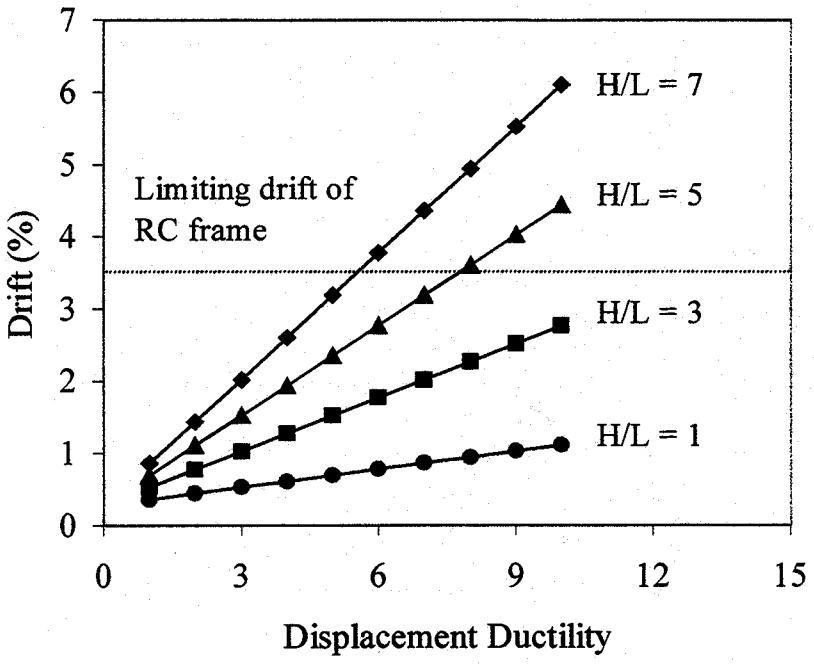

Fig. 4 Drift- displacement ductility curve

the structural ductility factor is required to be modified according to the period, it is reasonable to use a maximum ductility factor 8 for assessing a limiting drift based on structural testing. Then, Eq. (9) can be changed to Eq. (10) with the values α of 0.5 and β of 0.0025.

$$\frac{\delta_m}{h_w}(\%) = 0.67\left(\frac{h_w}{l_w}\right) + 0.52 \tag{10}$$

Where δ_m = maximum displacement at 0.80 P_m

3.5 Limiting drift ratios for shear walls

Two equations for the limiting drifts of shear walls have been proposed by analyzing the available test data and using simple curvature theory. Fig. 5 shows that the curve of Eq. (1) agrees with that of Eq. (10). An expression for the limiting drift ratio of a shear wall can be derived by taking 3.0% drift as the upper bound. That drift is also the value for 1.0 R for shear walls for BWS in Table 1. Also the least drift should be more than 1% to satisfy the limiting building drifts for each design code of section 3. Thus, an appropriate limiting drift expression for shear walls is:

$$1 \le \frac{\delta_m}{h_w}(\%) = 0.67\left(\frac{h_w}{l_w}\right) + 0.52 \le 3 \tag{11}$$

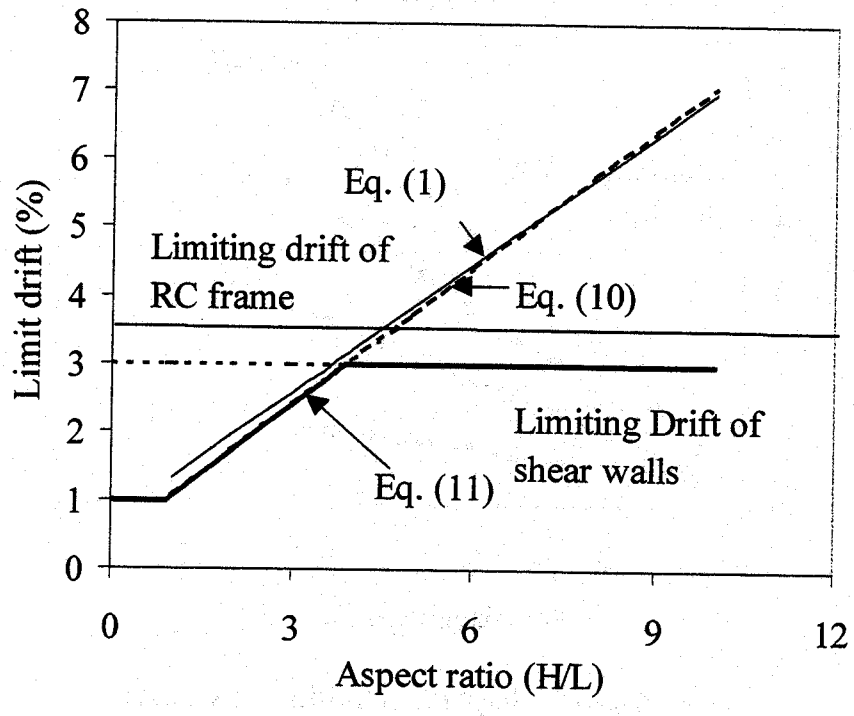

Fig. 5 Limiting drift ratio for shear walls

4. Relative energy dissipation ratio for shear walls

In the acceptance criteria (ACI, 1996), the limiting energy dissipation ratio for RC frame structure is set at 12% for the third complete cycle at or exceeding the maximum drift of 3.5%. This limit is to prevent the low cycle fatigue effects caused by inadequate damping and obviate possible displacement increases with cycling. Energy dissipation is best expressed as an equivalent viscous damping. In this paper, a procedure based on the relation between energy dissipation ratio and damping ratio is adopted to suggest a limiting energy dissipation ratio for shear walls based on testing.

Fig. 6 shows the hysteretic loop of the ACI (1996) acceptance criteria. The area of the parallelogram in Fig. 6 is :

$$(2D-2x_1)\times 2F = 4(D-x_1)F \tag{12}$$

Here, $K_1 = F/D$, $x_1 = D\dfrac{K_2}{K_1}$

Thus, Eq. (12) may be written as:

$$4(D-x_1DK_1) = 4(D-D\frac{K_2}{K_1})DK_1 \tag{13}$$

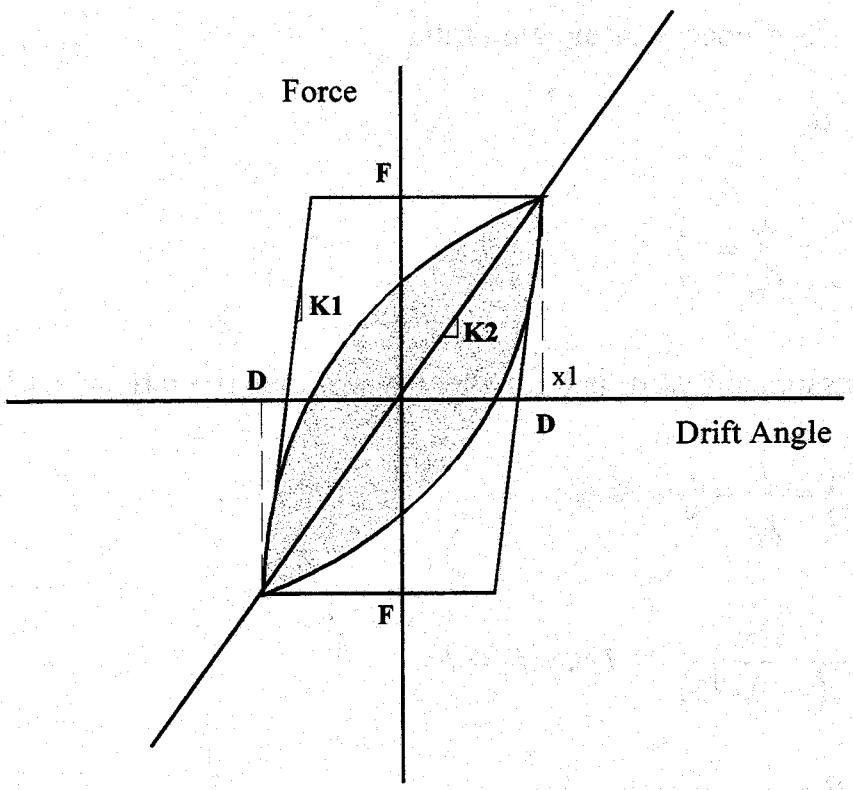

Fig. 6 Relative energy dissipation ratio

The energy dissipation ratio is

$$\frac{W}{\Delta W} = \frac{A_h}{4K_1 D^2 (1 - \frac{K_2}{K_1})} \tag{14}$$

$$\beta_I = \frac{A_h}{2\pi K_1 D^2}$$ From the NEHRP Provision (1994)

Where A_h = total area for a given cycle and β_I = effective damping

Eq. (14) can be rewritten as a relationship between energy dissipation ratio and damping ratio:

$$\frac{A_h}{2\pi K_1 D^2} \times \frac{\pi}{2\left(1 - \frac{K_2}{K_1}\right)} = E_R \tag{15}$$

$$\beta_I \times \frac{\pi}{2\left(1 - \frac{K_2}{K_1}\right)} = E_R \tag{16}$$

Where E_R = energy dissipation ratio

From Fig. 6

$$\frac{K_2}{K_1} = \frac{x_1}{D} = \frac{\delta_y}{\delta_m} = \frac{1}{\mu_\delta} \tag{17}$$

If it is assumed that μ_δ is 8 for shear walls, then the ratio of K_2/K_1 is

$$\frac{K_2}{K_1} = \frac{x_1}{D} = \frac{1}{\mu_\delta} = \frac{1}{8} = 0.125$$

$$\therefore \beta_I \times \frac{3.14}{2(1-0.125)} = 1.794 \times \beta_I = E_R \tag{18}$$

$$C \times \beta_I = E_R \tag{19}$$

Here, C = 1.794 is a coefficient to represent the relationship between damping and energy dissipation ratios at maximum drift angle.

Table 4 which is taken from Dowrick (1987) indicates representative values of damping for a range of construction. Those values are suitable for normal response spectrum or modal analysis in which viscous damping, equal in all modes, is assumed. Those damping values also assume that the structure is a normal risk structure expected to yield in the design earthquake, and hence the damping due to hysteresis is included, but no allowance for radiation damping has been made.

The minimum energy dissipation ratio specified in the ACI (1996) acceptance criteria are reviewed in here. The damping ratio of a RC frame structure can be estimated directly from the 12% energy dissipation ratio.

$$\beta_I = \frac{12(\%)}{1.794} = 6.99(\%)$$

That value is between 5 and 7 and is consistent with the damping ratios for concrete frames in Table 4.

Table 4 Typical damping ratios for structures (Dowrick,1987)

Type of construction	Damping ξ (percentage of critical)
(1) Steel frame, welded, with all walls of flexible construction	2
(2) Steel frame, welded, with normal floors and cladding	5
(3) Steel frame, bolted, with normal floors and cladding	10
(4) *Concrete frame, with all walls of flexible construction*	5
(5) *Concrete frame, with stiff cladding and all internal walls*	7
(6) Concrete frame, with concrete or masonry shear walls	10
(7) ***Concrete and /or masonry shear wall***	10
(8) Buildings, timber shear wall construction	15
Notes The term 'frame' indicates beam and column bending structures as distinct from shear structures. The term 'concrete' includes both reinforced and prestressed concrete in buildings. For isolated prestressed concrete members such as in bridge decks damping values less than 5 percent may be appropriate, e.g. 1-2 percent if the structure remains substantially uncracked.	

An appropriate limiting energy dissipation ratio for shear walls can be derived as follows:

$$E_R = 1.794 \times \beta_I$$

From Table 4

$$\beta_I = 10(\%)$$

The limiting minimum energy dissipation for a shear wall is then

$$E_R = 1.794 \times 10(\%) = 17.94(\%) \approx 18(\%) \qquad (20)$$

5. Conclusion

Appropriate limiting drift and energy dissipation ratios for shear walls for post-peak loads values equal to 80% of the ultimate load were studied. To derive a suitable limiting drift ratio for shear walls, available test data were analyzed and results compared to drift values calculated using a simple cantilever method. The result is a formula for drift that is a function of aspect ratio. A limiting energy dissipation ratio for shear walls was derived by using accepted damping ratio for structures. The limiting energy dissipation ratio for shear walls was 18% at a displacement ductility ratio of 8 and a damping ratio of 10%.

6. Acknowledgments

The work presented here was supported by funds from the advanced Structural RESearch Station which is one of the Engineering Research Centers of Korea, and was conducted as a joint research activity between STRESS and the Department of Civil Engineering of the University of Illinois at Urbana-Champaign.

7. References

ACI (1996), **Proposed Provisional Standard, Acceptance Criteria for Moment Frames Based on Structural Testing**

Alexander, C., Heifebrrecht, A., Tso, W. (1973), **Cyclic load tests on shear wall panel**, Proceedings of the Fifth World Conference on Earthquake Engineering.

Barda, F. (1972), **Shear strength of low-rise shear walls with boundary elements**, Ph. D. Dissertation, Lehigh University, Bethlehem, PA.

Benjamin, J.R., Williams, H.A. (1954), **Investigation of shear walls, part 6**, Department of Civil Engineering, Stanford University, Stanford, CA, Technical report No. 4, August.

Bertero, V.V. (1977), **Earthquake resistant reinforced concrete building construction**, Proceedings Workshop I, University Extension, University of California, Berkeley, California, July, pp.38-39.

Bertero, V.V., Anderson, J.C., Krawinkler, H., Miranda, E., Kajima research team (1991), **Design guidline for ductility and drift limits**, EERC Report No. UCB/EERC-91/15, University of California, Berkeley.

Bertero, V.V., et al., (1985), **Earthquake simulation tests and associated experimental and analytical correlation solution of one-fifth scale model**, SP-84 ACI, Detroit, Michigan, pp.375-424

Cervenka, V., Gerstle, K. (1971), **Inelastic analysis of reinforced concrete panels : Experimental verification and application,** Journal of the International Association of bridge and structural engineering, Vol. 32-II.

Corley, W.G., Fiorato, A.E., and Oesterle, R.G. (1981), **Structural walls,** ACI Journal SP-72-4. American Concrete Institute, 77-131.

Dowrick, D.J. (1987), **Earthquake resistant design for engineers and architects,** Wiley.

Duffey, T. A., Goldman, A. and Farrar, C. R. (1993), **Shear Wall Ultimate Drift Limits**, Report No. NUREG/CR-6104, LA-12649-MS, U.S. Nuclear Regulatory Commission.

Endo, T. (1982), **Hysteretic behavior of reinforced concrete shear walls**, Memories of Faculty of Technology, Tokyo Metropolitan University, No. 32 3195-3206.

Elnashai, A.S., Pilakoutas, K., and Ambraseys, N.N. (1990), **Experimental behavior of reinforced concrete walls under earthquake loading**, Earthquake Engineering and Structural Dynamics, Vol. 19, 389-407.

Farrar, C.R. and Bennet, J.G. (1998), **Experimental assessment of damping in low aspect ratio, reinforced concrete shear wall structure**, Report No. NUREG/CR-5154, LA-11325-MS, U.S. Nuclear Regulatory Commission.

FEMA (1995), 1994 **NEHRP recommended provisions for seismic regulations for new buildings.**

Fiorato, A.E., Oesterle, R.G., and Carpenter, J.E. (1976), **Reversing load tests of five isolated structural walls**, International Symposium on Earthquake engineering, St. Louis, MO, August.

Hiraishi, H, Shiohara, H., Kawashima, T., Tomatsuri, H., Kurosawa, A., Budo, Y. (1988), **Experimental study in seismic performance of multistory shear wall with flanged cross section**, Proceedings of ninth world conference on earthquake engineering,Vol. IV, Yokyo-Kyoto, -

IV.553-IVI.558.

Lefas, I.D., Kotsovos, M.D., and Ambraseys, N.N. (1990), **Behavior of reinforced concrete structural walls : strength, deformation characteristics, and failure mechanism**, ACI Structural Journal, 23-31, January-February.

Morgan, B.J., Hiraishi, H. (1986), **US-Japan quasi-static test of isolated wall planar reinforced concrete structure**, report to the NSF, Construction Technology Laboratories, PCA, Skokie, Illinois.

Park, R. (1989), **Evaluation of ductility of structures and structural assemblages from laboratory testing**, Bulletin of the the New Zealand national society for earthquake engineering, Vol. 22, No. 3, Sept. 155-166.

Paulay, T., Priestly, M.J.N., Synge, A.J. (1982), **Ductility in earthquake resistant shear walls**, Journal of the American Concrete Institue, 257-269, July-Aug.

Saatcioglu, M. (1991), **Hysteretic shear response of low-rise walls, Concrete shear in earthquake**, Proceeding of the International Workshop on Concrete Shear in Earthquakes, University of Houston, Texas, Elsevier.

Shiga, T., Shibata, A., Takahashi, J. (1973), **Experimental study of dynamic properties of renforced concrete shear walls**, Proceeding of Fifth World Conference on Earthquake Engineering, 1157-1156.

Standards Association of New Zealand (1992), **Code of practice for general structural design and design loadings for building**, NZS 4203.

Uang, C. M. and Maarouf, A. (1993), **Seismic displacement amplification factor in uniform building code**, Research Bulletin Board, BB93-3, pp.B-1

Vallenas, J.M., Bertero, V.V., Popov, E.P. (1979), **Hysteretic behavior of reinforced concrete structural walls**, EERC report No. UCB/EERC 79/20, University of California, Berkeley.

Veletos, A.S., Newmark, N.M. (1960), **Effects of inelastic behavior on the response of simple systems to earthquake motions**, Proceedings 2WCEE, Tokyo, Japan, Vol.2, pp.895-912.

Wallace J.W., Moehle, J.P. (1992), **Ductility and detailing requirements of bearing wall buildings**, Journal of structural engineering, ASCE Vol.118, No. 6, 1625-1644.

Wang, T.Y., Bertero, V.V., Popov, E.P. (1975), **Hysteretic behavior of reinforced concrete framed shear walls**, EERC report No. UCB/EERC 75/23, University of California, Berkeley.

Williams, H.A., Benjamin, J.R. (1952), **Investigation of shear walls, Part 1**, Technical Report No. 1, Department of Civil Engineering, Stanford University, Stanford, CA.

Wiradinata, S. (1989), **Behavior of squat shear walls subjected to load reversals**, Thesis, University of Toronto, Canada.

Yamada, M., Kawamura, H., and Katakihara, K. (1974), **Reinforced Concrete Shear Walls with Openings ; Test and Analysis**, ACI Publication SP-42, Paper No. 25, American Concrete Institute, Detroit, MI.

Workshop on Structural Design Issues for Moderate Seismic Zones
February 24-25, 1998, Urbana, Illinois

EFFECT OF PRIOR EARTHQUAKE DAMAGE ON RESPONSE OF SIMPLE STRUCTURES

M. Aschheim[1] and E. Black[2]
1) Assistant Professor, University of Illinois at Urbana-Champaign, USA
2) Graduate Research Assistant, University of Illinois at Urbana-Champaign, USA

Abstract
A systematic study involving over 22,000 single-degree-of-freedom (SDOF) analyses was made to determine the effects of prior earthquake damage on the peak displacement response of simple oscillators. Principle variables were oscillator strength, period of vibration, degree of prior damage, and load-deformation relation. Base input was provided by 18 recorded ground motions. The ground motions represent different frequency content, duration, and the presence or absence of near-field forward directivity effects.

The analyses show that prior damage has a relatively small effect on peak displacement response, as long as the degree of prior damage is less than what the undamaged structure would experience. This was observed for SDOF oscillators having the Takeda load-deformation relation with positive post-yield stiffness and for a modified Takeda relation incorporating pinched hysteresis and strength degradation. The Takeda oscillators with negative post-yield stiffness were prone to collapse, whether or not they had experienced prior damage.

1. Introduction

One of the most fundamental observations of seismology is that earthquake magnitudes are inversely proportional to their likelihood of occurrence. Structures built in seismic zones can thus be expected to be shaken numerous times by ground motions of lesser intensity prior to being subjected to a design-level earthquake. The analytical study described herein addresses the question of whether damage sustained under milder shaking significantly affects response to the design-level ground motion.

2. Previous Findings

Limited experimental and analytical observations have suggested that prior damage has little effect on peak displacement response. In shake table tests of ten-story reinforced concrete frames, Cecen (1979) found that the peak displacement response at each story of the frame was only slightly affected by previous shaking of the same intensity. Cecen also compared the displacement response of two nominally-identical reinforced concrete frames that were subjected to the same final motion after different sequences of prior shaking, and found that the peak displacement response over the height of the structures was nearly the same. In shake table tests of three-story reinforced concrete walls subjected to repeated shaking, Wolschlag (1993) found that the peak displacement response over the height of the structure was not affected significantly by prior shaking.

Analytical studies of Cecen's ten story frames conducted by Saiidi (1979) found that displacement maxima were not significantly affected by repeated motion; the double amplitude displacement response was 4 to 20% larger during the repeated ground motions for a large range of acceleration intensities. Mahin (1980) found that SDOF oscillators subjected to repeated ground motions exhibited moderate increases in displacement ductility demand across all periods, with weaker structures being prone to the largest increases. Given these findings, a broader investigation into the effects of prior damage on response was initiated.

3. Methodology

3.1 Analytical Framework

The analytical study was constructed to understand the relative influence of various factors on displacement response. The analytical framework explicitly accounts for the degree of prior damage for structures having different lateral strengths, periods of vibration, and load-deformation relations subjected to several suites of ground motions. The ground motions were selected to represent various frequencies, durations, and the presence or

absence of near field pulses. In order to keep the study simple while maintaining its breadth, many arbitrary choices and simplifying assumptions were made. These choices and assumptions are not necessarily appropriate for specific structures or structural types, which may require substantially more detailed modeling.

The effect of prior damage on displacement demand is the focus of this study. Two obvious approaches are available. In the first, a composite ground motion is created, comprised of the damaging ground motion, a quiescent period in which the structure comes to rest, and the design-level ground motion. For this approach, a possible criterion for establishing the damaging ground motion is that it should cause a pre-determined displacement ductility demand. Instead, the approach taken in this study is to prescriptively modify the SDOF load-deformation relation to analytically simulate prior ductility demand. Thus, prior ductility demand was explicitly modeled and the initially "damaged" oscillators were subjected to only the design-level ground motion. The peak displacement of each damaged oscillator, d_d', can then be compared with the peak displacement of an initially-undamaged oscillator, d_d.

A range of periods and strengths were of interest. Initially-undamaged oscillators had periods of vibration ranging between 0.1 and 2.0 sec (0.1, 0.2, 0.3, 0.4, 0.5, 0.6, 0.8, 1.0, 1.2, 1.5, and 2.0 sec). These periods correspond to the secant stiffness at yield of the undamaged oscillators. Regardless of the degree of prior damage, initially-damaged oscillators are referred to by the periods of their undamaged companions.

To obtain a range of lateral strengths while accounting for the inherently irregular features of recorded ground motions, the lateral strengths of the undamaged oscillators were set equal to the strengths required for an oscillator having a bilinear load-deformation relation to achieve ductility demands of 1 (elastic), 2, 4, and 8. These strengths are unique to each period and ground motion, and common to the different load-deformation relations. The bilinear oscillator had post-yield stiffness equal to 5% of the yield point secant stiffness, and viscous damping equal to 5% of critical damping. The design displacement ductility is subsequently referred to by the term DDD.

The effect of damage was investigated for three load-deformation relations. The first is the standard Takeda model (Takeda, 1970), referred to subsequently by the term Tak5. The post-yield stiffness of the Tak5 oscillators was set equal to +5% of the yield point secant stiffness, k, as shown in Figure 1a. The yield strength of each oscillator was identical to the strength required to achieve the specified displacement ductility demand for a bilinear oscillator having the same yield point secant stiffness. The exponent controlling the unloading stiffness was set equal to 0.5, indicating that at any instant the unloading stiffness is determined as the yield point secant stiffness divided by

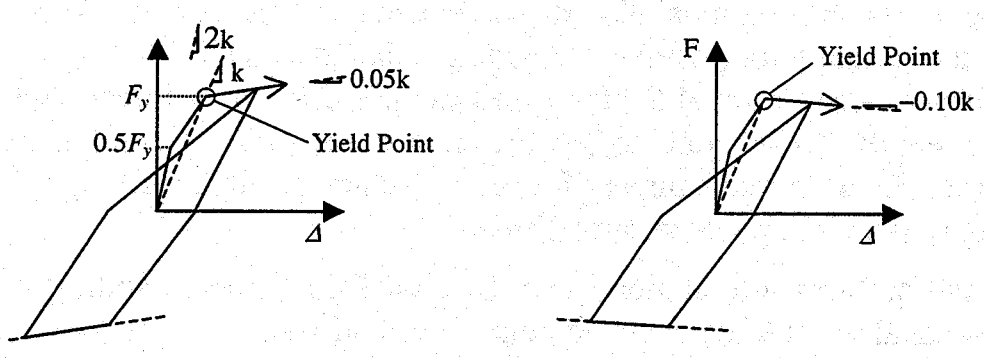

(a) TAK5 Model (b) TAK10 Model

Fig. 1. Standard Takeda models (Tak5 and Tak10) used in the analyses

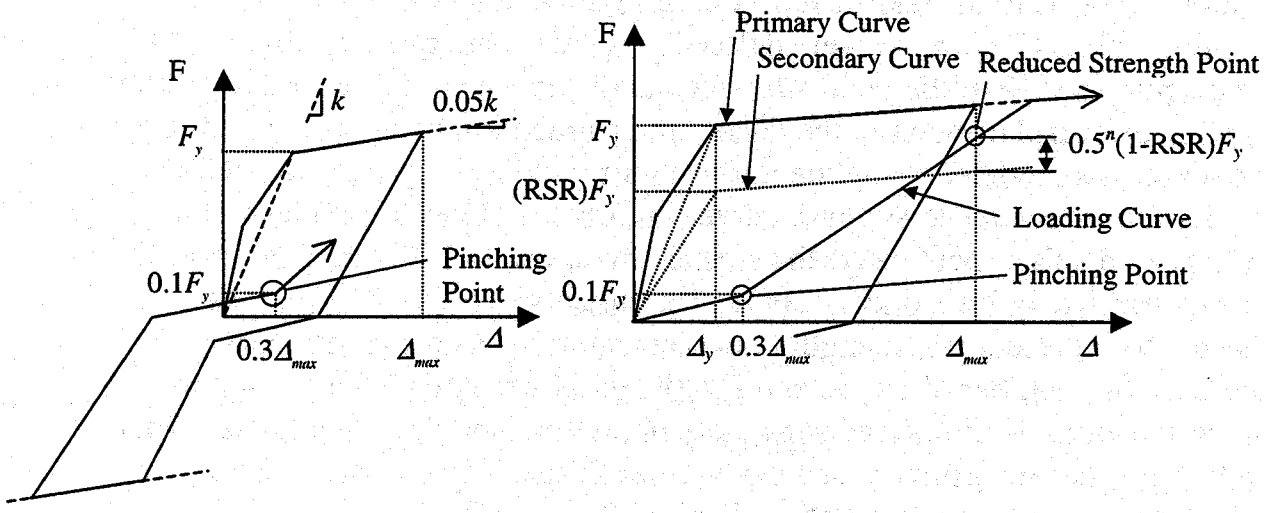

(a) Pinching point definition (b) Cyclic strength degradation

Fig. 2. Modified Takeda model (TakPinch) incorporating pinching and strength degradation

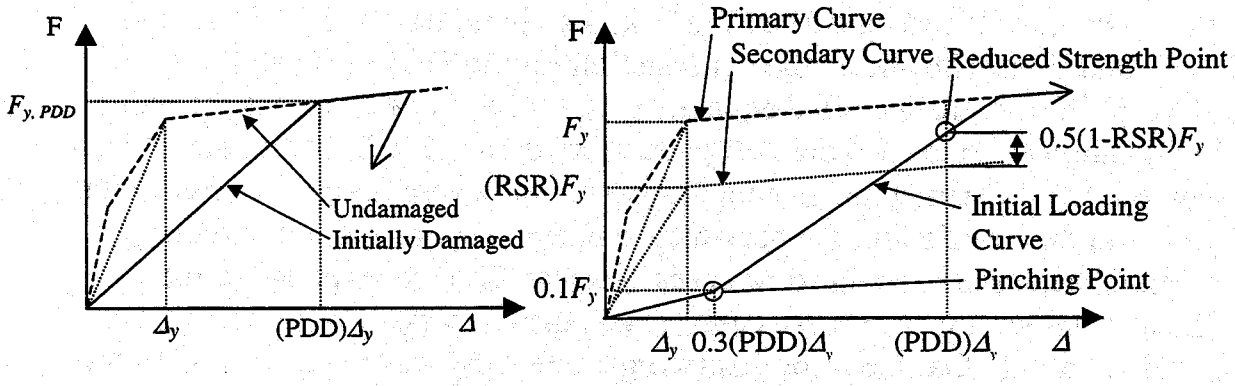

(a) Tak5 and Tak10 models (b) TakPinch model

Fig. 3. Construction of initially-damaged force-displacement response

the square root of the current maximum displacement ductility demand. This was monitored separately for positive and negative displacements. The uncracked stiffness was set equal to twice the yield point secant stiffness, and the cracking strength was set equal to half the yield strength. Viscous damping was set equal to 5% of critical damping for the frequency of vibration corresponding to the yield point secant stiffness.

The second load-deformation relation is the standard Takeda model with post-yield stiffness equal to -10% of the yield point secant stiffness. This model, subsequently referred to as Tak10, is shown in Figure 1b. Other parameter values are as for the Tak5 model.

To investigate the potential consequences of prior damage on systems with pinched hysteretic responses, a third load-deformation relation was used. This relation, referred to as TakPinch, is a modified Takeda model. Distinct pinching points (Figure 2a) were defined in the first and third quadrants at a force equal to 10% of the yield strength and displacement equal to 30% of the current peak displacement in the quadrant. Degradation of strength on cyclic reloading was modeled using the Reduced Strength Ratio parameter (RSR), which defines a reduced strength curve (Figure 2b). Repeated cycles to the same peak displacement cause the stiffness to asymptotically reduce towards the reduced strength secondary curve. The function $0.5^n(1 - RSR)F_y$ was selected to represent the strength in excess of the reduced strength curve, where n= the number of cycles and F_y= the yield strength of the oscillator. The parameter n is monitored separately in the first and third quadrants. When loading reaches the primary curve, n is reset to one. The parameter RSR was assigned values of 1 (no strength reduction), 0.8, and 0.6.

Prior damage was simulated by adjusting the initial loading curve and current displacement ductility maxima to correspond to a specified level of prior ductility demand (PDD). For example, Figure 3a shows the construction of the initially-damaged loading curve for a Tak5 oscillator having a PDD greater than 1, and Figure 3b shows the construction for the TakPinch oscillator. Values of PDD were specified equal to 1, 2, 4, or 8. In no case was the value of PDD allowed to exceed the design ductility demand (DDD), because it is assumed that the damaging ground motion is less severe than the design event. Even with this restriction, the peak displacement response of the undamaged Takeda-based oscillators in some cases was less than the response of their bilinear counterparts. For these cases, it was also necessary to restrict values of PDD to assure that the prior displacement demand was not greater than the peak displacement response of the initially undamaged oscillators.

The strengths of the oscillators were determined using the computer program PCNSPEC (Boroschek, 1991). Nonlinear response computations for the Takeda-based models were made using a computer program developed by Otani (1981)

and modified at the University of Illinois to consider prior ductility demands, pinching behavior, and strength degradation.

3.2 Ground Motions

It was desired to use a large enough sample of ground motions so that potential trends and deviations in the results could be observed. Furthermore, it was desired to separately assess whether ground motion duration or the presence or absence of near-field pulses associated with fault ruptures propagating towards the recording station influence the effect of prior damage on response. Three categories of ground motion were established: Short Duration (SD), Long Duration (LD), and Forward Directive (FD). Within each category, 6 ground motions were selected to span a range of frequency content. The ground motions are identified in Table 1, sorted in order of characteristic period within each category.

The selection of the ground motions was based on several objectives: (1) the ground motions should be strong enough to cause structural damage at their natural intensities; (2) the suite of records should include records that the research community is familiar with; (3) recent earthquakes should be represented; and (4) no one earthquake should be heavily represented to avoid systematic bias. No restriction was placed on the type of faulting mechanism.

Records were sorted into the SD and LD categories by simply judging the duration of the accelerogram. This was done in lieu of using available measures of duration because no one scalar measure can adequately represent the duration of inelastic response across different periods and strength levels. Because the physical rupture process correlates magnitude and shaking duration, records with magnitudes less than 7 often were judged to be SD motions while records from larger earthquakes tended to be classified as LD motions.

Records selected for the FD category contain near field pulses that are associated with fault rupture propagating towards the recording station (Somerville 1997). Recorded horizontal components were used, with orientations varying from approximately perpendicular to the fault trace to approximately parallel to the fault trace. Although the Tabas record (TB78TABS.344) is a near field record, it was place in the LD category because it has neutral directivity (Somerville 1997). The Lucerne motion (LN92LUCN.250) is believed to be the one corrected by Iwan (1994).

The characteristic period, T_g, of each ground motion was established considering equivalent velocity spectra and acceleration spectra for linear elastic oscillators having damping equal to 5% of critical damping. The characteristic period was identified using some judgment to correspond approximately to (1) the first (lowest period) peak of the equivalent velocity spectrum, and (2) the period at which the transition occurs between the constant acceleration and constant velocity portions

Table 1. Ground Motions Used in the Analyses

Earthquake Date	*Recording Station*	*Record Identifier*	*Component*	*PGA/g*	*Characteristic Period, T_g, sec*
Short Duration (SD)					
Whittier Narrows 1 Oct 87	Mount Wilson Caltech Seismic Station	WN87MWLN.090	90	0.17	0.20
Big Bear 28 Jun 92	Civic Center Grounds	BB92CIVC.360	360	0.54	0.40
Spitak 7 Dec 88	Gukasyan, Armenia	SP88GUKA.360	360	0.20	0.55
Loma Prieta 17 Oct 89	Corralitos Eureka Canyon Rd.	LP89CORR.090	90	0.48	0.85
Northridge 17 Jan 94	Century City	NR94CENT.360	360	0.22	1.00
Imperial Valley 15 Oct 79	Array #7-14	IV79ARY7.140	140	0.33	1.20
Long Duration (LD)					
Central Chile 3 Mar 85	Llolleo-Basement of 1-Story Building	CH85LLEO.010	10	0.71	0.30
Central Chile 3 Mar 85	University of Santa Maria Valparaiso	CH85VALP.070	70	0.17	0.55
Imperial Valley 18 May 40	El Centro Irrigation District	IV40ELCN.180	180	0.34	0.65
Tabas 16 Sep 78	Tabas	TB78TABS.344	344	0.93	0.80
Landers 28 Jun 92	Joshua Tree	LN92JOSH.360	360	0.27	1.30
Michoacan 19 Sep 85	SCT1-Secretary of Communication and Transportation	MX85SCT1.270	270	0.17	2.00
Forward Directive (FD)					
Landers 28 Jun 92	Lucerne	LN92LUCN.250	250	0.73	0.20
Imperial Valley 15 Oct 79	Brawley Municipal Airport	IV79BRWY.315	315	0.22	0.35
Loma Prieta 17 Oct 89	Saratoga Aloha Avenue	LP89SARA.360	360	0.50	0.40
Northridge 17 Jan 94	Newhall LA County Fire Station	NR94NWHL.360	360	0.58	0.80
Northridge 17 Jan 94	Sylmar County Hospital Parking Lot	NR94SYLH.090	90	0.60	0.90
Hyogo-Ken Nambu 17 Jan 95	Takatori-kisu	KO95TTRI.360	360	0.61	1.40

of an idealized smooth spectrum fitted to the actual spectrum, following guidance given by Shimazaki (1984), Qi (1991), and Lepage (1997). The fitting of a idealized smoothed spectrum typically leads to a slightly larger estimate of T_g than is obtained from equivalent velocity spectra.

4. Analytical Results

Over 20,000 SDOF responses were computed. Various cross sections or "slices"

The presentation for the Tak5 and TakPinch oscillators focuses on the displacement ratio, defined as the ratio of the peak displacement response of the initially-damaged oscillator and the peak response of the initially-undamaged oscillator. The displacement ratio is determined for a particular oscillator load-deformation relation, DDD, and ground motion record. The presentation for the Tak10 oscillators focuses on the percentage of oscillators that reached or exceeded their collapse displacement as a function of DDD and PDD.

4.1 Response of Tak5 Oscillators

Figure 4 plots the displacement histories and force-displacement responses of Tak5 oscillators subjected to the 1940 N-S El Centro record. The oscillators have a 1-sec period and lateral strength corresponding to DDD= 8. The solid line plots the response of the initially-undamaged oscillator while the dashed and dotted lines plot the response of companion oscillators having PDD= 1, 4, and 8. The first 40 seconds of response are plotted in the uppermost figure, and below this is shown a detailed view of the first 10 seconds of response. Force-displacement curves show the first 10 seconds of response.

The displacement histories in Figure 4 are similar to one another, having similar phasing and amplitude regardless of the degree of prior damage. Significant differences appear only within the first five seconds of response. Peak displacements were similar in magnitude and time of occurrence. While the force-displacement responses differ in the first seconds of response, they become similar in the cycles in the vicinity of the peak positive and negative displacements. The initial details of response at small displacements are influence by prior damage. At larger displacements, the oscillators with little or no initial damage differ little from those having prior damage. This suggests that the unloading and reloading stiffnesses at larger displacements have a greater influence on peak displacement response than does the initial stiffness or initial period of vibration. These trends were observed at other periods as well.

Figure 5 presents the effect of prior damage on peak displacement response for a large number of earthquakes and reference periods. In Figure 5, the displacement ratio is plotted as a function of the period ratio, T/T_g, for oscillators having strengths defined by DDD= 8. The period ratio, T/T_g, is defined as the ratio of the oscillator reference period and the characteristic period of the ground motion. Figure 5a plots results for oscillators having PDD equal to 1, while results for PDD= 8, are plotted in Figure 5b. In this and subsequent figures, results for the SD motions are presented in the uppermost plot, while the LD and FD results are presented in the middle and lower plots. Within each plot, the ground motions are sequenced in order of increasing characteristic period.

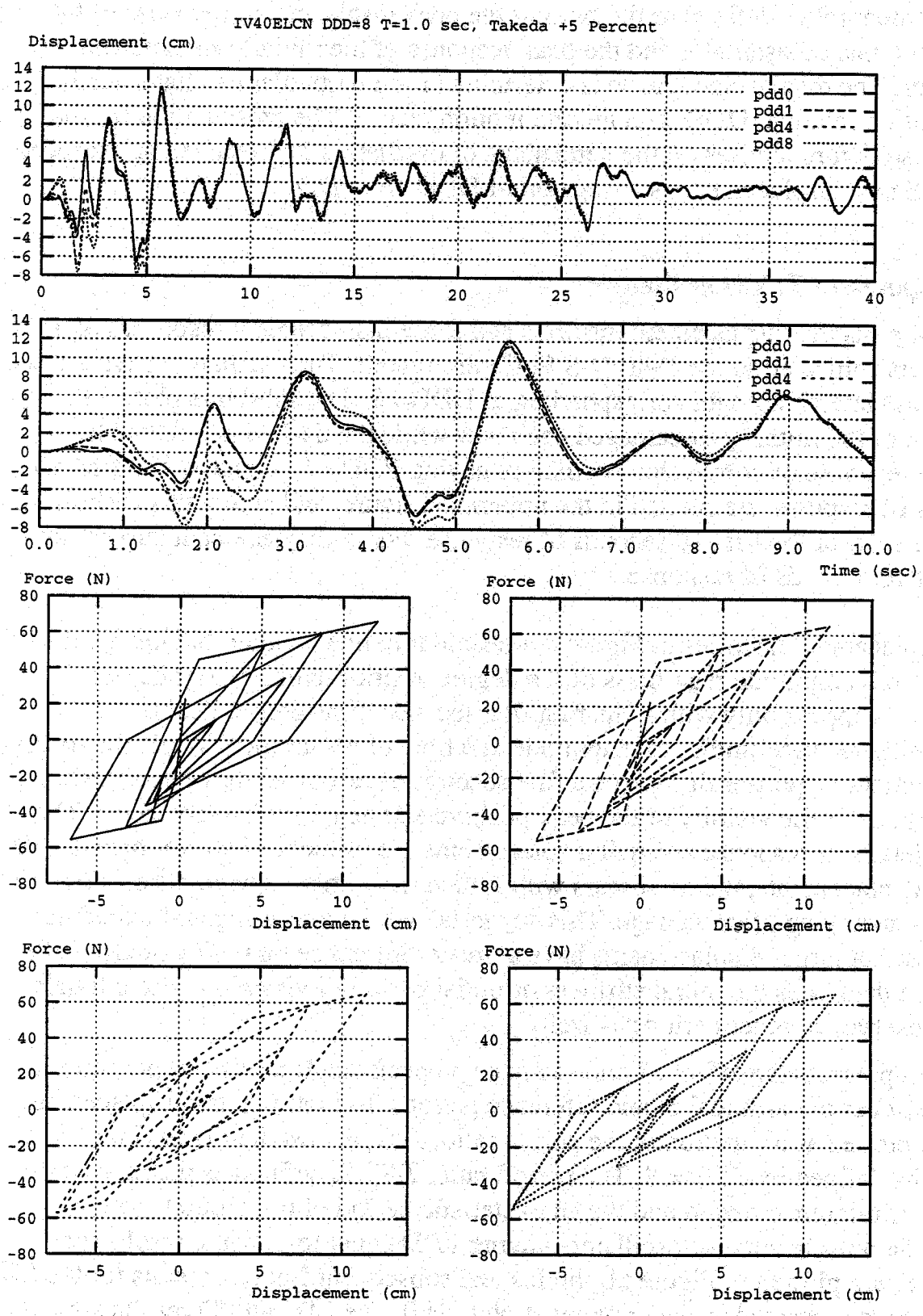

Fig. 4. Effect of damage on response of a Tak5 oscillator to El Centro (IV40ELCN.180), T= 1.0 sec

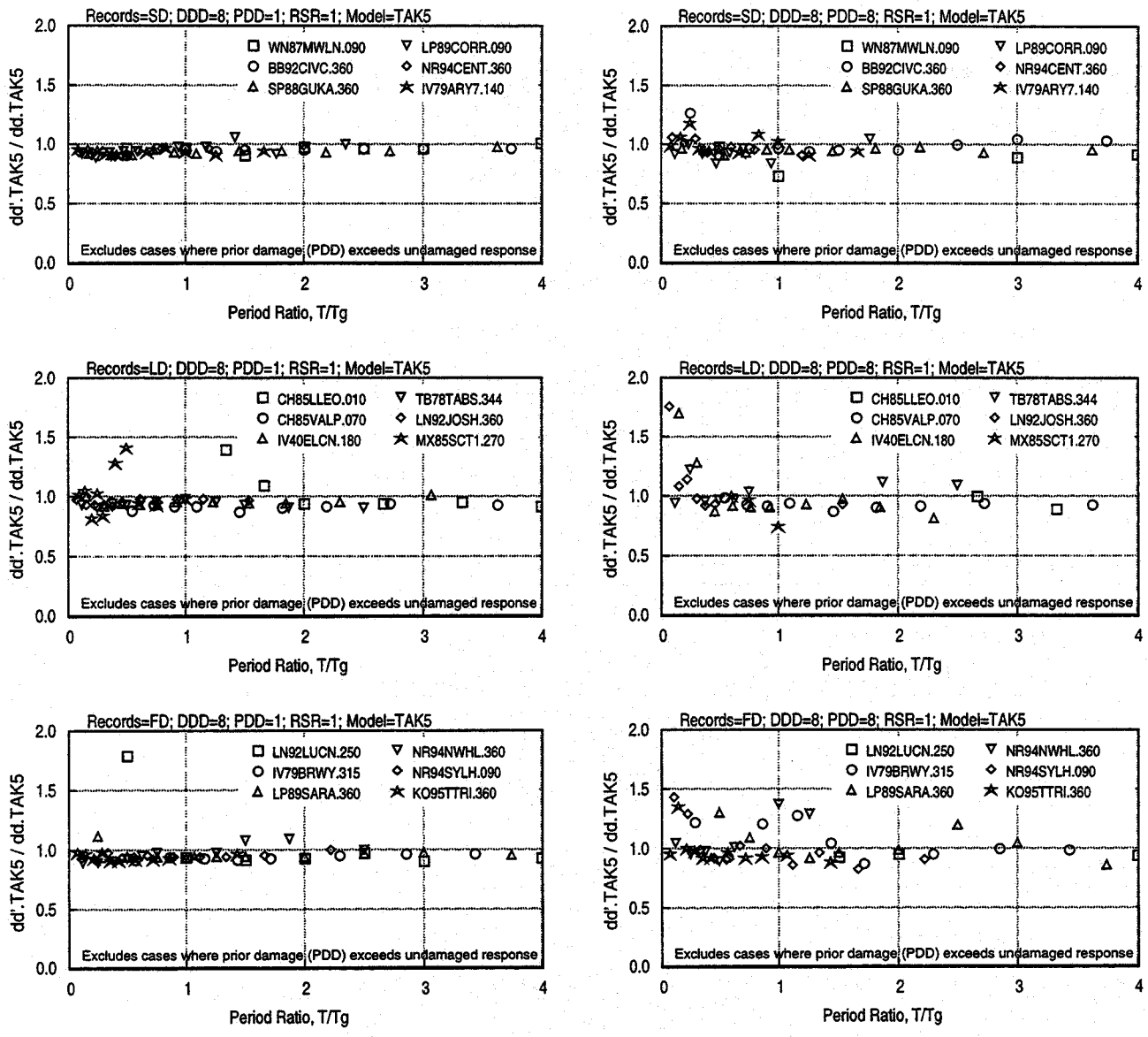

Fig. 5. Displacement ratios for Tak5 oscillators: (a) PDD= 1, and (b) PDD= 8

The displacement ratio is frequently slightly less than unity in the six plots of Figure 5. For the plots in Figure 5a (PDD= 1), prior damage frequently causes a slight reduction in peak displacement response. In Figure 5b (PDD= 8), prior damage rarely causes the peak displacement response to increase by more than 10% for the Short and Long Duration motions, or about 30% for the Forward Directive motions. Scatter about the mean is smallest for the SD motions for both cases of PDD, and tends to be greater for PDD= 8 than PDD= 1. These results indicate that minor cracking has a negligible effect on peak displacement response, while more substantial prior damage occasionally results in small increases in displacement demand, for Tak5 oscillators with strengths corresponding to DDD= ♀

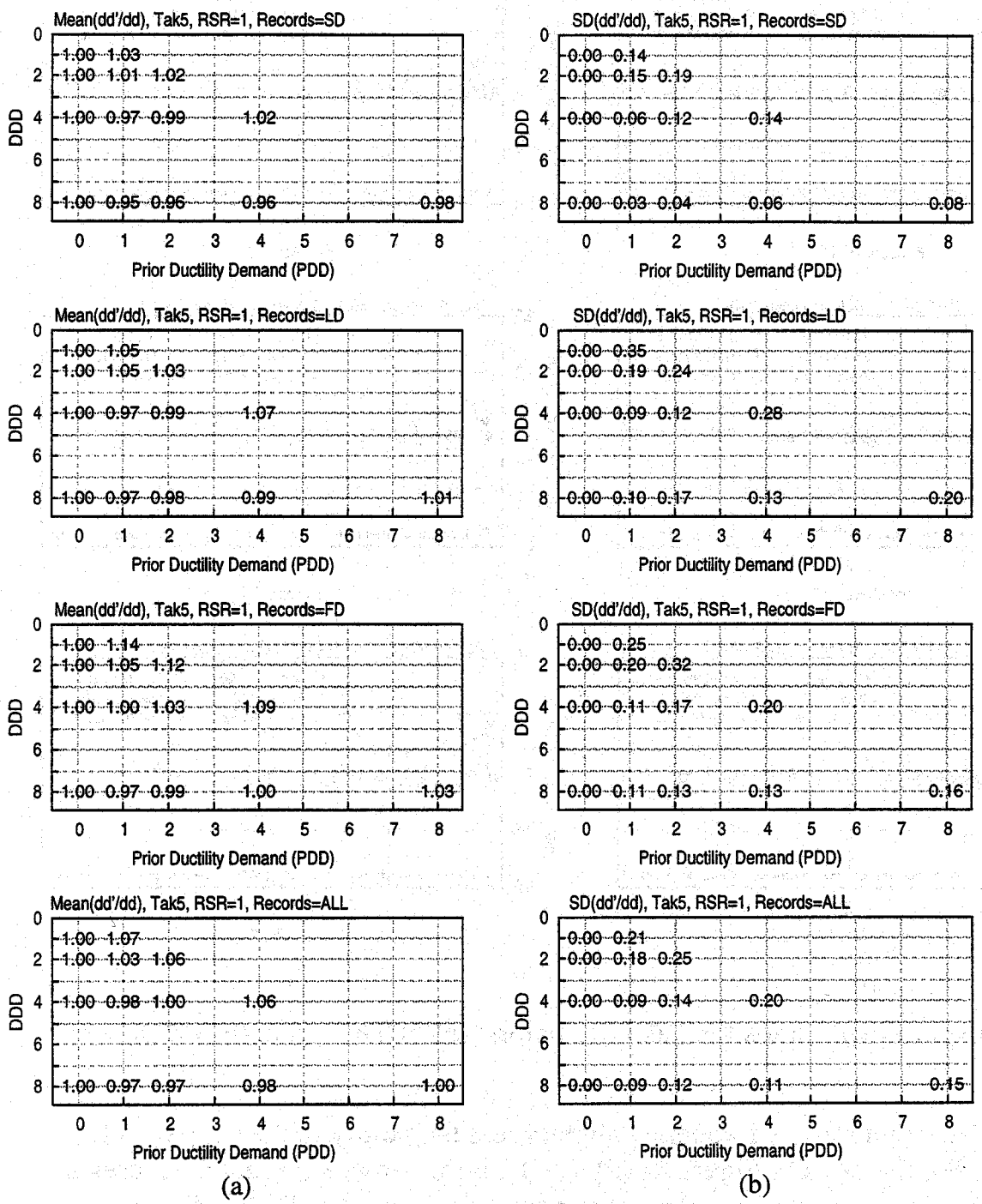

(a) (b)

Fig. 6. Displacement ratio statistics for Tak5 oscillators: (a) mean and (b) standard deviation

Figure 6 presents response statistics for Tak5 oscillators for all values of DDD and PDD. Mean values of the displacement ratio are presented in Figure 6a. The upper plots present results for the SD, LD, and FD ground motions; the lowest plots present summary statistics for the entire collection of ground motions. Mean displacement ratios range between 0.95 and 1.14 within the individual ground motion categories and between 0.97 and 1.07 when computed for the entire set of

ground motions. Changes in initial period resulting from different PDD are seen to have little effect on peak displacement response across all values of DDD and PDD for the Tak5 oscillators. Peak displacement response appears to be regulated more substantially by the unloading and reloading stiffnesses at the cycles during which the peak displacement response occurs.

Mean displacement ratios tend to be lower for the SD motions and higher for the LD motions, although the differences are small. Mean displacement ratios exceed unity for PDD = DDD, and are slightly less than unity for PDD < DDD. For weaker structures (DDD= 8), small prior ductility demands cause a slight reduction in peak displacement response, on average, while larger prior ductility demands have negligible effects on peak displacement response, on average. Thus, for the weaker Tak5 oscillators, prior damage does not cause larger peak displacement responses to occur in subsequent design events, provided that the prior displacement response is not greater than anticipated for the undamaged structure in the design event, and provided that residual drifts are negligible.

Variability in the displacement ratio, as measured by the standard deviation statistic, is plotted in Figure 6b. It can be observed that standard deviations tend to be largest for low DDD and for PDD = DDD. The larger standard deviations for low DDD are attributed to the more prominent role that the uncracked stiffness and cracking behavior play on the response of relatively strong oscillators, for which low ductility demands can be expected. Variability in response amplitude is reduced for small PDD, but as larger prior ductility demands are imposed, differences in stiffnesses and displacements at the start of the cycle during which peak response occurs lead to the observed increase in the standard deviation.

4.2 Response of TakPinch Oscillators

Figure 7 plots the peak displacement of previously damaged TakPinch oscillators normalized by the peak displacement of initially-undamaged TakPinch oscillators. The oscillators of Figure 7 have lateral strengths corresponding to DDD= 8, and strength degradation was not modeled (RSR= 1). Figure 7a plots results for PDD= 1. Results are similar to those of the Tak5 model (Figure 5a), and have a similar degree of scatter. This indicates that minor prior ductility demands (PDD= 1) typically have negligible effects on the peak displacement response of stiffness-degrading oscillators, regardless of the degree of pinching in the hysteresis. Both the Tak5 and TakPinch oscillators quickly progress beyond the undamaged portions of their load-deformation curves, and thereafter the displacement response is similar. Differences in the first cycles of response frequently are of little or no consequence in subsequent cycles, and it is in these later cycles that the peak displacement response usually occurs.

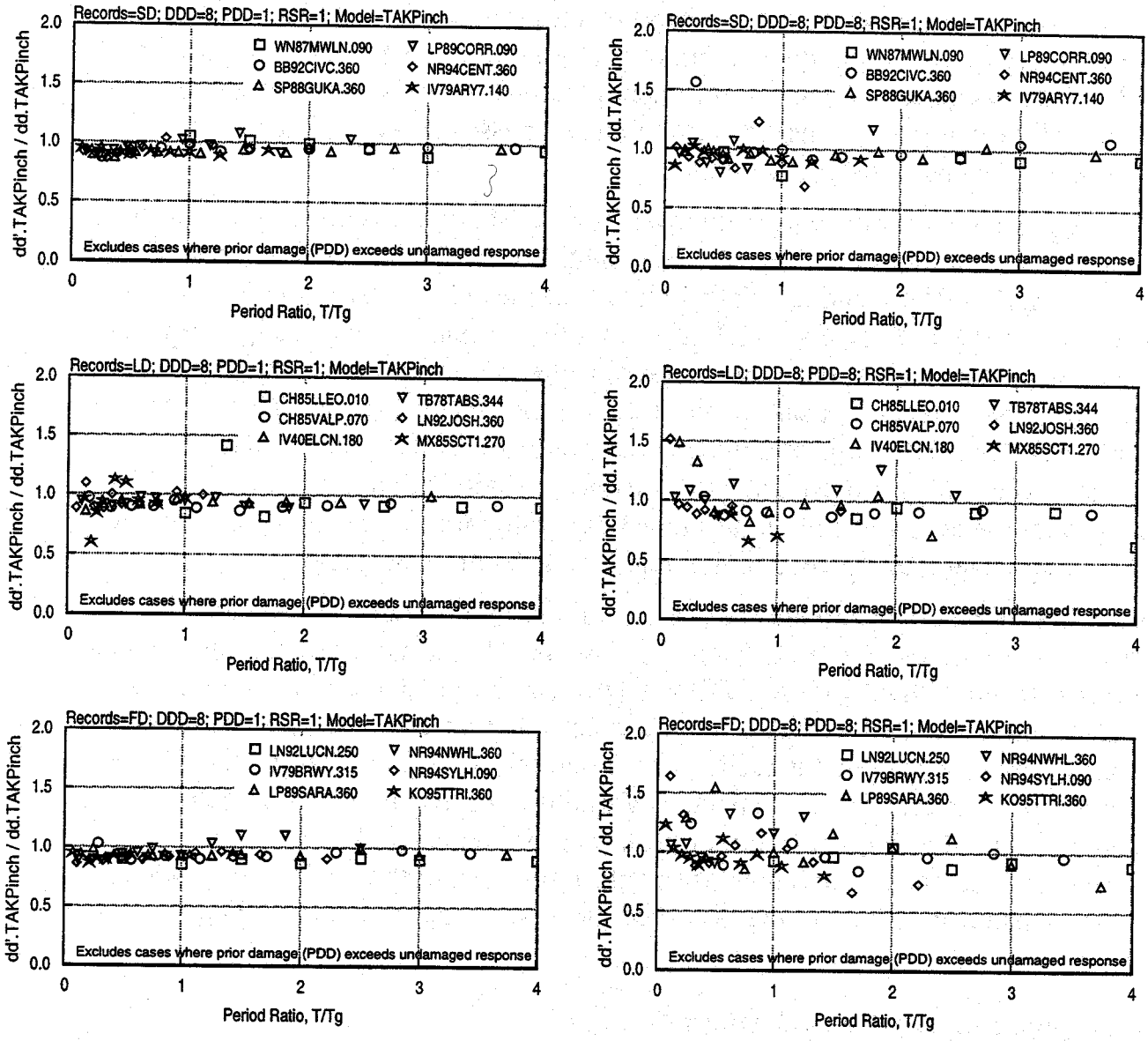

(a) (b)

Fig. 7. Displacement ratios for TakPinch oscillators with no strength degradation: (a) PDD= 1, and (b) PDD= 8

Figure 7b plots peak displacement demands for TakPinch oscillators having PDD= 8, normalized by the peak responses of the initially-undamaged TakPinch oscillators. Results are similar to those for the TAK5 oscillators of Figure 5b in that prior damage frequently causes a slight decrease in peak displacement response. However, the displacement ratios for the TakPinch oscillators appear to deviate more from the mean across all ground motion categories relative to the Tak5 oscillators. The deviation is larger for the Forward Directive motions.

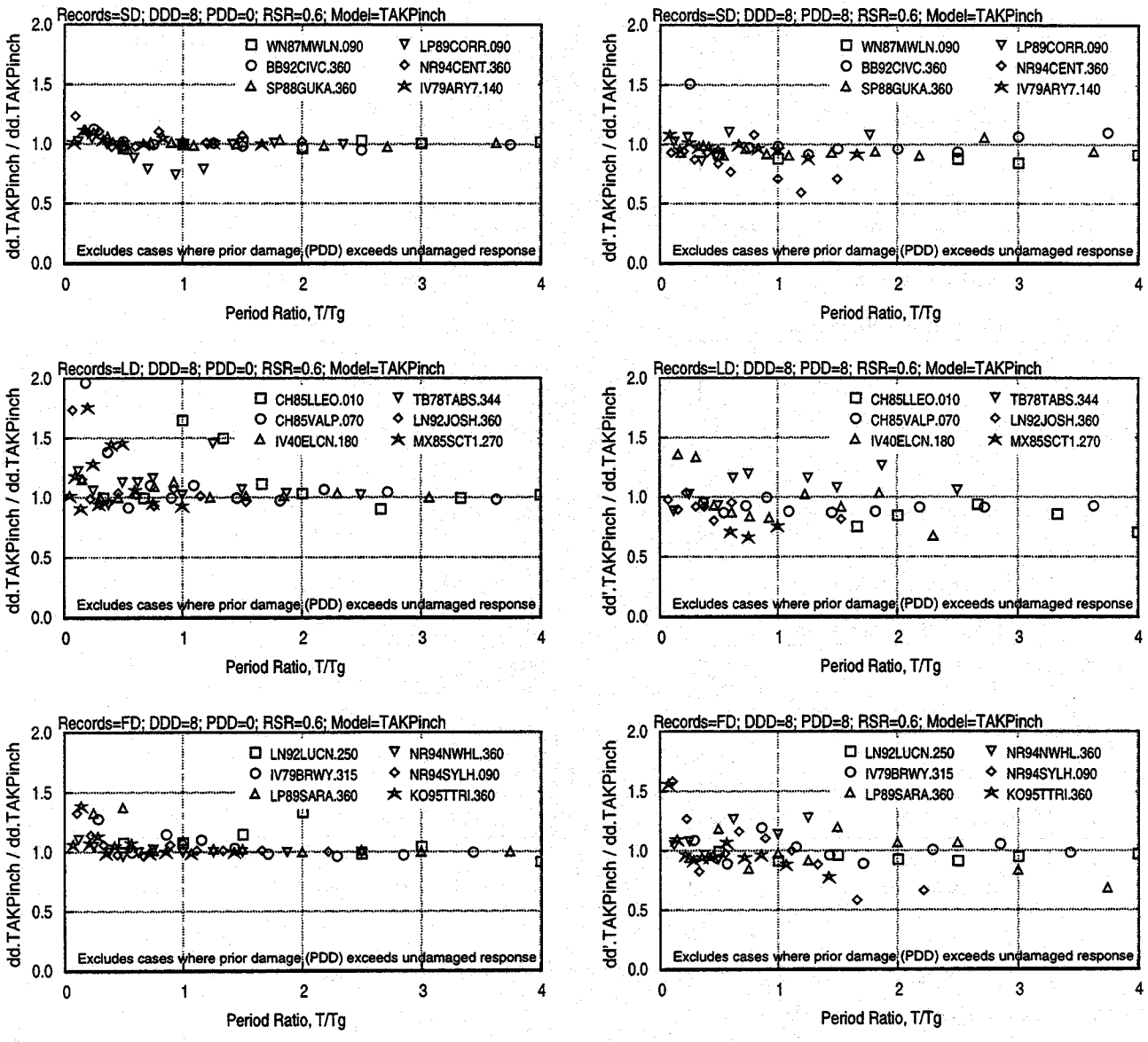

Fig. 8. (a) Effect of strength degradation (RSR= 0.6) on undamaged TakPinch oscillator response (DDD= 8) and (b) displacement ratios for TakPinch oscillators with RSR= 0.6 and PDD= 8

The effect of cyclic strength degradation on the displacement response of undamaged TakPinch oscillators is shown in Figure 8a, for oscillators having strengths corresponding to DDD= 8. Figure 8a plots the peak displacement response of oscillators having RSR= 0.6 normalized by the peak response of corresponding oscillators having no cyclic strength degradation (RSR= 1). It can be observed that cyclic strength degradation oscillators often has little or no effect on the peak displacement response of initially undamaged TakPinch oscillators. In other cases, displacements increase or decrease. When peak displacements increase due to strength degradation, the tendency is more prevalent for shorter period structures, and the increase appears to be greatest for the Long Duration motions.

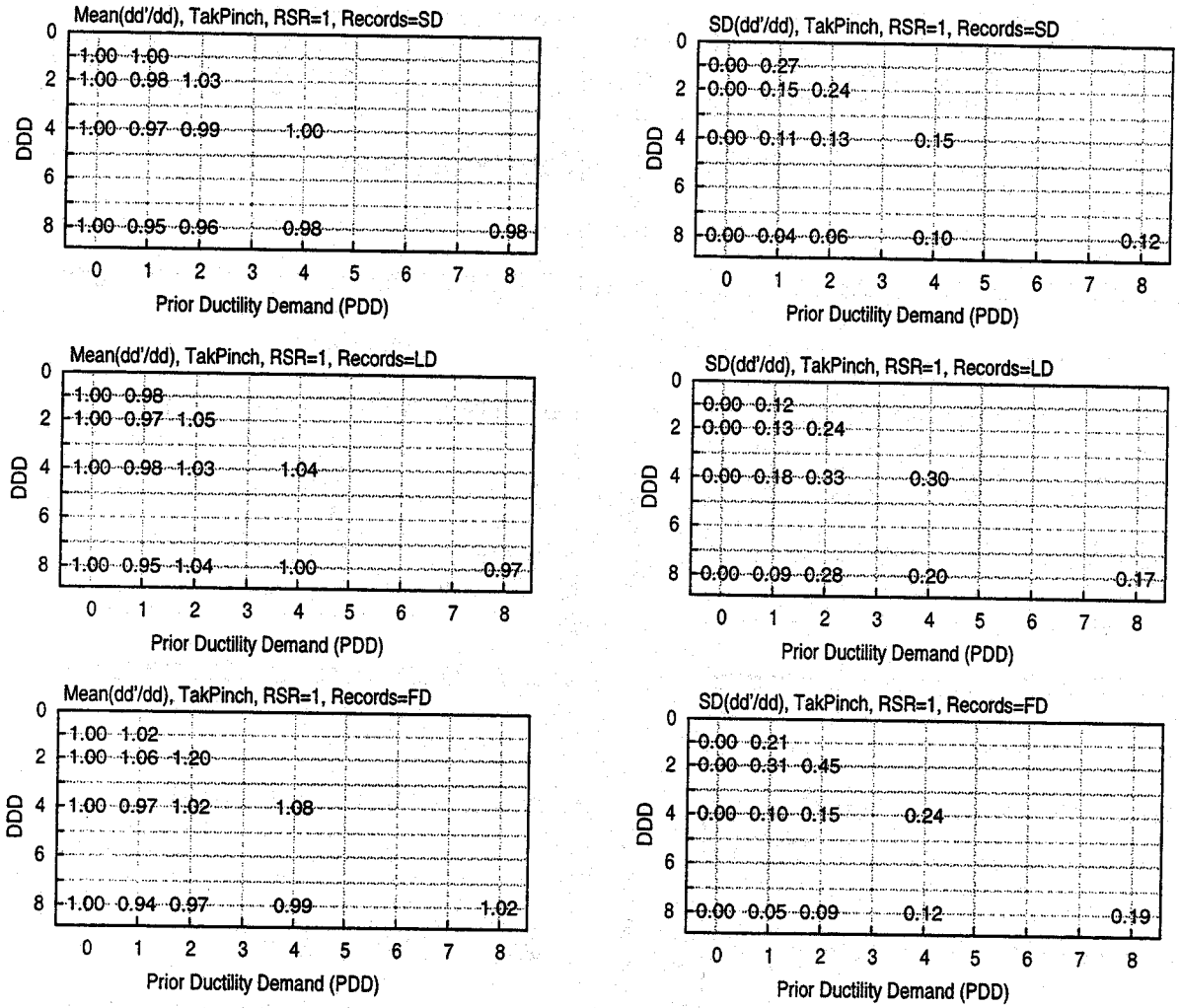

(a) (b)

Fig. 9. Displacement ratio statistics for TakPinch oscillators (RSR=1): (a) mean and (b) standard deviation

This can be understood in terms of several phenomena: (1) the tendency for short period structures to have multiple cycles at or near the peak displacement response, resulting in cyclic reduction in stiffness that further influences peak displacement response; and, (2) the greater likelihood that a larger number of cycles will occur at or near the peak displacement response for the LD motions.

The effect of prior ductility demand on the strength degrading TakPinch oscillators is shown in Figure 8b, which plots the ratio of peak displacement response for PDD= 8 and the peak response of undamaged TakPinch oscillators (PDD= 0).

The oscillators have strengths corresponding to DDD= 8 and strength degradation defined by RSR= 0.6. In Figure 8b it can be observed that prior ductility demands tend to reduce the peak oscillator displacements in a mean sense. Relative to the TakPinch oscillators with RSR= 1 (Figure 7b), the RSR= 0.6 oscillators appear to exhibit more deviation about the mean for the Long Duration motions.

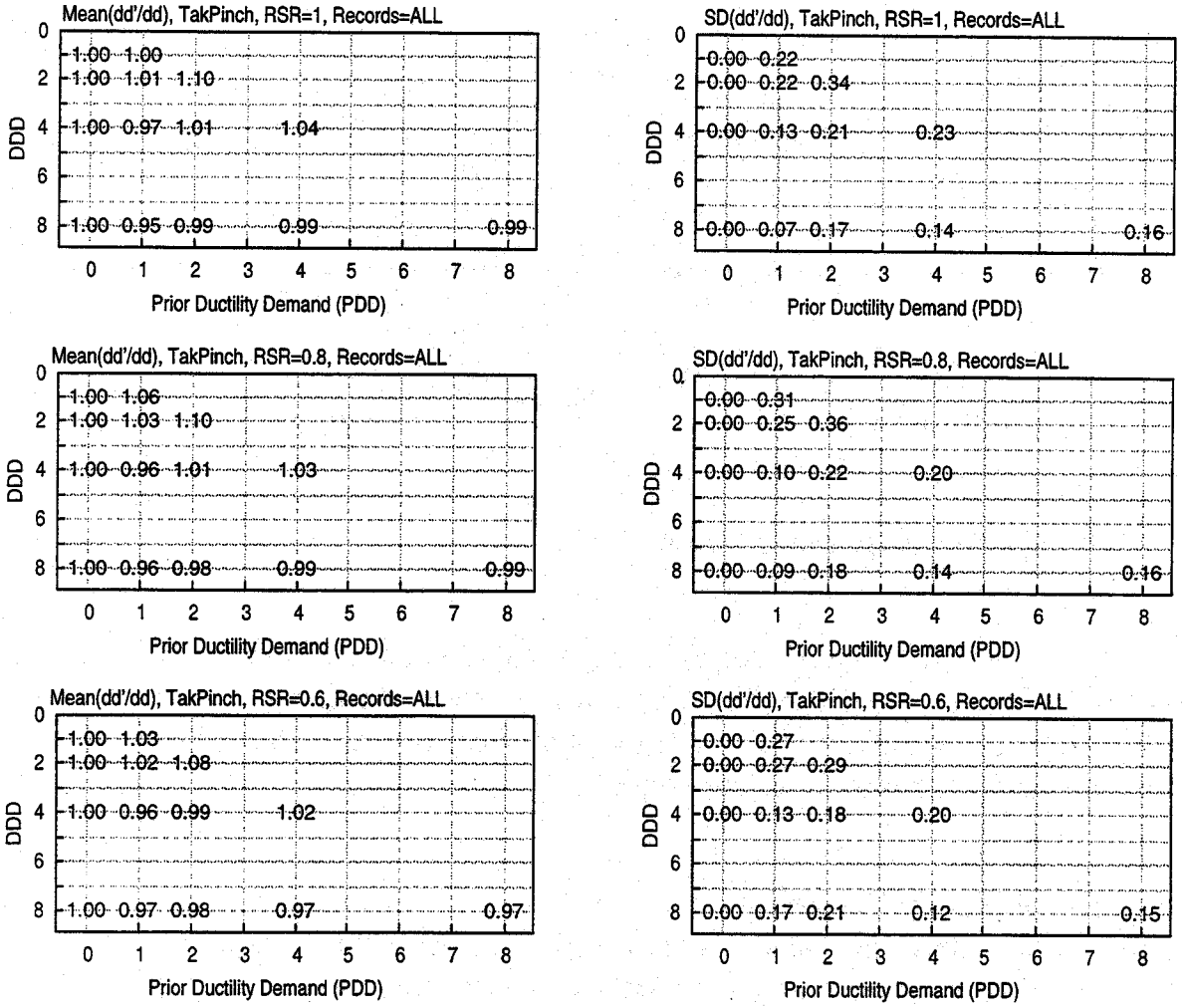

Fig. 10. Displacement ratio statistics for TakPinch oscillators (RSR=1, 0.8, and 0.6): (a) mean and (b) standard deviation

Response statistics for the TakPinch oscillators are plotted in Figures 9 and 10 as a function of design displacement ductility (DDD) and prior ductility demand (PDD). Figure 9 presents results for RSR=1 for each ground motion category; mean values of the displacement ratio are presented in Figure 9a and the standard deviation of this ratio is presented in Figure 9b. Summary statistics for the collection of ground motions are presented in Figure 10 for oscillators having strength degradation given by RSR=1, 0.8, and 0.6.

The trends shown for the TakPinch oscillators in Figure 9 are similar to those observed for the Tak5 oscillators in Figure 7. Mean displacement ratios range from 0.94 to 1.20, with higher values generally occurring for PDD=DDD. Mean displacement ratios tend to be less than unity for lower strength oscillators (DDD= 8) and small PDD. Standard deviations were larger for the stronger oscillators (low DDD) and tend to increase as PDD approaches DDD.

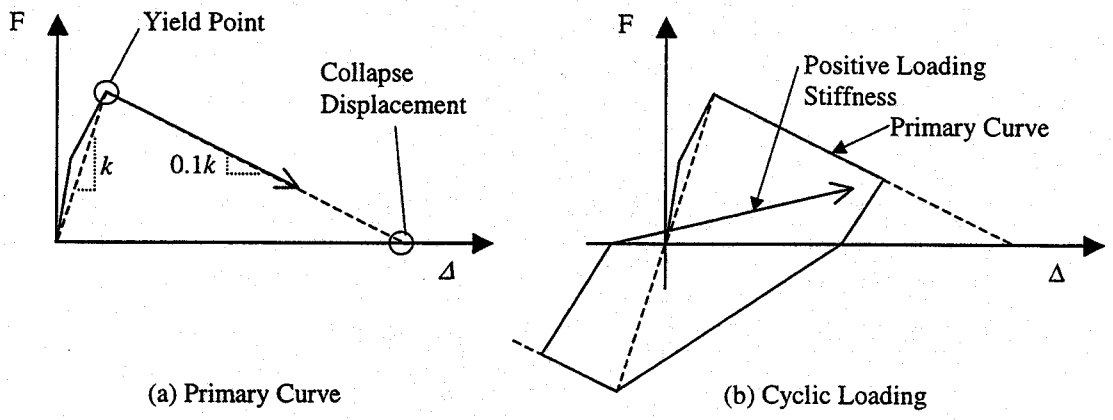

Fig. 11. Tak10 load-deformation relations

Figure 10 indicates that strength degradation, as modeled using RSR=1, 0.8, and 0.6, has little effect on the mean displacement ratio for any pairing of PDD and DDD. The standard deviation of this ratio was more sensitive to the value of RSR, but no pattern in its variation was apparent.

4.3 Response of Tak10 Oscillators

The primary curve defining Tak10 oscillator load-deformation response is characterized by a negative post-yield stiffness. Under static loading conditions, the collapse displacement can be defined as the point where the descending branch of the load-displacement curve intersects the abscissa (Figure 11a). It seems possible under dynamic conditions for a structure to momentarily exceed this displacement and not collapse provided that suitable base accelerations are present. Nevertheless, it is reasonable and conventional to consider dynamic displacements in excess of the collapse displacement as signifying structural collapse.

Collapse according to this definition was observed numerous times for both the undamaged and damaged Tak10 oscillators. For example, Figure 12 plots the displacement history and force-displacement response of a 1-sec Tak10 oscillator having various degrees of prior damage, subjected to the NS El Centro record. It can be observed that the oscillator with PDD= 1 manages to avoid collapse, while the undamaged oscillator collapses in the positive direction and the oscillators with larger PDD collapse in the other direction. The response of this oscillator, having strength defined by DDD= 8, can be compared with that of the Tak5 oscillator shown in Figure 4.

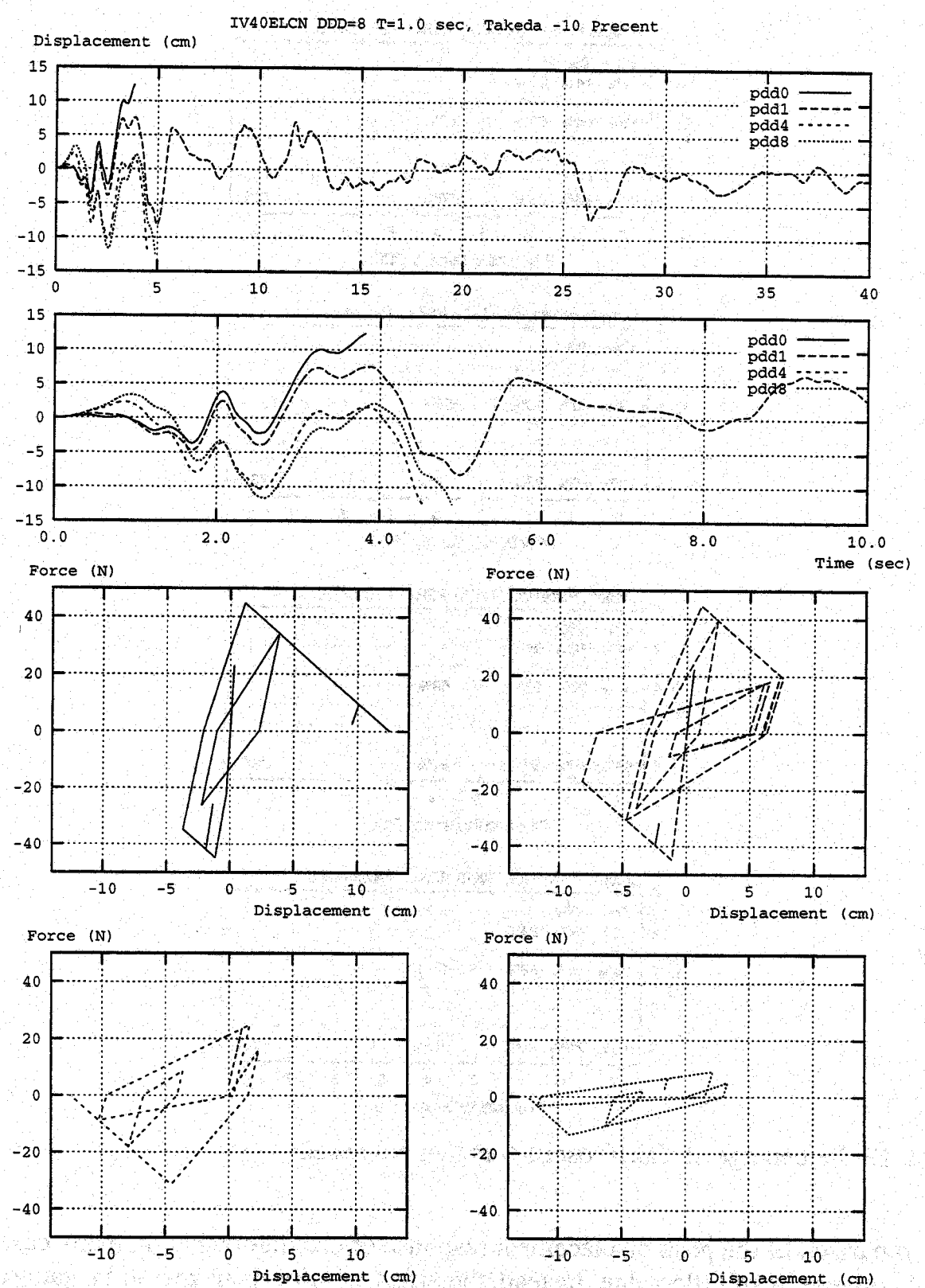

Figure 12. Effect of damage on response of a Tak10 oscillator to El Centro (IV40ELCN.180) record, T=1 sec.

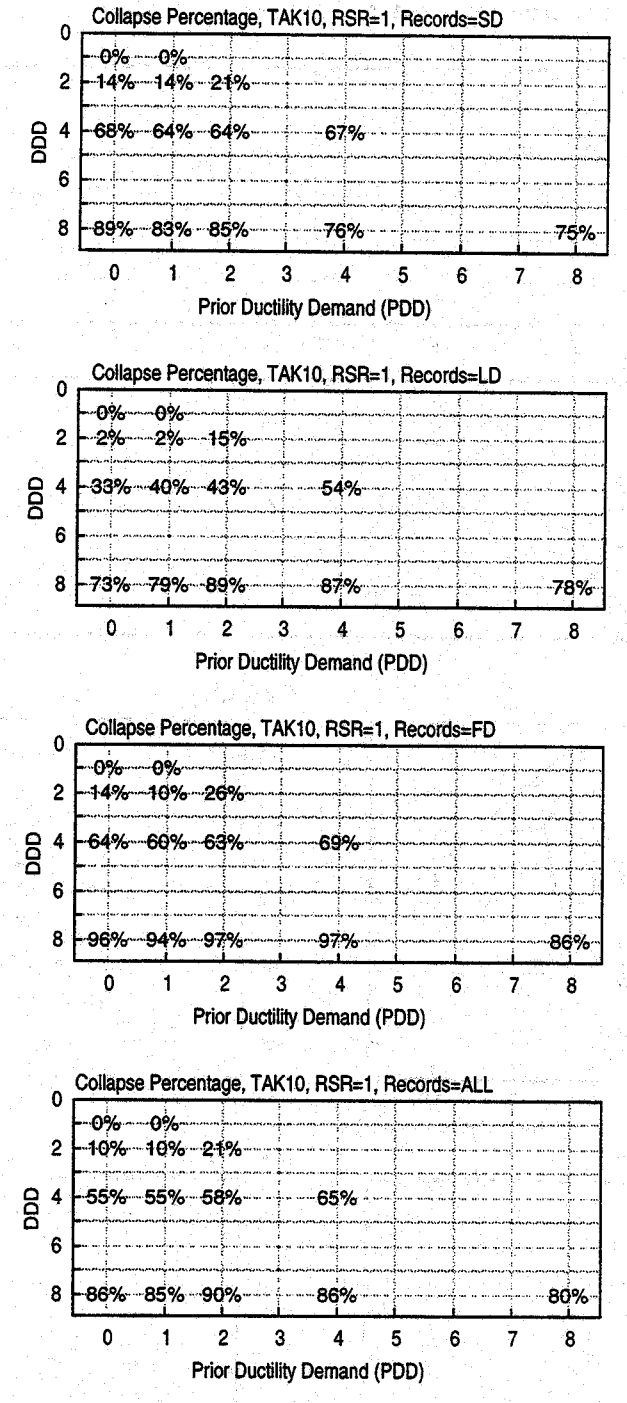

Fig. 13. Percentage of Tak10 oscillators that collapsed

Comparison of the peak displacement response of oscillators that, in many cases, did collapse, is of little value. Instead, the effect of prior damage will be gauged by the propensity of damaged and undamaged oscillators to collapse.

Figure 13 plots the percentage of Tak10 oscillators that collapsed as a function of DDD and PDD, for each ground motion category and for the entire collection of

motions. It can be observed that 73 to 96% of the undamaged DDD=8 oscillators collapsed, and 2 to 14% of the DDD=2 oscillators collapsed. This indicates the need to assure nearly elastic response in systems having negative post-yield stiffness where their collapse must be prevented. Prior ductility demand can increase or decrease the collapse percentage by relatively small amounts, but the strength level (indicated by DDD) is clearly more significant. Collapse percentages were typically larger for the SD and FD motions, and the largest collapse percentages tended to occur for the relatively weak structures (DDD= 8) subjected to the FD motions.

In Figure 11b and in Figure 12, it can be observed that while the primary Tak10 curve has a negative slope, the oscillator often unloads from and reloads towards a primary curve with positive stiffness. The observation that the SD and FD motions tended to be more damaging for a given strength (or DDD) level may reflect a tendency for these motions to have few strong pulses that cause peak response to occur predominantly by loading along the primary curve. In contrast, the LD motions may have more cycles in which the oscillator unloads from and reloads towards the primary curve, thereby spending a greater portion of its response with positive stiffness. Stiffness degrading models, which exhibit this positive stiffness even when governed by a negative post-yield primary curve, may be less prone to collapse than bilinear models for which the unloading and reloading stiffnesses remain equal to the initial stiffness.

5. Conclusions and Implications

The analytical results demonstrate that prior ductility demand has a very minor influence on peak displacement response on average. This conclusion holds across the full range of periods and ground motions investigated for SDOF oscillators exhibiting stiffness degradation, and is independent of the presence or absence of pinching of the hysteretic response. This conclusion also holds for the form of cyclic strength degradation investigated in conjunction with pinched hysteretic response. In all cases it is assumed that the prior displacement demand is less than what the undamaged structure would experience, and that residual displacements resulting from the prior demands are negligible. Small prior ductility demands caused slight reductions in peak displacement response, on average, while larger prior ductility demands caused slight increases in these means.

These results indicate that initial stiffness has little influence on peak displacement response; rather, the unloading and reloading stiffnesses at the cycles nearest the peak displacement are much more important. Initially-undamaged oscillators crack and yield in the early portions of their response, and often catch up to the response of their previously-damaged companions.

Earthquake engineering occurs in the context of substantial uncertainties and approximations, including uncertainties associated with the ground motion input, the evaluation and modeling of structural properties, analytical simplifications and approximations, and in the estimation of deformation capacities. It is in this context that most engineers would accept any of the damaged oscillator displacement histories given in Figure 4 as adequate representations of the PDD= 0 response for a known base input. Thus, prior damage is seen to exert a relatively minor influence on peak displacement response; issues relating to ground motion estimation, modeling, analysis, and capacity evaluation are likely to be of far greater significance in determining response amplitudes and their acceptability.

A significant number of collapses were computed for structures having negative post yield stiffness. Considering the entire set of ground motions, 10% of the relatively strong structures (given by DDD= 2) collapsed, while 86% of the structures having strengths corresponding to DDD= 8 collapsed. Prior damage in some cases increased and in other cases reduced the number of oscillators that collapsed. Regardless of prior damage, it is clear that these structures must remain nearly elastic if their collapse is to be prevented.

6. Acknowledgments

The response studies were partially funded by the Federal Emergency Management Agency through the Partnership for Response and Recovery, and were conducted as part of the ATC-43 project of the Applied Technology Council. The work is more fully described in FEMA publications 306-308 (1998). Any findings or recommendations expressed in this paper are those of the authors and not necessarily those of ATC or FEMA.

7. References

Borsoschek, 1991. Boroschek, R.L., *PCNSPEC Manual.*

Cecen, H., 1979. *Response of Ten Story, Reinforced Concrete Model Frames to Simulated Earthquakes*, Doctoral Thesis, Department of Civil Engineering, University of Illinois at Urbana.

FEMA-306, 1998. *Evaluation of Earthquake Damaged Concrete and Masonry Wall Buildings: Basic Procedures Manual,* Federal Emergency Management Agency, in press.

FEMA-307, 1998. *Evaluation of Earthquake Damaged Concrete and Masonry Wall Buildings: Technical Resources,* Federal Emergency Management Agency, in press.

FEMA-308, 1998. *Repair of Earthquake damaged Concrete and Masonry Wall Buildings,* Federal Emergency Management Agency, in press.

Iwan, Wilfred D., 1994. "Near-Field Considerations in Specification of Seismic Design Motions for Structures", *Proceedings of the Tenth European Conference on Earthquake Engineering*, Vienna, Austria.

Lepage, A., 1997. *A Method for Drift Control in Earthquake-Resistant Design of RC Building Structures,* Doctoral Thesis, Department of Civil Engineering, University of Illinois at Urbana.

Mahin, S.A., 1980. "Effects of Duration and Aftershocks on Inelastic Design Earthquakes," *Proceedings of the Seventh World Conference on Earthquake Engineering*, Istanbul, Vol. 5.

Otani, S., 1981. "Hysteresis Models of Reinforced Concrete for Earthquake Response Analysis," Journal (B), The Faculty of Engineering, University of Tokyo, Vol. XXXVI, No. 2, pp. 125 - 159.

Wolschlag, C., 1993. *Experimental investigation of the response of R/C structural walls subjected to static and dynamic loading*, Doctoral Thesis, Department of Civil Engineering, University of Illinois at Urbana.

Qi, X., Moehle J.P., 1991, *Displacement Design Approach for Reinforced Concrete Structures Subjected to Earthquakes*, Report No. UCB/EERC 91/02, Earthquake Engineering Research Center, University of California at Berkeley.

Saiidi, M., and Sozen, M.A., 1979. *Simple and Complex Models for Nonlinear Seismic Response of Reinforced Concrete Structures*, Structural Research Series No. 465, Civil Engineering Studies, University of Illinois, Urbana, August.

Shimazaki, K., Sozen, M.A., 1984. *Seismic Drift of Reinforced Concrete Structures*, Research report, Hasamma-Gumi Ltd, Tokyo (in Japanese), and draft research report (in English).

Somerville, P., 1997. "Engineering Characteristics of Near Fault Ground Motion", *Proceedings of the SMIP97 Seminar on Utilization of Strong Motion Data*, Strong Motion Instrumentation Program, 8 May.

Takeda, Toshikazu, Sozen, M.A., and Nielson, N., 1970. "Reinforced Concrete Response to Simulated Earthquakes," Journal of the Structural Division, American Society of Civil Engineers, Vol. 96, No. ST12, Dec. 1970.

Workshop on Structural Design Issues for Moderate Seismic Zones
February 24-25, 1998, Urbana, Illinois

SPREADING BEAM PLASTIC HINGING ZONE FOR THE DUCTILE BEHAVIOR OF HIGH-STRNGTH RC BEAM-COLUMN JOINTS USING VERTICALLY-ANCHORED INTERMEDIATE REINFORCEMENTS

W.H. Yi
Associate Professor, Dept. of Architectural Eng., Kwang Woon Univ., Seoul, Korea
L.H. Lee
Professor, Dept. of Architectural Eng., Han Yang Univ., Seoul, Korea,
Y.C. You
Senior Researcher, Building Structure and Production Div., Korea Institute of Construction Technology, Seoul, Korea

Abstract
The reinforcing details which can make beam plastic hinging zones moved and spreaded from the column face was proposed to insure the ductile behavior of high-strength (f'_c=700kg/cm^2) RC beams. Also, the optimum reinforcing range of the vertically-anchored intermediate reinforcement was investigated. Based on the test results, It was concluded that the beam plastic hinging zone can be moved and expanded in case of being reinforced by the vertically-anchored intermediate reinforcements about 1.0*d*. And energy dissipation capacity of the specimen, IV-1.0D10 which is reinforced by vertically anchored intermediate reinforcements about 1.0*d* is 1.6 times as high as the specimen CM-STAN which is designed by ACI 318-89. On the other hand, the specimen IV-0.5D10 which is reinforced by vertically anchored intermediate reinforcements about 0.5*d* shows the diagonal tension failure at the center of the moved plastic hinging zone.

1 Introduction

It is well recognized that the reinforced concrete frame building designed for code seismic forces will be stressed beyond the elastic limit during a major earthquake. The critical regions in reinforced concrete buildings, in this case, are usually the beam to column connections. Therefore, the design philosophy of "strong column-weak beam" is recommended to minimize the probability of

structural collapse or loss of structural serviceability. Design of reinforced concrete beam-column joints according to the present recommendation of ACI-ASCE Committee 352 results in the development of a beam plastic hinge at the column face (ACI318-89). A plastic hinge formed at this location usually cause the stiffness and strength deterioration in the connection.

An alternative approach of moving beam plastic hinge away from the column face is proposed to solve the beam to column connection problem (Abdel-Fattah and Wight, 1987; Al-Haddad and Wight, 1988; Bahjat and Wight, 1985; Mohammed and Wight, 1986).

This design concept can keep the beam section adjacent to the column faces essentially elastic, but relocating the beam plastic hinging zones lead to a larger rotational ductility demand in the beams. Moreover brittle shear failure can be occurred at the relocated plastic hinge because the damage is concentrated with in a narrow area. On the other hand, the reinforcing region of cut-off intermediate longitudinal reinforcements can not be quantified by the irregular bond deterioration of cut-off intermediate longitudinal reinforcements. The primary purpose of this investigation is to propose the reinforcing details which can make beam plastic hinging zones moved and spreaded from the column face using vertically anchored intermediate longitudinal reinforcements (Fig. 1). Also, the optimum reinforcing range of the vertically-anchored intermediate reinforcement is investigated.

2 Test procedures

2.1 Test specimens

Five exterior beam-column joints are manufactured and tested according to the scheduled loading history in laboratory unit. Intermediate longitudinal reinforcements consisted of four bars placed in two layers at approximately the third points between the tension and compression reinforcement.

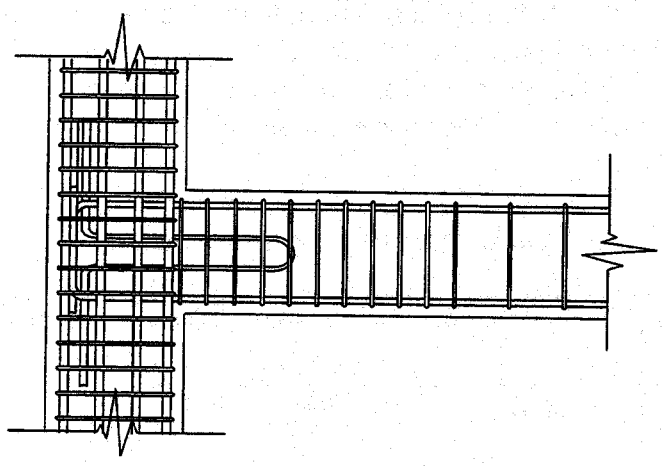

Fig. 1. Vertically-anchored intermediate longitudinal reinforcement

The specimen named 'CM-STAN' is reinforced by the Conventional Method and selected as a STANdard specimen. The specimen 'IC-1.5D10' is reinforced by the cut-off Intermediate reinforcements which is Conventional in reinforcing beam plastic hinge about 1.5D from the column face. Also, the specimen 'IV-0.5D10', 'IV-1.0D10' and 'IV-1.5D10' are reinforced by Intermediate reinforcements which were Vertically-anchored and placed 0.5d, 1.0d and 1.5d region from column face, respectively. All specimens are designed by ACI 318-89 Code. The details and dimension of the representative specimens are shown in Fig. 2. and Table 1.

Table 1. Specimen list

Specimen	b x D (cm)	Flexural Reinforcement A_s, (cm^2)	Flexural reinforcement ratio ρ (%)	Intermediate reinforcement A_i (cm)	Intermediate reinforcement			Stirrup diameter & spacing (cm)
					hook	length	A_i / A_s	
CM-STAN	20 x 35	4-D16	1.06	-	-	-	-	φ 6-@65
IC-1.5D10	20 x 35	4-D16	1.06	2-D10	Cut-off	1.5d	0.18	φ 6-@55
IV-0.5D10	20 x 35	4-D16	1.06	2-D10	Vertical	0.5d	0.18	φ 6-@55
IV-1.0D10	20 x 35	4-D16	1.06	2-D10	Vertical	1.0d	0.18	φ 6-@55
IV-1.5D10	20 x 35	4-D16	1.06	2-D10	Vertical	1.5d	0.18	φ 6-@55

f_y = Yield strength of flexural reinforcement (4000 kg/cm^2)
f_{yi} = Yield strength of intermediate reinforcement (4000 kg/cm^2)
f_{ys} = Yield strength of shear reinforcement (4000 kg/cm^2)
f'_c = Compressive strength (700 kg/cm^2)
Dimension of column section : 40 x 40 cm

2.2 Material

Concrete, with 13 mm nominal maximum size aggregate, is obtained from local ready-mixed plant. Compression cylinders measuring 10×15 cm are prepared for each beam. Concrete strengths are listed in Table 3. The flexural reinforcements for the beams consist of No. 4 ASTM A615 Grade 60 deformed bars. The longitudinal reinforcements for the column-stub consist of No. 5 deformed bars. Column ties and Hoops are made of No 1. (6 mm) deformed bars.

Table 2. Tensile test of the reinforcements

Type	Elastic modulus (t/cm^2)	Yield strength (t/cm^2)	Yield strain ($x10^{-6}$)	Tensile strength (t/cm^2)	Elongation (%)
HD19	2117	4.12	1946	6.70	21.0
HD16	1987	4.09	2058	6.45	19.8
HD10	1928	3.87	2007	5.75	21.4
HD6	1807	4.38	2420	5.70	15.3

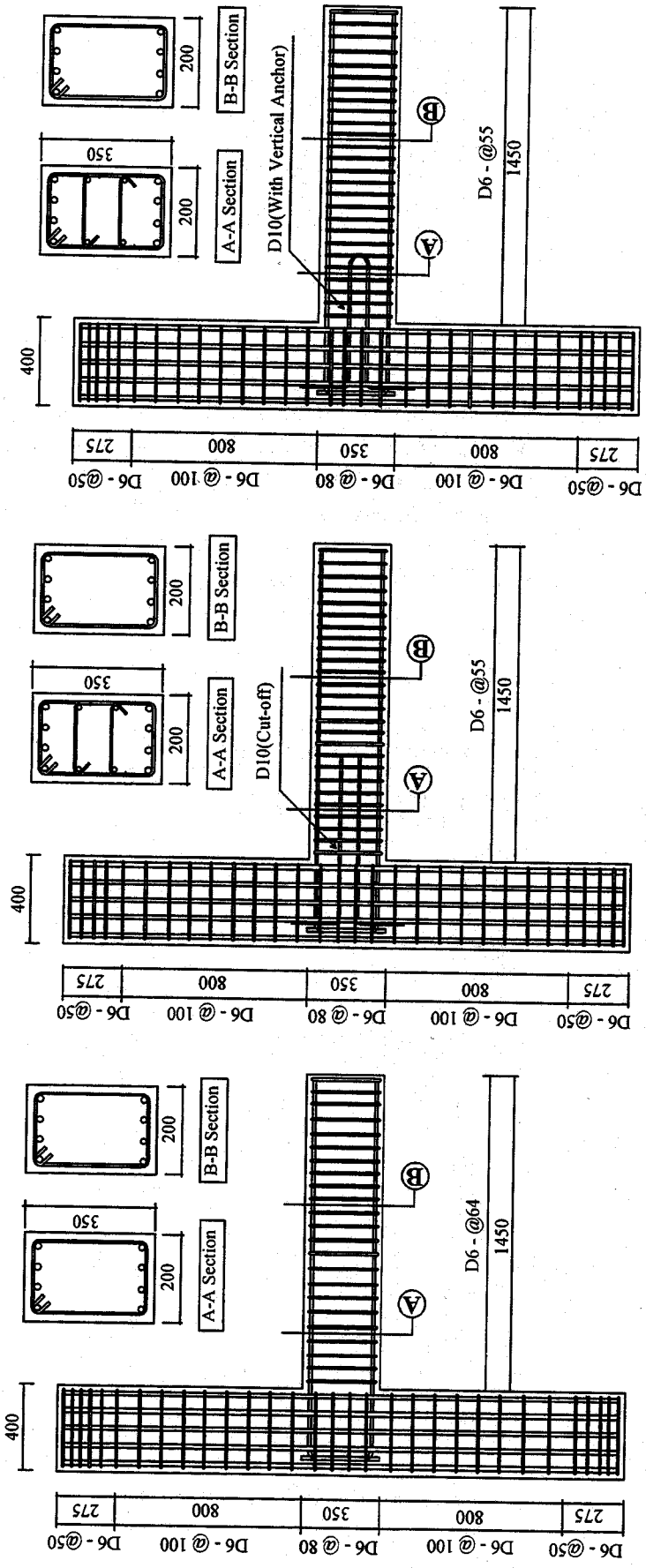

(a) CM-STAN (b) IC-1.5D10 (c) IV-1.0D10

Fig. 2 Detail and dimension of test specimens

Table 3. Compressive test of the concrete

Compressive strength (kg/cm^2)			Height	Area	Elastic modulus	Slump
7	14	28	(cm)	(cm^2)	(t/cm^2)	(cm)
610	620	710	20.2	78.6	217	21.4

2.3 Test set-up

The specimens are held vertically in a steel frame with pin supports near the end of the beam and column during testing (Fig. 3). The actuator is attached to a steel frame prestressed to the structural floor of the laboratory. Electrical resistance strain gages are bonded to the longitudinal reinforcement and to stirrups placed within a distance equal to the beam depth from the column face. Linear variable displacement transformers (LVDTs) are used to measure the beam deflection at a distance of 1.2 m from the column face and the shear deformation over three regions, $0.5d$ adjacent to the column face, $0.5d \sim 1.0d$ and $1.0d \sim 2.0d$.

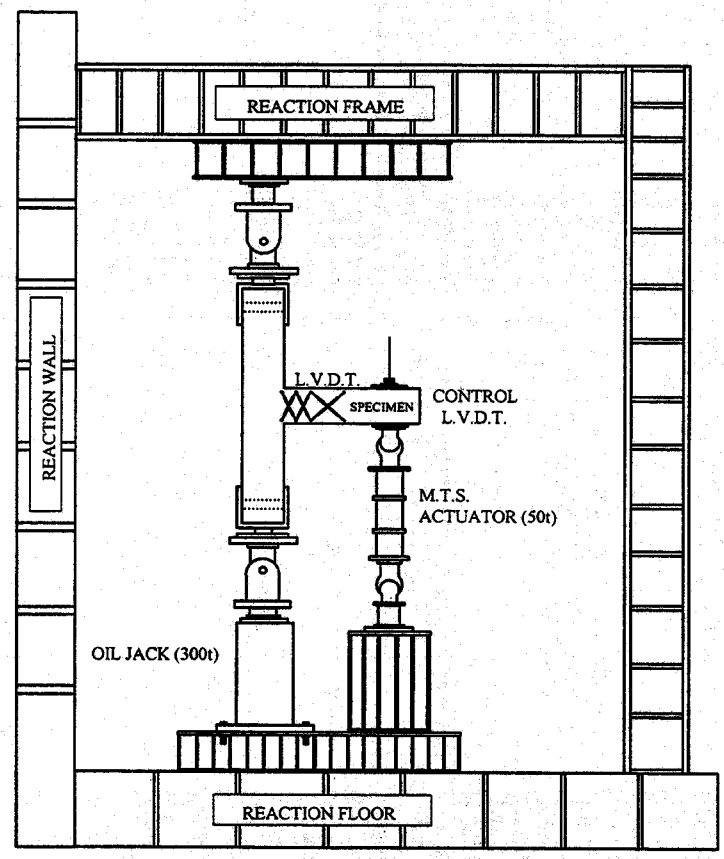

Fig. 3. Schematic drawing of the testing frame

2.4 Test procedure

The constant axial force corresponding to $0.2f'_c$ (192 ton) is applied at the column prior to the hysteretic beam loading. Load is applied using a 50 ton servo-hydraulic actuator under displacement control.

The beam is, first, loaded upward (positive bending) slightly beyond the yield strain of the longitudinal reinforcement. The yield displacement, δ_y, is set when the flexural reinforcement reaches its yield strain. The direction of loading is then reversed. The loading history scheduled is shown in Fig. 4. Test is proceeded until the maximum cycle load, P_n, drop 75% of its yield load P_y, which is defined as the collapse load (Hwang and Scribner, 1984; Darwin and Nmai, 1986) .

3 Test results

3.1 Load-displacement curve

Each specimen undergoes the same loading history. The load-deflection curve of specimen 'CM-STAN' showed the drastic strength deterioration after 12 cycle ($6\delta_y$) and it was finally collapsed at 14 cycle due to the shear fracture of the core concrete. That of the specimen 'IC-1.5D10', also showed the strength deterioration after 13 cycle but less serious than specimen 'CM-STAN' and finally it was collapsed at 16 cycle as the intermediate reinforcement is being buckled.

The load-displacement curve of the specimen 'IV-0.5D10' shows the abrupt strength deterioration with the diagonal tension failure occurred at 0.5d from the column face after 9 cycle. On the other hand, that of specimen 'IV-1.0D10' showed sustained load-carrying capacity up to the final failure cycles with the stable hysteretic loops. It is originated by the fact that the intermediate longitudinal reinforcement was to inhibit opening of crack in the beam hinging zone, promoting a more uniform distribution of cracking of concrete and preventing localized failure. Therefore, the beam plastic hinging zone of the specimen 'IV-1.0D10' is moved and spreaded by rein- forcing the vertically anchored intermediate longitudinal reinforcements over the 1.0*d* region from the column face.

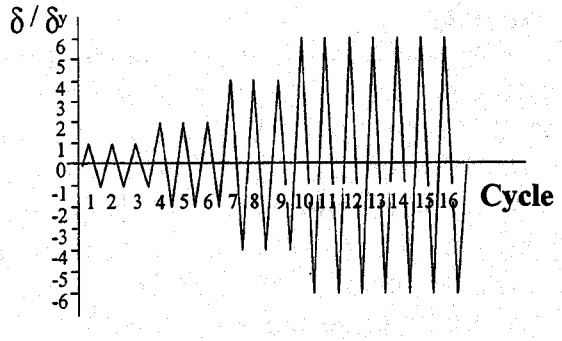

Fig. 4. Loading history

3.2 Cracking pattern up to failure and shear deformation of plastic hinge

Fig. 6 shows the cracking pattern of each specimen up to failure and Fig. 7 shows the relationships between the maximum shear deformation at each load cycle. The shear deformation of three regions (column face~0.5*d*, 0.5*d*~1.0*d*, 1.0*d*~2.0*d*) adjacent to the column face is measured by the six LVDTs attached to the beam plastic hinging zone. The failure of specimen CM-STAN was initiated by the spalling of the cover concrete and finally collapsed by the diagonal shear fracture of the core concrete at 0.5*d* from the column face. And the magnitude of shear deformation at D_1 (0.5*d*) region is much greater than that of D_2 (0.5*d*~1.0*d*) and D_3 (1.0*d*~2.0*d*) as shown in Fig. 7. Also the spalling of the cover concrete at 0.5*d* caused the failure of specimen IC-1.5D10. However the severe fracture of the core concrete was not observed up to 13 cycle, and finally it was collapsed as the cut-off intermediate longitudinal reinforcements was being buckled. Such delayed failure mode can be observed in the relationships between shear deformation and load cycle at each region, but its relative magnitude of shear deformation at each region is similar to that of specimen CM-STAN. In this manner, the spalling of the cover concrete at 0.5*d* caused the failure of specimen IV-0.5D10 and the concentrated damage was found at the 0.5*d* from the column face with drastic strength deterioration after 10 cycle. And finally it was collapsed by the fracture of the transverse reinforcements at 13 cycle.

On the other hand, the failure of specimen IV-1.0D10 was initiated at 1.0*d* from the column face and propagated to the column face. Finally a dispersed cracking pattern was found. Also the magnitude of shear deformation at D_1 (0.5*d*) region is similar to that of shear deformation at D_2 (0.5*d*~1.0*d*). Moreover the shear deformation of specimen IV-1.0D10 at D_1 (0.5*d*) region is reduced compared with that of specimen CM-STAN and IC-1.5D10 about 60 percents. It is originally based on the fact that the shear resistance capacity of specimen IV-1.0D10 is increased by the additional confining effects of the core concrete and dowel action provided by the intermediate longitudinal reinforcement. The increased shear resistance capacity made the beam plastic hinging zone spread, lead to the decreased rotational ductility demand of a beam. The failure mode of specimen IV-1.5D10 is similar to that of specimen IV-1.0D10, but the plastic hinging region is reduced about 0.7*d*.

3.3 Energy dissipation capacity

The dissipated energy '*E*' of test specimens is calculated for each cycles of which the peak load P_n is greater than 75 percent of the initial yield load P_y. The energy dissipation capacity of specimen 'IV-1.0D10', which is reinforced by vertically anchored intermediate longitudinal reinforcements about 1.0*d* is 1.6 times as high as that of the specimen 'CM-STAN' which is designed according to ACI 318-89. Also the energy dissipation capacity of specimen 'IV-1.0D10' is 1.4 times as high as that of the specimen 'IC-1.5D10', which is additionally reinforced by cut-off intermediate longitudinal reinforcements.

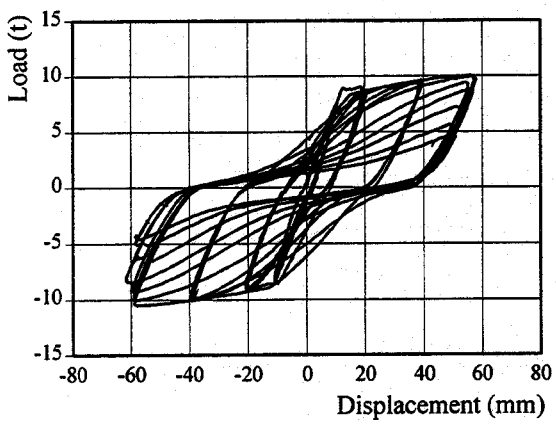

(a) CM-STAN

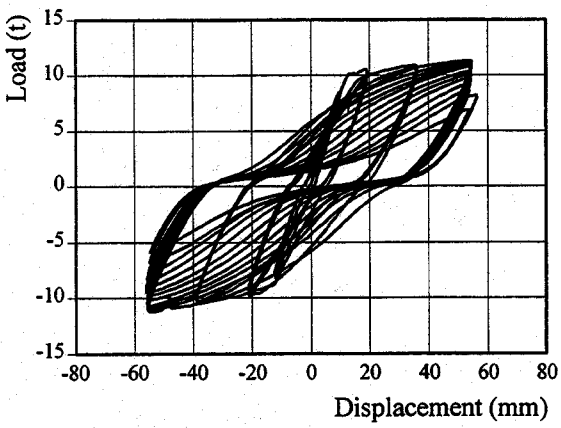

(d) IV-1.0D10

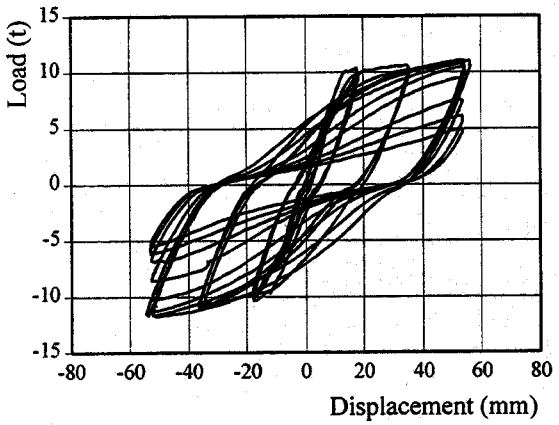

(b) IC-1.5D10

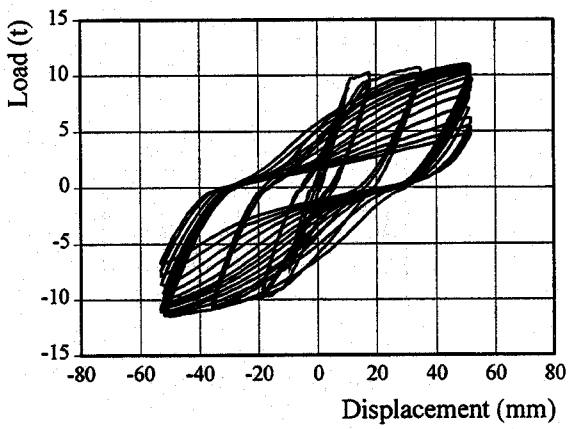

(e) IV-1.5D10

Fig. 5. Load-displacement curve

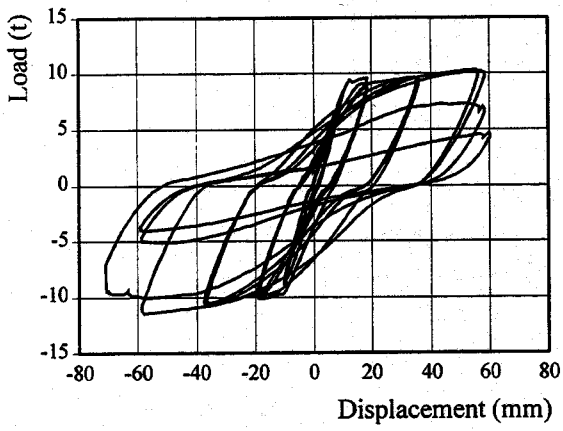

(c) IV-0.5D10

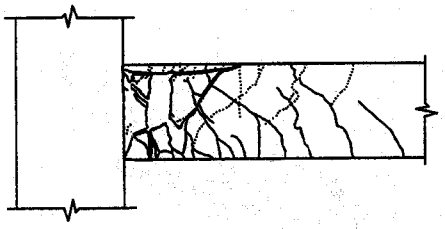

(a) CM-STAN

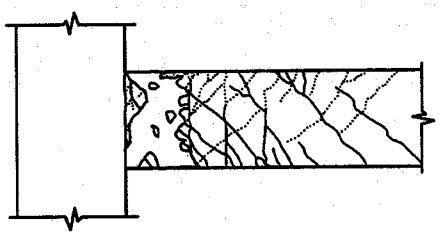

(b) IC-1.5D10

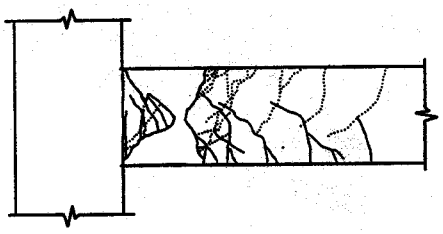

(c) IV-0.5D10

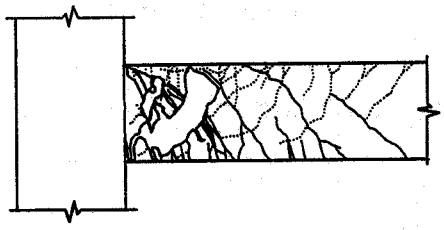

(d) IV-1.0D10

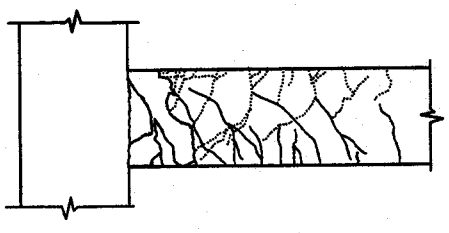

(e) IV-1.5D10

Fig. 6. Cracking pattern at failure

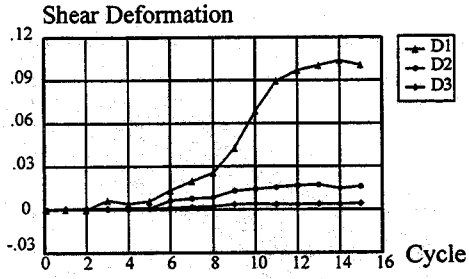

(a) CM-STAN

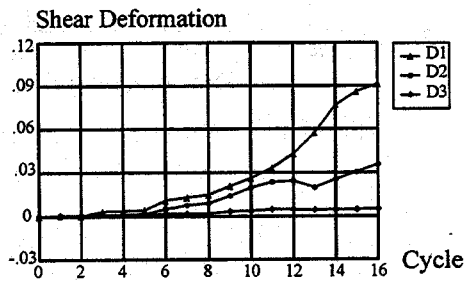

(b) IC-1.5D10

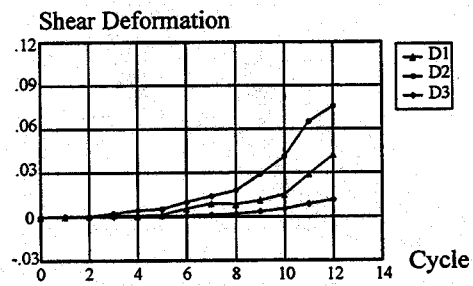

(c) IV-0.5D10

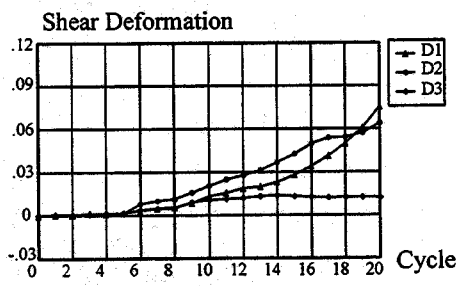

(d) IV-1.0D10

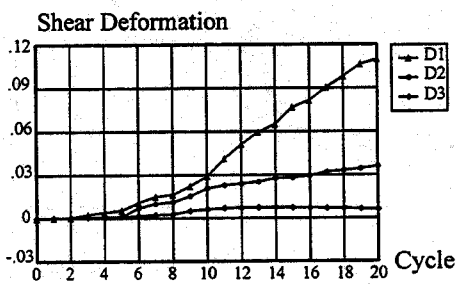

(e) IV-1.5D10

Fig. 7. Shear deformation vs. load cycle

Table 4. Test results

Specimen	Yield load P_y(t)		Maximum Load P_m(t)		Yield displacement Δ_y (cm)		Maximum displacement Δ_m (cm)		Cycle (n)			Dissipated energy (t cm)
									$P_n>0.75P_y$		Total	
	+	-	+	-	+	-	+	-	+	-		
CM-STAN	7.33	8.30	10.07	10.45	0.99	1.09	5.80	6.14	14	13	15	565.5
IC-1.5D10	7.31	6.94	10.84	11.62	0.91	0.87	5.60	5.28	15	15	16	677.4
IV-0.5D10	7.70	8.83	10.11	11.19	0.94	1.02	6.01	5.86	11	10	12	472.1
IV-1.0D10	8.37	7.95	11.25	10.92	0.95	1.21	5.62	5.59	20	19	20	898.8
IV-1.5D10	8.44	6.90	10.92	11.32	0.97	0.91	5.23	5.29	18	20	20	840.4

4 Conclusions

Five reinforced concrete cantilevers beam specimens were constructed and tested to study the effects of the vertically anchored intermediate longitudinal reinforcement in moving and spreading beam plastic hinging zone away from the column face. Based on the results of these tests, the following conclusions can be drawn.

The beam plastic hinging zone can be moved and spreaded in case of being reinforced by the vertically-anchored intermediate reinforcements about 1.0*d*.

The energy dissipation capacity of specimen IV-1.0D10 is the most excellent; the energy dissipation capacity of specimen IV-1.0D10, which is reinforced by adding vertically anchored intermediate longitudinal reinforcements about 1.0*d* is 1.6 times as high as that of the specimen CM-STAN, which is designed according to ACI 318-89.

From the load-displacement curve and failure mode, the optimum reinforcing range of the vertically-anchored intermediate reinforcement is 1.0*d* from the column face.

5 Acknowledgement

The reported research was supported by the Korea Science and Engineering Foundation under Grant No. KOSEF92-29-00-13 and STRESS. These supports are greatly acknowledged.

6 References

ACI Committee 318. (1989) **Building Code Requirements for Structural Concrete(ACI 318-89) and Commentary.**

Abdel-Fattah, B.A. and Wight, J.K. (1987) Study of Moving Beam Plastic Hinging Zones for Earthquake Resisting Design of R/C Buildings. **ACI Structural Journal**, 84, Jan-Feb., 31～39.

Al-Haddad, M.S. and Wight, J.K. (1988) Relocating Beam Plastic Hinging Zones for Earthquake Resisting Design of Reinforced Concrete Buildings. **ACI Structural Journal**, 86, March-April, 123～133.

Bahjat, A.A. and Wight, J.K. (1985) **Experimental Study of Moving Beam Plastic Hinging Zones for Earthquake Design of R/C Building**. Report No. UMCE 85-11, Department of Civil Engineering, The University of Michigan, December.

Mohammed, S.A. and Wight, J.K. (1986) **Feasibility and Consequence of Moving Beam Plastic Hinging Zones for Earthquake Resistant Design of R/C Buildings**. Report No. UMCE 86-1, Department of Civil Engineering, The University of Michigan, 48109, July.

Hwang, T.H. and Scribner, C.F. (1984) R/C Member Cyclic Response During Various Loadings. **Journal of Structural Engineering**, ASCE, 110, No. 3, Mar., 477～489

Darwin, D., and Nmai, C.K., (1986) Energy Dissipation in RC Beams Under Cyclic Load. **Journal of the Struc. Div.**, ASCE, 83, Aug., 1829～1846.

Workshop on Structural Design Issues for Moderate Seismic Zone
Feburary 24-25, 1998, Urbana, Illinois

COMPUTATIONAL METHODOLOGY AND DESIGN EQUATION FOR ULTIMATE STRESS OF UNBONDED TENDON

J-H Moon
Department of Architectural Engineering, Hannam University
Taejon, Korea 306-791

J-H Lim
director ALT structural research group
51 SamSung-Dong KangNam-Gu, seoul, Korea 135-090

L-H Lee
advanced STructure RESearch Station, Hanyang University
Seoul, Korea 133-791

ABSTRACT

The present study is the first phase of research with the subject of the application of unbonded tendons to structures. It describes the computational method of the unbonded tendon stress at the flexural failure of the member containing unbonded tendons. The previous design equations, first, were examined in order to find whether any modifications are needed. The previous experimental results were used to examine ACI and AASHTO Code equations as well as other proposed equations. Then, a new design equation was proposed with the consideration of the plastic hinging zone and the global compatibility requirement. Main parameters and their combination were obtained from the theoretical study and then the coefficients for them were found by the regression with test data. The purpose equation showed a good agreement with previous test data.

1. INTRODUCTION

The behavior of the members with unbonded tendon is different from that of the members with bonded tendon. For the members with bonded tendon, equilibrium and compatibility equations can be applied assuming that tendon and concrete behave as a body since they are completely bonded in the member. For the members with unbonded tendon, however, tendon and concrete deform independently except at the ends of the member. Therefore, the analysis must be based on the global compatibility rather than on the local compatibility. The local compatibility means that tendon and concrete elongate equally at a given section of the member. The global compatibility means that, along the location of the tendon, the overall elongation of the concrete equals to the total lengthening of the tendon.

Many researches have been carried out as to the members with unbonded tendon, on the basis of which various design equations such as ACI code have been proposed so far. But it is hard to say that global compatibility is fully considered in the existing codes that have been proposed or put into use. Furthermore, those design equations are often based on the very limited parameters and experiments, and they also generalize the data derived from limited parameters of one or two.

The purpose of this study is to perform a comprehensive analysis of the problems mentioned above employing the existing experimental results, and to develop a new design equation using the equilibrium condition, the characteristics of the materials, and the global compatibility. A newly proposed equation will be developed while examining the experimental results of the existing tests in such a way that the coefficients of the parameters used in the design equation be found by the regression method using the test results. In other words, main parameters and their combination will be obtained from the theoretical study and the coefficients for the parameters will be found by the regression.

Finally it has to be mentioned that this is the first phase of continuous researches with the subject of the unbonded tendon. Since the first phase of research was completed, authors are planning continuous research programs for the application of unbonded tendon to the beam-column connection and the wall horizontal connection at seismic zone.

2. EVALUATION OF PREVIOUS DESIGN EQUATIONS

Although much effort for the computational method of unbonded tendon stress has been devoted for the last four decades, it is still in question if any

methods proposed previously are general and consistent at all. To solve the problem, Naaman and Alkhairi[10,11] recently carried out a comprehensive study about the existing code equations and many of proposed design equations. They gathered virtually all the experimental data obtained for more than four decades. Then, they proposed a design equation based on the comparative study with the previous design equations and the experimental results. However, their propose equation needs further research mostly due to complexity. Since then, many researchers have proposed new design equations to provide a general and consistent computation method.

In this study, thus, existing design equations as well as the ACI 318-95 equation were examined before proposing a design equation of authors. The ACI code equation[3] is written as

$$f_{ps} = f_{se} + 10{,}000 + \frac{f_c'}{k\rho_p} \text{ psi} \tag{1}$$

but

$$f_{ps} \le f_{se} + C, \text{ and } f_{py} \text{ psi}$$

in which k=100 and C=60,000 for $L/d_p < 35$, and k=300, C=40,000 for $L/d_p > 35$, where L is the span and d_p is the depth from the extreme compression fiber to the center of the prestressing steel.

Naaman and Alkhairi's design equation[4,10,11] uses the bond reduction factor Ω_u to calculate the average strain of the concrete strain along the tendon profile. The cross sectional equilibrium equation, then, is written in terms of the neutral axis depth which is formulated with the bond reduction factor. It has an advantage that the last of computational processes can be identical to the member containing bonded tendons. In consequence, the design equation is written in a simple form as

$$f_{ps} = f_{se} + \Omega_u E_{ps} \varepsilon_{cu} \left(d_{ps}/c - 1\right) L_1/L_2 \tag{2}$$

but

$$f_{ps} \le 0.94 f_{py} \text{ psi}$$

Their proposed equation was compared with experimental results and a good agreement was obtained. Later, the equation was adopted in the AASHTO LRFD Code[1].

Harajili and Kanj[7] proposed an equation written as

$$f_{ps} = f_{se} + \gamma_o f_{pu}[1.0 - 3.0\omega] \le f_{py} \quad (3a)$$

$$\omega = \rho_{ps}\frac{f_{se}}{f_c'} + \rho_s\frac{f_y}{f_c'}\frac{d_s}{d_p} \quad (3b)$$

$$\gamma_o = (n_0/n_1)\left[0.12 + 2.5/(L/d_p)\right] \quad (3c)$$

in which ρ_{ps} and ρ_s are prestressing and reinforcing ratios, respectively; n_0 is length of tendons between the anchorage ends; n_1 is length of loaded span(s). The proposed equation includes various influential parameters such as the partially prestressing ratio, the span-depth ration(L/d_p), and the pattern loading (n_0/n_1).

Chakrabarti tested thirty-three beams posttensioned with unbonded tendons. Then, a design equation was suggested for computing the design ultimate stress.

$$f_{ps} = f_{se} + k\left[\frac{f_{se} + 10{,}000 + A}{1 - B} - f_{se}\right] \le f_{se} + C, \text{ and } f_{py} \text{ psi} \quad (4a)$$

$$A = (f_c'/100\rho_s)\cdot(d_p/d_s)(60{,}000/f_y)\cdot(1 + \rho_s/0.25) < 20{,}000 \text{ psi} \quad (4b)$$

$$B = r f_c'/(100\rho_s)\cdot f_{se} < 0.25 \quad (4c)$$

in which

$$k=1.0,\ r=1.0, \text{ and } C=60{,}000 \text{ for } L/d_p \le 33; \quad (4d)$$

$$k=0.65,\ r=0.8, \text{ and } C=40{,}000 \text{ for } L/d_p > 33 \quad (4e)$$

In this study, a similar body of experimental results as those of Naaman and Alkhairi was used to analyze the above design equations. The statistical distributions obtained from the competitive analysis are illustrated in Fig. 1. The stress increases of unbonded tendon Δf_{ps} are compared with the experimental results. The correlation coefficients for each equation is shown in Table 1.

Table 1 Comparison of Correlation coefficient R

Design equation	ACI	AASHTO	Harajili/Kanj	Chakrabarti
Correlation coefficient	0.64	0.71	0.55	0.64

As indicated in Fig. 1, Δf_{ps} by the ACI code is conservative about the experimental results. Naaman and Alkhairi mentioned from their study that the values obtained by ACI equation were deviated far from the experimental values. It seems to be the reason because the ACI equation takes only f_{se}, ρ_p, and f_c' into account without considering amount of bonded reinforcements and loading type which can influence significantly on the stress of unbonded tendon. In addition, the span/depth ratio is considered rather empirically than logically. Authors had already carried out a experimental program on this subject and it was proven that the effect of the span/depth ratio be reconsidered in the ACI code in future.

On the other hand, the AASHTO LRFD is regarded to be comparatively nice since it contains the parameters such as the depth of stress block at a section and the loading type. As the depth of stress block is influenced by the amount of the tendons and amount of reinforcements, it is reasonable to include the amount of reinforcements as an important parameter. This equation, however, is somewhat complex for the design purpose because the neutral axis depth should be computed in advance. It means that the procedure is lengthy because a quadratic equation has to be solved to compute the tendon stress.

The results by the equation of Harajli and kanj show that the degree of the scatter is high and the correlation coefficient R is smaller than the result by the ACI code. The reason seems to be that the parameter on the loading type is not taken into consideration while the parameters on the span/depth ratio $\left(L/d_p\right)$ and on the amount of reinforcements are taken into consideration.

It is not clear how the coefficients in the equation by Chakrabarti were determined. For example, the limit of span-depth ratio is ambiguously 33 in contrast to ACI Code equation. Also, Eq. 4e uses the ratio of 0.65 to take into account the effect of high span-depth ratio. Further, it is hard to forecast the effects of many variables with the equation. For example, ρ_s and f_{se} are used in the denominator and the numerator simultaneously. Thus, designers may hardly expect their effects when an adjustment in prestressing force has to be made during the design stage.

From the previous studies so far, it was concluded that important variables on the stress of unbonded tendon are those of effective, area tendon, concrete strength, amount of reinforcements, span/depth ratio and loading type. The design equations can be classified into two groups such as theoretical and empirical. Eq. 1 and 4 are categorized as the empirical equation while Eq. 2 and 3 can be said as partially theoretical. Although it is not easy to determine which type of equation is better than the other, it is desirable if the design equation can be explained with any theoretical backgrounds. In this study, thus, a theoretical approach was used to derive a new design equation with using the analytical

method which is usually called as 'the strain compatibility method' by Naaman and Harajili. However, further developments of the strain compatibility method were made to consider geometrical locations of tendons and bonded reinforcements.

3. THEORETICAL SOLUTION

The theoretical approach begins with three basic requirements of an equilibrium equation, a constitutive equation, and a compatibility equation. The requirements were set up considering a flexural failure state of a member. Naaman and Harajili derived an equilibrium equation in terms of cross sectional forces. In this study, however, a moment equilibrium equation was derived to take into account geometrical locations of tendons and bonded reinforcements. (see Fig. 2) Thus, the equilibrium equation is written as

$$0.85f_c'b\beta_1c(d_e-\beta_1c/2) = A_{ps}f_{ps}(d_p-\beta_1c/2) + A_sf_y(d_s-\beta_1c/2) - A_s'f_y(d_e-\beta_1c/2) \quad (5a)$$

where

$$d_e = \frac{A_{ps}f_{ps}d_p + A_sf_yd_s}{A_{ps}f_{ps} + A_sf_y} \quad (5b)$$

The global compatibility requirement was applied assuming that the strain increase in the unbonded tendon is the same at any section along the span. Thus, the frictional effects were ignored. The strain of unbonded tendon will be the average value that is computed from the idealized curvature distribution shown in Fig. 3. Thus, the stress of unbonded tendon is

$$\varepsilon_{ps} = \varepsilon_{se} + \left[\varepsilon_{cu}\frac{d_p - c}{c}\right]*(L_o/L) \quad (6)$$

in which L_o is the equivalent plastic hinge length, and L is the total length between anchorages. Then, the neutral axis depth is obtained as

$$c = \frac{\left(\frac{L_o}{L}\right)\varepsilon_{cu} d_p}{\varepsilon_{ps} - \varepsilon_{se} + \left(\frac{L_o}{L}\right)\varepsilon_{cu}} \tag{7}$$

From Eq. 5a and 7, the ultimate stress of unbonded tendon f_{ps} is computed as

$$f_{ps} = \frac{1}{\alpha_p A_{ps}} \frac{0.85 f_c' b \beta_1 \varepsilon_{cu} (L_o/L) d_p}{\varepsilon_{ps} - \varepsilon_{se} + \varepsilon_{cu}(L_o/L)} + \frac{(A_s' - \alpha_s A_s) f_y}{\alpha_p A_{ps}} \tag{8a}$$

where

$$\alpha_p = (d_p - \beta_1 c/2)/(d_e - \beta_1 c/2) \tag{8b}$$

$$\alpha_s = (d_s - \beta_1 c/2)/(d_e - \beta_1 c/2) \tag{8c}$$

The equivalent plastic hinge length L_o can be obtained as shown in Fig. 3.

$$L_o = \frac{L}{f} + 2L_p \tag{9}$$

in which f is the coefficient with regard to the loading type. It can be determined from Harajli, Naaman and Alkhairi, or previous experimental results. If there is 1-point loading, f=10, and if 2-point loading or uniform loading, then f=3. Assuming $L_p = 0.5 d_p$, the plastic hinge length ratio is determined as

$$\frac{L_o}{L} = \frac{1}{f} + \frac{1}{L/d_p} \tag{10}$$

It is important to know that the span/depth ratio L/d_p is the function of the plastic hinge length ratio which can affect the stress increase of unbonded tendon significantly. Although ACI code also takes into account the span/depth ratio, it has to be considered together with the loading type. It is due to the fact that the effect of span/depth ratio is important in case of 1-point loading while it is trivial in case of uniform loading or 2-point loading. For example, fig. 4 shows that the effect of span/depth ratio is minimal in comparison with the effect of loading condition for the case of the uniform loading.

The material property of tendon was modeled with the following constitutive equation of Monegatto and Pinto.

$$f_{ps} = E_{ps}\varepsilon_{ps}\left\{Q + (1-Q)/\sqrt[n]{1+P}\right\}$$
$$P = \left[E_{ps}\varepsilon_{ps} / (kf_{py})\right]^n \qquad (11)$$

With the above three requirements, an iterative computational method, called strain compatibility analysis, can be done to get the unbonded tendon stress. Then, the analysis were compared with the Δf_{ps} of the previous experiments in Fig. 5. The correlation coefficient R=0.78 from the strain compatibility method was the most accurate value compared with the other design equations. Therefore the strain compatibility method was proven to be an appropriate approach. In consequence, a design equation was derived using the concept of the strain compatibility method.

4. PROPOSED DESIGN EQUATION

In order to propose an equation which makes possible a simple computation while preserving the accuracy of the strain compatibility method, it was assumed that the unbonded tendon behaves elastically. Most of previous experiments showed that the unbonded tendon did not develop the nonlinear strain even at the failure of the member. It is because the tendon stresses are distributed all through the member length. Thus it is hardly probable that the tendon develops the nonlinear strain because there is no concentration of strain. Thus, the constitutive equation can be simple as

$$f_{ps} = E_{ps}\varepsilon_{ps} \qquad (12)$$

However, the other requirements of equilibrium and compatibility are not modified.

By multiplying E_{ps} to the denominator and the numerator of first term of right hand side of Eq. 8a,

$$f_{ps} = \frac{1}{\alpha_p A_{ps}} \frac{0.85 f_c' b \beta_1 \varepsilon_{cu} E_{ps} (L_o/L) d_p}{f_{ps} - f_{se} + \varepsilon_{cu} E_{ps} (L_o/L)} + \frac{(A_s' - \alpha_s A_s) f_y}{\alpha_p A_{ps}} \qquad (13)$$

Adding $-f_{se} + \varepsilon_{cu}(L_o/L)$ to both sides, it can be written in terms of Δf_{ps} as

$$\Delta f_{ps} + \varepsilon_{cu} E_{ps} (L_o/L) = \frac{1}{\alpha_p A_{ps}} \frac{0.85 f_c' b \beta_1 \varepsilon_{cu} E_{ps} (L_o/L) d_p}{\Delta f_{ps} + \varepsilon_{cu} E_{ps} (L_o/L)} + \frac{(A_s' - \alpha_s A_s) f_y}{\alpha_p A_{ps}} - f_{se} + \varepsilon_{cu} E_{ps} (L_o/L) \quad (14)$$

To get Δf_{ps} through (14), a quadratic equation is written as

$$X^2 - 2BX - C = 0 \quad (15a)$$

in which

$$X = \Delta f_{ps} + \varepsilon_{cu} E_{ps} (L_o/L) \quad (15b)$$

$$2B = \frac{(A_s' - \alpha_s A_s) f_y}{\alpha_p A_{ps}} - f_{se} + \varepsilon_{cu} E_{ps} (L_o/L) \quad (15c)$$

$$C = \frac{0.85 f_c' b \beta_1 \varepsilon_{cu} E_{ps} (L_o/L) d_p}{\alpha_p A_{ps}} \quad (15d)$$

The solution of the quadratic equation is

$$X = B + B\sqrt{1 + (\sqrt{C}/B)^2} \quad (16)$$

Assuming $\sqrt{1 + (\sqrt{C}/B)^2} \approx 1 + \frac{1}{2}\frac{\sqrt{C}}{B}$ (17)

$$X = 2B + \sqrt{C}/2 \quad (18)$$

Although Eq. 18 can be solved directly, the result may not be accurate because of the approximation by Eq. 17. Thus, the coefficients of the equation were replaced by arbitrary constants Q1, Q2, and Q3.

$$\Delta f_{ps} = -Q_1 f_{se} + Q_2 \frac{(A_s' - \alpha_s A_s) f_y}{\alpha_p A_{ps}} + Q_3 \varepsilon_{cu} E_{ps} (L_o/L) + Q_4 \sqrt{\frac{0.85\beta_1 \varepsilon_{cu} E_{ps} (L_o/L) f_c'}{\alpha_p \rho_p}} \quad (19)$$

The third and fourth terms of the equation (19) share the same parameters so that it can be written as follows.

$$\Delta f_{ps} = -Q_1 f_{se} + Q_2 \frac{(A_s' - \alpha_s A_s) f_y}{\alpha_p A_{ps}} + \sqrt{\frac{f_c'}{\alpha_p \rho_p} (L_o/L)} * \left[-Q_3 \varepsilon_{cu} E_{ps} \frac{\sqrt{(L_o/L)}}{\sqrt{f_c'/(\alpha_p \rho_p)}} + Q_4 \sqrt{0.85\beta_1 \varepsilon_{cu} E_{ps}} \right] \quad (20)$$

In the first term inside [ ] of (20), L_o/L is less than 1 and the denominator is comparatively high. Thus the term can be neglected. By replacing L_0/L with Eq. 10, then, f_{ps} can be generalized as follows with new coefficients K_1, K_2, K_3, and K_4.

$$f_{ps} = K_1 + K_2 f_{se} + K_3 \frac{(A_s' - A_s) f_y}{A_{ps}} + K_4 \sqrt{\frac{d_s}{d_p} \frac{f_c'}{\rho_p} \left[\frac{1}{f} + \frac{1}{L/d_p} \right]} \quad (21)$$

By regression analysis with test data, the coefficients were determined as

$$f_{ps} = 30{,}000 + 0.75 f_{se} + \frac{1}{12} \frac{(A_s' - A_s) f_y}{A_{ps}} + 82 \sqrt{\frac{d_s}{d_p} \frac{f_c'}{\rho_p} \left[\frac{1}{f} + \frac{1}{L/d_p} \right]} \text{ psi} \quad (22)$$

Then, a design equation was derived while considering safety factor. With additional regression analysis, a new design equation was obtained as

$$f_{ps} = 10{,}000 + 0.8 f_{se} + \frac{1}{15} \frac{(A_s' - A_s) f_y}{A_{ps}} + 80 \sqrt{\frac{d_s}{d_p} \frac{f_c'}{\rho_p} \left[\frac{1}{f} + \frac{1}{L/d_p} \right]} \text{ psi} \quad (23)$$

but

$$f_{se} + 10{,}000 \le f_{ps} \le f_{py} \text{ psi}$$

In this study, Eq. 22 and 23 will be called as the analysis equation and the design equation, respectively.

5. EVALUATION OF PROPOSED DESIGN EQUATION

To ascertain the accuracy of the proposed design equation, the correlation coefficients were compared with all the equations mentioned in this paper. The correlation coefficient (R=0.77) of the proposed design equation is better than those of ACI code, Harajli and kanj's design equation, Chakrabarti's equation. But the AASHTO LRFD code showed similar accuracy. However, the proposed design equation has a merit that it can predict the ultimate stress of unbonded tendon in a comparatively simple way. But the AASHTO LRFD needs a lengthy computation to solve the quadratic equation. The comparisons of tests with results obtained by the strain compatibility analysis, the analysis equation, and the design equation are shown in Fig. 5, 6, and 7, respectively. The proposed design equation has six characteristics and merits compared with others.

First, the proposed design equation contains the effective prestress f_{se} as a parameter. If the design equation is transformed for the stress increment Δf_{ps}, - $0.2f_{se}$ turns out to be a parameter which affects on Δf_{ps}. But the ACI equation does not recognize the effect of f_{se} on the tendon stress increment. It means that the higher the effective stress, the higher the ultimate stress. However, previous test results showed that Δf_{ps} decreases if the value of f_{se} increases.

Second, the proposed equation can compute accurately the f_{ps} of unbonded tendon in the partially prestressed member. The ACI code cannot take into account the bonded reinforcements even if they are used together with the tendon. Eq. 5, however, illustrates that the area of reinforcement affects on the equilibrium state of section. It, in turn, affects the curvature of the member, and finally affects the stress of the tendon.

Third, the proposed equation contains the term f_c'/ρ_p which is the same parameter as the ACI code. But the parameter is included in the form of a square root. Its validity can be found from Eq. 15d. As the term f_c'/ρ_p is contained in the third term of Eq. 15a, it should be represented as a square root in the design equation.

Fourth, the plastic hinge length ratio is an important parameter. It can be influenced by the loading type and the span/depth ratio. Though the ACI code regards the span/depth ratio as a parameter empirically, the proposed design equation shows that the effect of span/depth ratio can be evaluated in a

mechanically valid way with the concept of plastic hinge length.

Fifth, the proposed design equation can consider the effect on the area and the locations of reinforcement and tendon

At last, while neither Harajli and kanj's design equation nor AASHTO LRFD code equation can provide a mechanically valid ground for the method to evaluate the ultimate stress of unbonded tendon in continuous members, the proposed equation can predict it accurately with the concept of plastic hinge length.

6. CONCLUSIONS

(1) It is desirable to evaluate the tendon stress through the analysis of the whole member by considering the strain of the tendon between both ends of the member.
(2) ACI code evaluates the ultimate stress of unbonded tendon only with the concrete strength and the amount of tendons. However, the parameters on the reinforcement area and the load type may have to be reflected in the design equation.
(3) Unlike in the ACI code, the stress increase of unbonded tendons is proportional to the square root of f_c'/ρ_p.
(4) The effect of span/depth ratio has to be considered together with the concept of plastic hinge length.
(5) The strain compatibility method can closely predict the stress of unbonded tendon at the ultimate load.

ACKNOWLEDGMENTS

The authors would like to thank STRESS (advanced STructure RESearch Station) at Hanyang University and Kumho Construction & Engineering for providing financial support for this study.

6. REFERENCES

1. AASHTO, AASHTO LRFD Bridge Design Specification, SI unit 1st Ed., American Association of State Highway and Transfortation Officials, 1994.
2. ACI-ASCE Committee 423, "Recommendations for concrete members prestressed with unbonded tendon." ACI Journal, May-June 1989.
3. ACI Committee 318, "Building code requirements for structural concrete

(ACI 318-95) and commentary (ACI 318R-95)." American Concrete Institute, Detroit, 1995.

4. Alkhairi, F. M., "On the flexural behavior of concrete beams prestressed with unbonded internal and external tendons." Ph.D thesis, University of Michigan at Ann Arbor, 1991.
5. Chakrabarti, P. R., "Ultimate stress for unbonded post-tensioning tendons in partially prestressed beams." ACI Journal, Nov.-Dec., 1995, pp 689-697.
6. Harajli, M. H., and Naaman, A. E., "Evaluation of the ultimate steel stress in partially prestressed flexural members." PCI Journal, Sept.-Oct., 1985, pp 54-81.
7. Harajli, M. H., and Kanj, M. Y., "Ultimate flexural strength of concrete members prestressed with unbonded tendons." ACI Journal, VOl. 88, No. 6, 1991, pp 663-673.
8. Moon, J.-H., and Burns, N. H., "Flexural behavior of members with unbonded tendons. II : application." J. of Struct. Engrg., ASCE, Vol. 123, No. 8, Aug., 1997.
9. Mattock, A. H., Discussion of "Rotational capacity of concrete beams." by W. Corley, Proceeding, ASCE, Apr., 1967, pp 519-522.
10. Naaman, A. E., and Alkhairi, F. M., "Stress at ultimate in unbonded post-tensioning tendons. Part Ⅰ : Evaluation of the state-of-the art." ACI Journal, Sept.-Oct., 1991, pp 641-651.
11. Naaman, A. E., and Alkhairi, F. M., "Stress at ultimate in unbonded post-tensioning tendons. Part Ⅱ: Proposed methodology." ACI Journal, Nov.-Dec., 1991, pp 683-692.

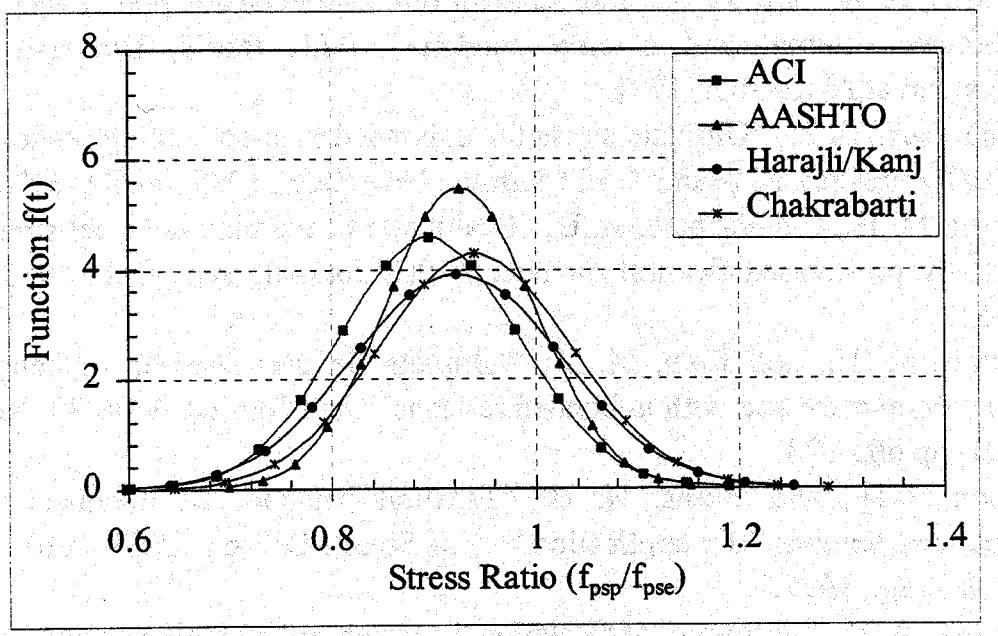

(a) Ultimate stress of unbonded tendon

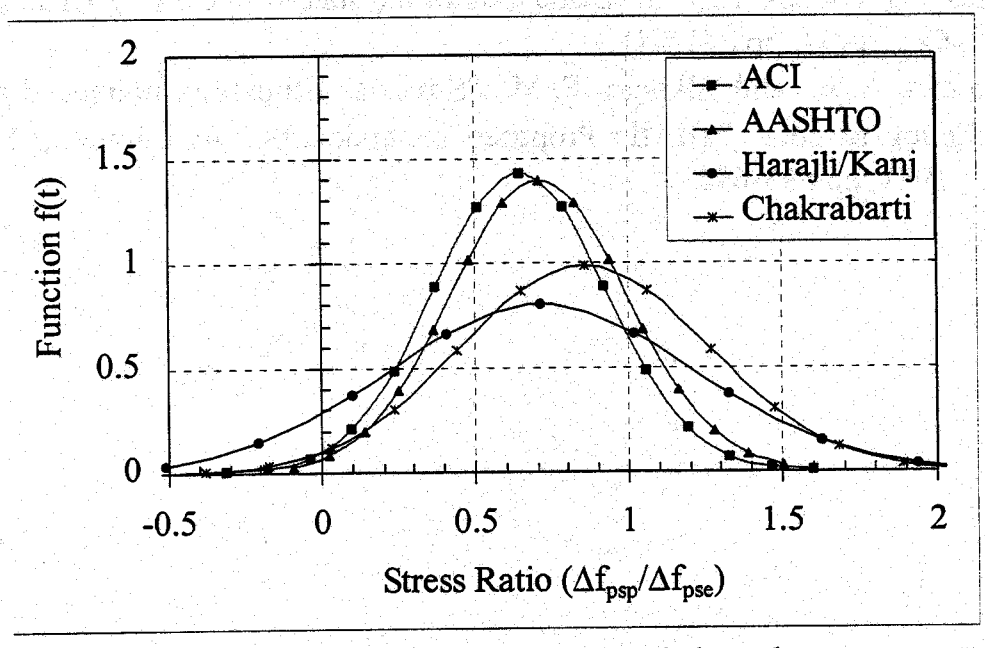

(b) Stress increase of unbonded tendon

Fig. 1 Statistical distribution of unbonded tendon stress

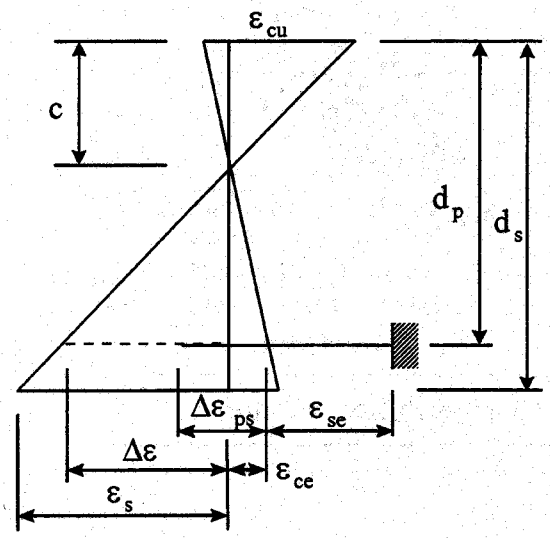

Fig. 2 Strain distribution

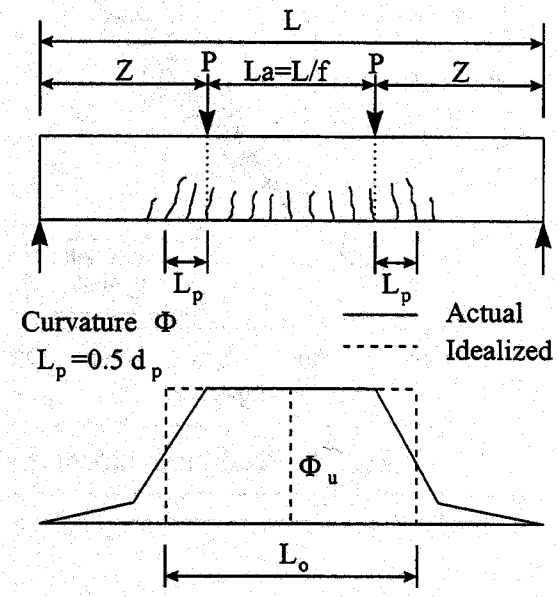

Fig. 3 Idealized curvature distribution

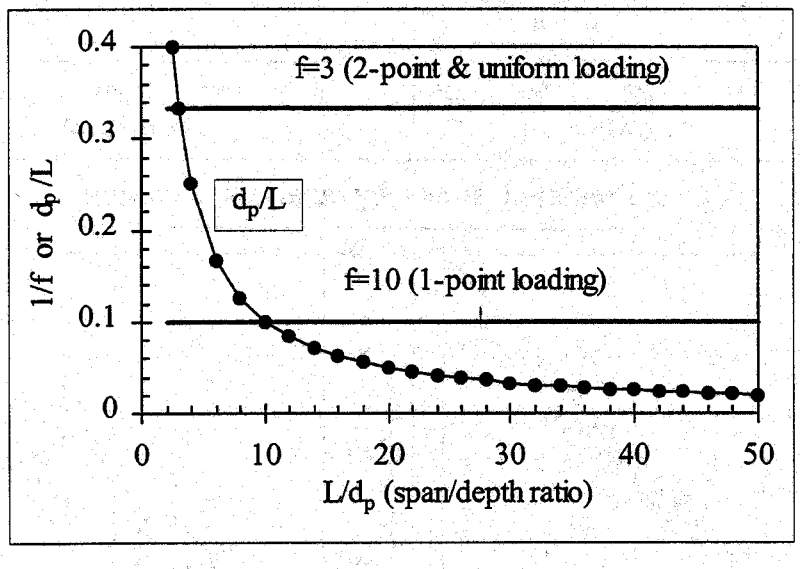

Fig. 4 Effect of plastic hinge length

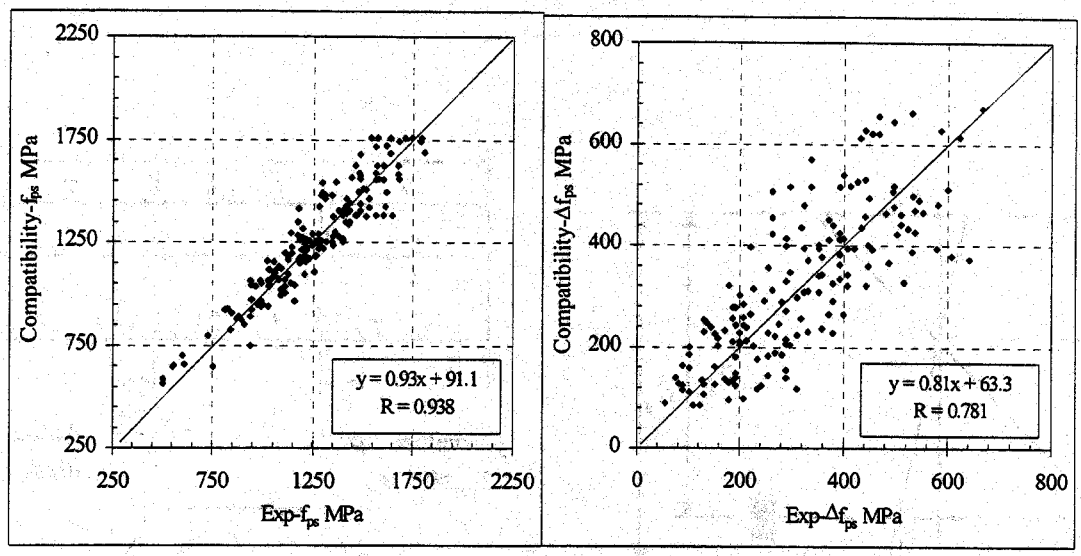

Fig. 5 Predicted stress by strain compatibility method

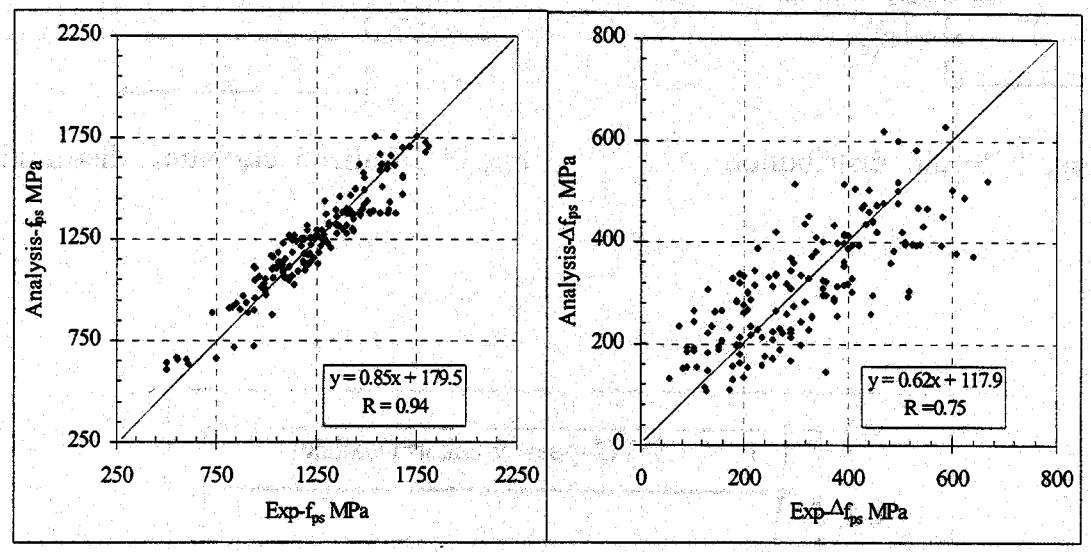

Fig. 6 Predicted stress by analysis equation

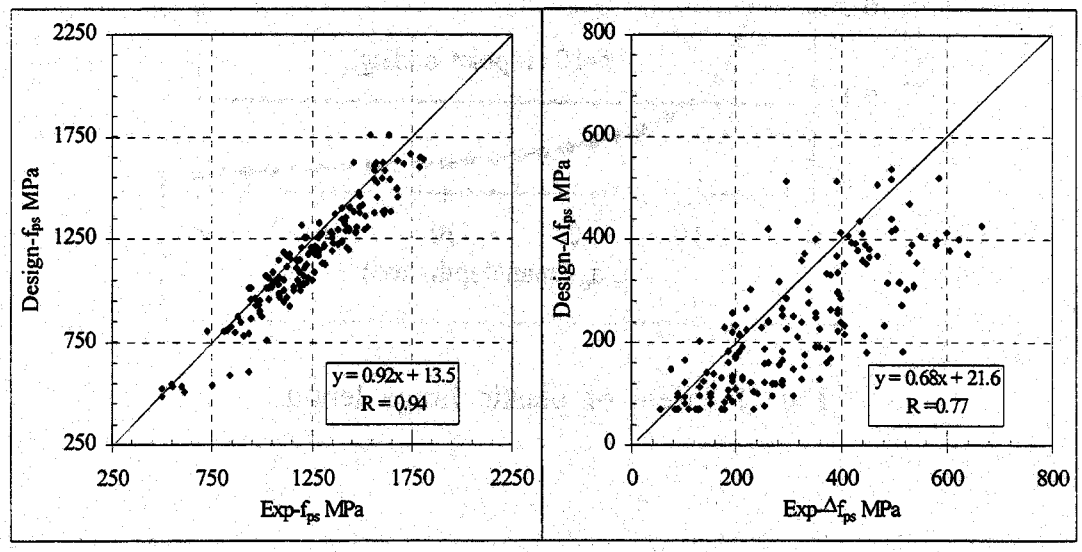

Fig. 7 Predicted stress by design equation

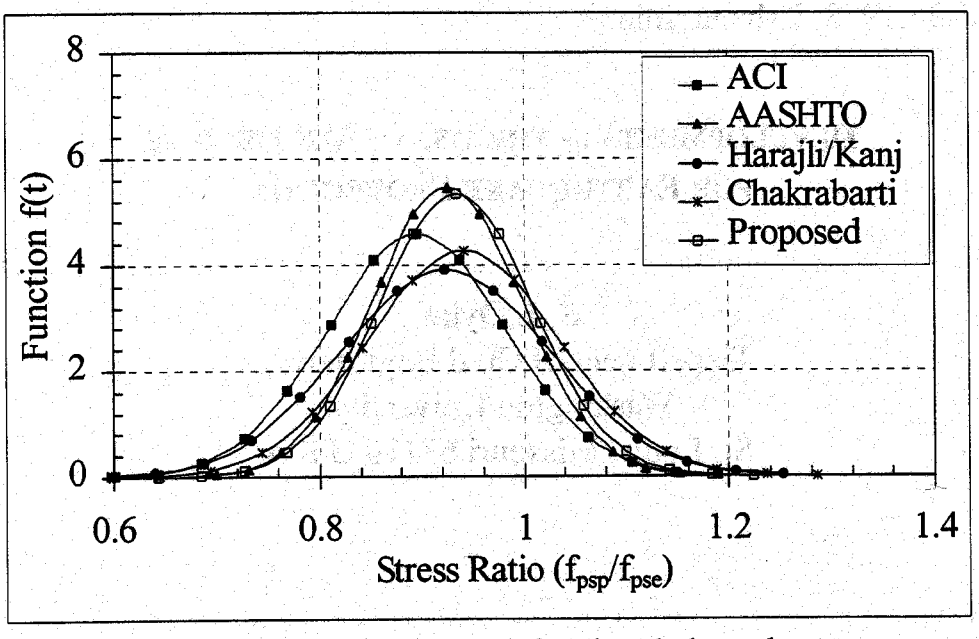

(a) Ultimate stress of unbonded tendon

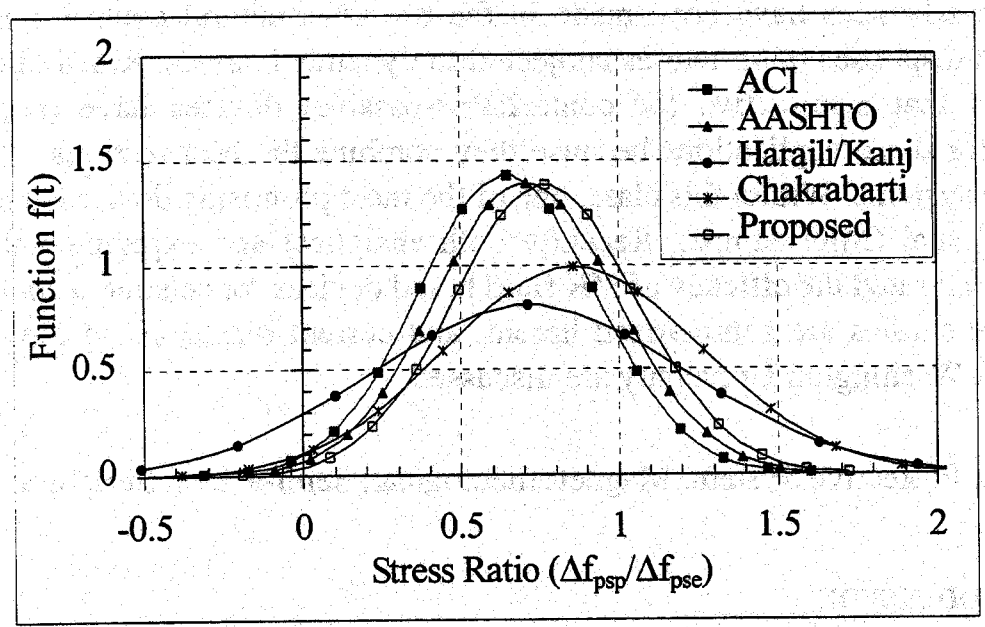

(b) Stress increase of unbonded tendon

Fig. 8 Statistical distribution of unbonded tendon stress

Workshop on Structural Design Issues for Moderate Seismic Zones
February 24-25,1998, Urbana, Illinois

DEVELOPMENTS IN THE USE OF MR DEVICES FOR EARTHQUAKE PROTECTION

S. J. Dyke
Department of Civil Engineering
Washington University
St. Louis, Missouri 63130 U.S.A.

ABSTRACT

One of the top priorities in the civil engineering community is the development of effective means for increasing the seismic resistance of structures. Recently significant advances have been made in the use of structural control systems to reduce the responses of structures subjected to dynamic hazards. Researchers have recognized that semi-active (or controllable-passive) devices have tremendous potential for these applications because they combine the best features of passive and active systems. Within this class, one of the most promising devices is the magnetorheological (MR) damper. Recently both analytical and experimental studies have demonstrated the efficacy of MR fluid based devices for seismic response control. These studies are summarized herein, and current directions of the ongoing research at Washington University are discussed.

Keywords: Protective System, Magnetorheological, Semi-active, Structural control

1 INTRODUCTION

The development of effective strategies to minimize losses and reduce the devastating consequences of earthquakes is a problem of widespread importance. Advances made in this field will have tremendous social and economic implications. One recent emphasis in earthquake resistant design considers the use of structural control systems as a means of reducing the responses of structures subjected to severe dynamic loading [11–13, 18]. These approaches, also termed protective sys-

tems, offer exciting new possibilities for the future of seismic design.

Significant advances have been made in the design, development and verification of protective systems. This technology has now reached the point where control systems have been designed and installed in full-scale buildings and bridges [11, 14, 15]. These systems have the potential to revolutionize earthquake engineering. One of the most promising class of control systems uses semi-active, or controllable-passive devices. According to presently accepted definitions, a semi-active control device is one that cannot increase the mechanical energy in the controlled system (*i.e.*, including both the structure and the device), but has properties which can be dynamically varied to optimally reduce the responses of a structural system. These devices have attracted much attention recently because they address most of the concerns brought forth about structural control [15]. Examples of such devices include variable-orifice fluid dampers, controllable friction devices, variable stiffness devices, controllable liquid sloshing/column devices, and controllable fluid dampers.

Magnetorheological (MR) dampers are new semi-active devices that are particularly suitable for civil engineering applications. These devices utilize MR fluids, which have the ability to reversibly change from a Newtonian liquid to a semi-solid upon application of a magnetic field. Devices based on MR technology offer mechanical simplicity, low power requirements, environmental robustness, and demonstrated potential for developing forces sufficient for full-scale applications at a reasonable cost, and can be viewed as fail-safe in that they revert to passive dampers should the control hardware malfunction. Preliminary experimental results have proven that MR dampers can be built that are capable of generating the forces required for full-scale implementation. A 20-ton MR damper was designed and constructed by Lord Corporation, a leader in MR fluid technology (see http://www.rheonetic.com), and is currently being tested at the University of Notre Dame [1–2, 16]. Recently other researchers have also developed in interest in this technology for related civil engineering applications [19, 20].

The purpose of this paper is to summarize some of the recent activities in the use of MR devices for seismic control of buildings, and to discuss some current and future research directions. Direct comparisons between MR devices and passive devices have demonstrated that MR devices have the ability to achieve greater performance levels than similar passive systems [4–9]. Additionally, these studies indicated that semi-active systems have the potential to achieve, or even surpass, the performance of fully active systems [7]. Current analytical and experimental research activities are studying the implementation of MR devices to achieve effec-

tive seismic response control for a variety of loading conditions and performance objectives. Experimental investigations will be conducted in the recently established Washington University Structural Control and Earthquake Engineering Laboratory (see http://www.seas.wustl.edu/research/quake).

2 CURRENT STATUS OF MR DAMPERS FOR SEISMIC HAZARD MITIGATION

Recently a number of investigations, both analytical and experimental, have been conducted to demonstrate the efficacy of MR devices for seismic response control of buildings. The results of these studies are summarized in the following sections.

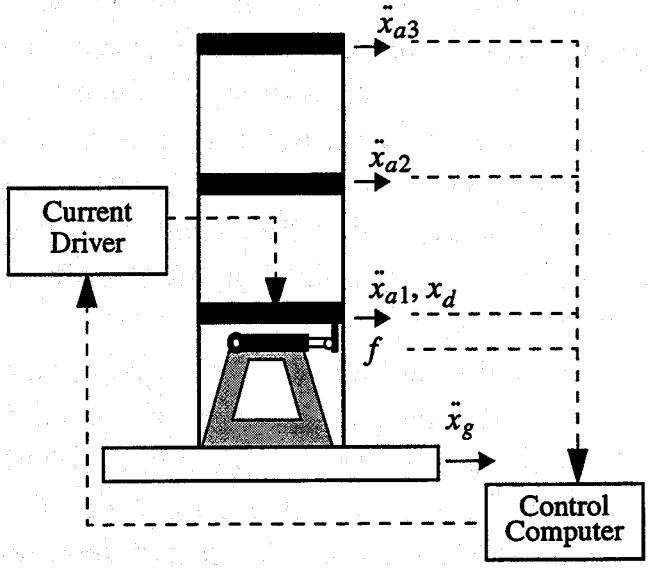

Figure 1. Diagram of MR Damper Implementation.

2.1 EXPERIMENTAL STUDIES

Dyke *et al.* [8–9] conducted the first successful experiments demonstrating the great potential of MR technology for earthquake hazard mitigation. In these experiments a single MR damper was employed to control a three-story test structure at the Structural Dynamics and Control/Earthquake Engineering Laboratory (SDC/EEL) at the University of Notre Dame. A diagram of the experimental setup is shown in Fig. 1.

To evaluate the potential of MR dampers in structural control applications and to take full advantage of the unique features of the device, a phenomenological model was developed that can effectively reproduce the behavior of an MR damper [17], shown in Fig. 2. This model reproduces the behavior of a typical MR damper over a wide variety of loading conditions. The model is valid for both time-varying displacement and control inputs, making it suitable for control applica-

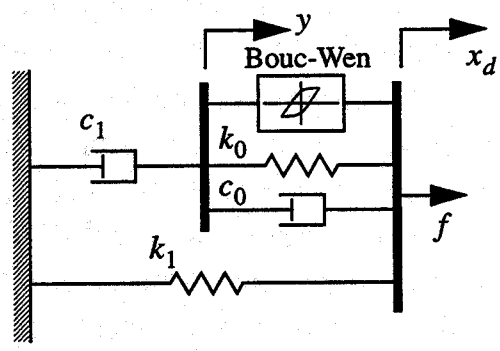

Figure 2. Simple Mechanical Model of the MR Damper.

tions. To account for fluctuating inputs, certain parameters of the model are dependent upon the magnetic field strength. The model also accounts for the dynamics involved in the fluid reaching rheological equilibrium and in driving the electromagnet in the MR damper (see [17] for further details).

To perform the initial investigations, a clipped-optimal control algorithm based on acceleration feedback was developed and shown to be effective for seismic response reduction [4–9]. For the El Centro earthquake experiments, this control system achieved a 78%, 79%, and 36% reduction in peak third floor relative displacement, maximum interstory displacement, and peak third floor absolute acceleration, respectively, over the uncontrolled values. A comparison of the uncontrolled and controlled responses are shown in Fig. 3. Additionally, the results clearly demonstrated that the performance of a semi-active system based on the MR damper can surpass that of similar passive systems (an additional 15–30% reduction in the structural responses). Furthermore, simulation studies indicate that the performance of this semi-active control system has the potential to surpass that of a comparable active control system [7].

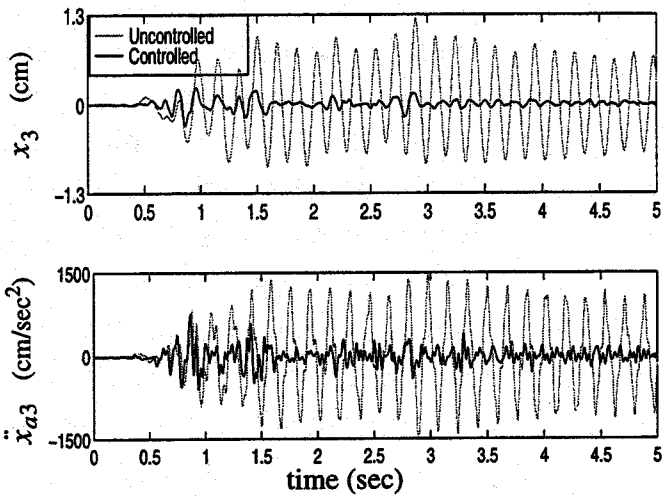

Figure 3. Controlled and Uncontrolled Responses due to El Centro Earthquake.

2.2 Analytical Studies

A number of analytical studies have been conducted to provide further evidence of the potential of the MR damper for seismic hazard mitigation. The results of these studies are summarized in the following sections.

Evaluation of Semi-Active Control Algorithms

Because of the inherent nonlinear nature of MR devices, one of the challenging aspects of utilizing this technology to achieve high levels of performance is in the development of appropriate control algorithms that can take advantage of the unique characteristics of the device. Because the characteristics of the various semi-active devices are different (*e.g.*, variable friction, fluid-orificing, controllable flu-

ids, *etc.*), a control algorithm that performs well for one device may not be suitable for use with another device. Recently, four semi-active control algorithms proposed in the literature were evaluated for use with the MR damper [5].

To examine the suitability of each algorithm for use with the MR damper, the performance of the resulting control systems were compared through numerical simulations, and the advantages of each algorithm were discussed. In these numerical studies, a single MR damper was used to control a three story building subjected to seismic loading. To assess the effectiveness of each of the control algorithms, they were evaluated in their ability to reduce the peak responses of the model building for the N-S component of the El Centro earthquake excitation.

The results of this analytical study demonstrated that the performance of the resulting controlled system and the requirements of the control device are highly dependent on the control algorithm employed. Most of the semi-active control systems performed noticeably better than the passive controllers in some way. Specifically, some algorithms were able to achieve high reduction in structural accelerations, some were able to achieve large reductions in structural displacements, and some could achieve both of these goals simultaneously. Thus the choice of control algorithm is highly dependent on the control objectives.

Investigating the Use of Multiple Control Devices

Because it is likely that multiple control devices will be used to reduce the responses of a full-scale structure, the effective utilization of multiple control devices is another important consideration. Recently, Dyke and Spencer [4] considered the use of multiple MR dampers for seismic response control. In this work, the clipped-optimal control algorithm developed for use with the MR damper was extended to the multiple-input case, and evaluated through a numerical example in which two dampers were employed to control a model of a five story, linear structure. In the example, one MR damper was attached between the base and first floor of the structure, and another was attached between the first and second floors of the structure. In this example, the clipped optimal controller was designed to minimize the absolute acceleration of the top floor of the structure.

The performance of the semi-active control system was evaluated for the El Centro earthquake at three different magnitudes including full-scale, half-scale, and quarter-scale. The response of the passive-on and the passive-off systems were included as a basis for comparison. The results indicated that both passive systems achieve a reasonable level of performance. At all amplitudes the passive-on system performed better than the passive-off system, achieving approximately a 60%

reduction in the maximum interstory displacements and greater than a 50% reduction in the maximum absolute accelerations.

Because the MR damper has the ability to dynamically modify its properties, the performance of the semi-active system surpassed that of both passive systems. In reducing the peak accelerations of the three different earthquakes, the clipped-optimal controller achieves a 22% (full-scale), 28% (half-scale), and 32% (quarter-scale), reduction over the better passive results. Furthermore, these performance levels are achieved while maintaining approximately the same reduction in maximum interstory displacements as in the best passive case.

It is interesting to note that in this study the MR damper was found to be particularly effective in reducing the absolute accelerations of the floors of the structure. This result occurs because the semi-active system has the flexibility to adjust the control forces to an appropriate level for the corresponding excitation magnitude. Generally the control forces provided in the passive-on case are significantly larger than those provided by the semi-active control system, because the passive-on system applies the maximum control force possible at all times. However the results of this study clearly demonstrate that this approach is not the best strategy, particularly if the goal is to reduce the structural accelerations.

3 MR Research in Earthquake Engineering

Based on the encouraging results of the research summarized herein, the future of MR devices for civil engineering applications appears to be quite promising. However, before this technology will become widely accepted and routinely implemented in seismic resistant structural design, a number of issues must be investigated. The following sections address some of the current directions in structural control research at Washington University.

3.1 Washington University Seismic Simulator Facility

Experimental verification of new approaches is an important step in demonstrating the potential of protective systems. The Washington University Structural Control and Earthquake Engineering Laboratory [10] (also see *http://www.seas.wustl.edu/research/quake*) was developed to provide a testbed for experimental verification of new approaches in seismic resistant design. This experimental facility houses a uniaxial seismic simulator (Fig. 4) that is capable of imparting the motion generated by an earthquake to a structural system, and will assist the civil engineer in the effective design of control systems. The simulator consists of a

1.5×1.5 m^2 (5×5 ft^2) aluminum sliding table mounted on high-precision, low-friction, linear bearings. The sliding table is driven with an 80 kN (18 kip) hydraulic actuator. The seismic simulator was designed to have an operational frequency range of 0–50 Hz, a stroke of 15 cm (6 in), can achieve velocities of over 75 cm/sec (30 in/sec), and is capable of imparting accelerations of greater than 4 *g*'s to a 900 kg (1 ton) test load.

A six-story, single bay test structure has been constructed for laboratory testing (Fig. 5). The structure is 180 cm (74 in) tall and has a mass of 136 kg (300 lb). This model will be the test specimen for the experimental investigations described in the following section.

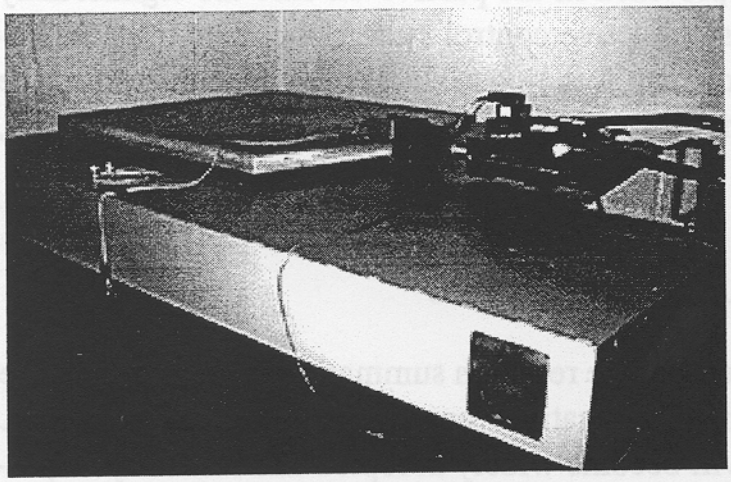

Figure 4. Photograph of the Seismic Simulator in the Washington University Structural Control and Earthquake Engineering Laboratory.

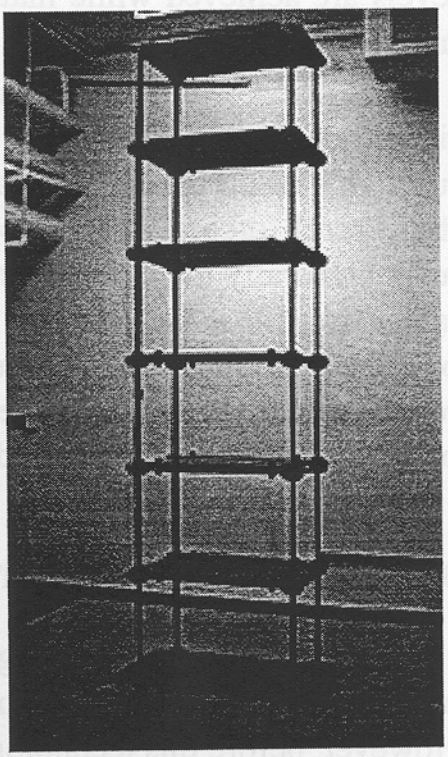

Figure 5. Photograph of Six-Story, Single Bay Test Structure.

3.2 Current Directions in Structural Control Research

Based on previous results, MR devices have a great deal of potential in structural control systems. To implement these devices in full-scale structures, a number of issues should be addressed. For instance, just as numerous passive devices are necessary to control a full-scale structure, more than one semi-active device will likely be used in these applications. Thus, analytical studies were performed to demonstrate that multiple MR devices can be used simultaneously to control a structure. Experimental verification of the efficacy of multiple control devices in a

structure is underway. In this experiment, the six story structure in the earthquake engineering laboratory at Washington University (Fig. 5) will be used as the test specimen. MR devices will be placed on multiple floors of the structure to achieve significant global response reduction. The control system will be evaluated by comparing the resulting structural responses to those of comparable passive systems.

Another facet of the current research activities is in the use of MR devices for controlling larger structures with more complex behavior. Recently a second generation benchmark problem in structural control for seismically excited buildings was presented to the structural control community by the ASCE Subcommittee on Structural Control (problem statement is available on the World Wide Web at: http://www.nd.edu/~quake/, or at http://www.seas.wustl.edu/research/quake). The subject of these analytical studies is a full-scale, 20-story structure designed for the Los Angeles area as part of the SAC Phase II Steel Project. Efforts are currently underway at Washington University to develop a MR-based control system to reduce the responses of this structure. Proposed control system designs are required to include accurate models of all control devices and sensors, device location and orientation, and a description of the control algorithm. The performance of each of the proposed control systems will be compared to other proposed strategies through a set of performance criteria. The results of this study will be presented at the Second World Conference on Structural Control in the summer of 1998.

4 SUMMARY

Magnetorheological devices offer an exciting alternative in structural control applications. They are versatile, inexpensive, and stable, and can generate forces of the scale required for civil engineering structures. A number of recent studies summarized in this paper demonstrate the significant potential of these devices. Further experimental and analytical studies are being performed to examine the efficacy of these devices in a variety of situations.

Further information on the facilities and ongoing research activities in the Washington University Structural Control and Earthquake Engineering Lab are available on the World Wide Web at: http://www.seas.wustl.edu/research/quake.

5 ACKNOWLEDGMENTS

The Washington University Structural Control and Earthquake Engineering Laboratory was established with support from the School of Engineering and Applied Sci-

ences at Washington University in St. Louis. In addition, the author would also like to express her appreciation to Lord Corporation of Cary, North Carolina for providing the prototype damper used in the experimental work summarized herein.

6 REFERENCES

[1] Carlson, J.D. and Spencer Jr. B.F. (1996). "Magneto-Rheological Fluid Dampers for Semi-Active Seismic Control," *Proc. of the 3rd Int. Conf. on Motion and Vibr. Control*, Chiba, Japan, Vol. 3, pp. 35–40.

[2] Carlson, J.D. and Spencer Jr., B.F. (1996). "Magneto-Rheological Fluid Dampers: Scalability and Design Issues for Application to Dynamic Hazard Mitigation," *Proc. 2nd Int. Wkshp. on Struc. Control*, Hong Kong, pp. 99–109, Dec.

[3] Dyke, S.J., Spencer B.F. Jr., Quast, P., and Sain, M.K. (1995). "The Role of Control-Structure Interaction in Protective System Design." *J. of Engrg. Mech., ASCE*, Vol. 121 No. 2, pp. 322–38.

[4] Dyke S.J. and Spencer Jr. B.F., (1996). "Seismic Response Control Using Multiple MR Dampers," *Proc. 2nd Int. Wkshp. on Struc. Control*, Hong Kong, pp. 163–173.

[5] Dyke, S.J. and Spencer Jr., B.F. (1997). "A Comparison of Semi-Active Control Strategies for the MR Damper," *Proc. of the International Conf. on Intelligent Information Systems*, Bahamas, December 8–10.

[6] Dyke, S.J., Spencer Jr ., B.F., Sain, M.K. and Carlson, J.D. (1996). "Seismic Response Reduction Using Magnetorheological Dampers." *Proc. of the IFAC World Congress*, San Francisco, CA, June 30–July 5.

[7] Dyke, S.J., Spencer Jr., B.F., Sain, M.K. and Carlson, J.D. (1996). "Modeling and Control of Magnetorheological Dampers for Seismic Response Reduction," *Smart Materials and Structures,* Vol. 5, pp. 565–575.

[8] Dyke, S.J. (1996). "Acceleration Feedback Control Strategies for Active and Semi-Active Systems: Modeling, Algorithm Development and Experimental Verification.," Ph.D. Dissertation, University of Notre Dame, Notre Dame, IN.

[9] Dyke, S.J., Spencer Jr., B.F., Sain, M.K., and Carlson, J.D. (1996). "Experimental Verification of Semi-Active Structural Control Strategies Using Acceleration Feedback," *Proc. of the 3rd Intl. Conf. on Motion and Vibr. Control*, Vol. 3, pp. 291–296, Chiba, JAPAN, September.

[10] Dyke, S.J. (1998). "Design and Development of the Washington University Seismic Simulator Facility," *Proceedings of the 12th ASCE Engineering*

Mechanics Conference, La Jolla, California, May 17–20 (in press).

[11] Fujino, Y., Soong, T.T. and Spencer Jr., B.F. (1996). "Structural Control: Basic Concepts and Applications," *Proc. of the ASCE Struct. Cong.*, Chicago, Illinois, pp. pp. 361–370.

[12] Housner, G.W., Masri, S.F. and Chassiakos, A.G. (Eds.), (1994). *Proc. of the First World Conf. on Structural Control*, Pasadena, CA, August 3-5.

[13] Housner, G.W., Bergman, L.A., Caughey, T.K. Chassiakos, A.G., Claus, R.O., Masri, S.F., Skelton, R.E., Soong, T.T., Spencer Jr., B.F. and Yao, J.T.P., 1997. "Structural Control: Past, Present, and Future", *J. Engrg. Mech.*, ASCE, Special Issue, Vol. 123, No. 9, pp. 897-971.

[14] Sack, R.L., Kuo, C.C., Wu, H.C., Liu, L. and Patten, W.N. (1994). "Seismic Motion Control via Semiactive Hydraulic Actuators." *Proc. of the U.S. Fifth National Conf. on Earthquake Engrg.*, Chicago, Illinois, Vol. 2, pp. 311–320.

[15] Spencer Jr., B.F. (1996). "Recent Trends in Vibration Control in the U.S.A.," *Proc. of the 3rd Int. Conf. on Motion and Vibr. Control*, Chiba, Japan.

[16] Spencer Jr. B.F., Carlson, J.D., Sain, M.K., and Yang, G. (1997). "On the Current Status of Magnetorheological Dampers: Seismic Protection of Full-Scale Structures," *Proc. of the Amer. Control Conf.*, pp. 458–62.

[17] Spencer Jr., B.F., Dyke, S.J., Sain, M.K., and Carlson, J.D. (1996). "Phenomenological Model for Magnetorheological Dampers," *J. Engrg. Mech.,* ASCE, Vol. 123, No. 3, pp. 230-238.

[18] Spencer Jr., B.F., and Sain, M.K., (1997). "Controlling Buildings: A New Frontier in Feedback," *Control Systems: Breaking Through with Emerging Technologies*, IEEE, Vol. 17, No. 6, pp. 19–35.

[19] Hansen, B.C., Gordaninejad, F., Saiidi, M. and Chang, F-K. (1997), "Control of Bridges Using Magneto-Rheological Fluid Dampers," *Proc. of the International Workshop on Health Monitoring*, Stanford University, September.

[20] Gordaninejad, F., Saiidi, M., Chang, F-k and Hansen, B. C. (1998), "Control of Bridges Using Magneto-Rheological Fluid Dampers and Fiber-Reinforced, Composite-Material Columns," *Proc. of 1998 SPIE Conf. on Smart Structures and Materials*, San Diego, California.

Workshop on Structural Design Issues for Moderate Seismic Zone
February 24-25, 1998, Urbana, Illinois

BEHAVIOR OF CONCRETE-FILLED BOX COLUMN TO H-BEAM CONNECTIONS

K. J. Shin
Associate Professor, Department of Architectural Engineering,
Hannam University, Korea
Y. S. Oh
Associate Professor, Department of Architectural Engineering,
Taejon University, Korea
T. S. Moon
Professor, Department of Architectural Engineering,
Hanyang University, Korea

Abstract
This paper describes a test program conducted on the behavior of cold-formed, concrete-filled box column to H-beam connections. Specimens representative of interior columns in a steel building frame were fabricated with connections stiffened by bent plates through a box section and T-stiffeners at the junction of the beam and column flange. They were tested to failure under static and cyclic loads applied separately. Ultimate load-carrying capacity and typical load-deflection obtained experimentally are presented. The result for those specimens tested under static loading are compared with the results using the nonlinear finite element analysis. Close agreement is observed between the experimental and numerical load deflection curves. Monotonic test results show that the bent plates are enough to develop load-carrying capacity in excess of the plastic capacity of the beam. Cyclic test results show that T-stiffeners are useful to increase the energy dissipation capability. Results show that cold-formed section should be used carefully to satisfy the basic requirements: sufficient strength, sufficient deformation capacity, and adequate rigidity as a rigid connection.
Key words: Box column, Connection, T-stiffener, Cyclic load

1. Introduction

Concrete filled tube (CFT) column have excellent strength properties in terms of increasing axial loading capacity, especially for the short to medium length columns. Use of CFT is therefore increasing in modern steel construction. The conventional connection details are not practical to a CFT beam-to-column connection because they have diaphragms that make the concrete filling difficult. External diaphragms are required for concrete filling in box column connection. The connection details using rectangular box columns are complicate because a box column has the closed shape. Connection between beam and column is one of the main areas where potential cost saving can be achieved. Various types of connections using box column have been reported. Giroux and Picard (1977) suggested rigid frame connections for tubular column using strap angles. Dawe and Grondin (1990) tested ten tube connections using tension plates and angles to study the failure modes and analytical model. Recently, Shanmugan and Ting (1995) have investigated the structural performance for the connections externally stiffened by T-sections. Experiments have been done on four-way connections

Nine tests were performed on two-way connections stiffened by bent plates and T-stiffeners as shown in Fig. 1. The connections were tested to failure under monotonic and cyclic load applied separately. The objective of this study was to collect data on the performance of connections using cold-formed, concrete-filled box column.

2. Experimental Program

Nine half-scale specimens consisting of connections stiffened by bent plate internally or T-stiffeners externally were designed. Fig.1 shows a typical four-way connection shape. Fig 2 shows the bent plates penetrated through a box column. The plates connecting both beam flanges each other are bent shapes to make a four-way connection. The bent plates are inserted through the holes made in flange of a box column. The cold-formed box column could be used without cutting at the connection, which may reduce the welding cost of column. The angle of bent plate was 30° to cross each other. The beam flanges were cut out to insert the bent plate and fillet welded to the beam flange. T-stiffeners were built-up by welding the plates of thickness 9mm. The T-stiffeners were welded to columns and beam flanges using partial-penetration single groove welds. The length of T-stiffener was fixed as 150mm long. The test parameters of T-stiffener are the length of welding to box column, which is 150mm

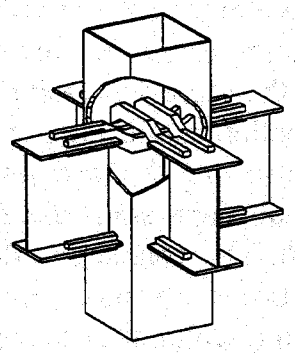

Fig. 1. Connection shape

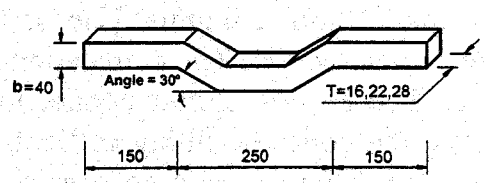

Fig. 2. A bent plate

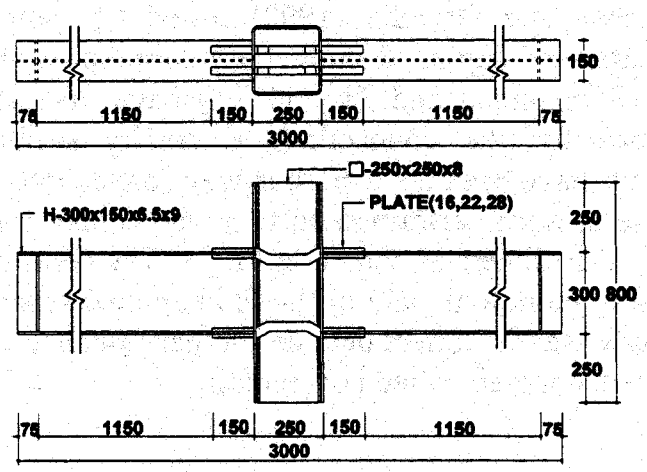

Fig. 3. Dimensions of monotonic test specimens (unit:mm)

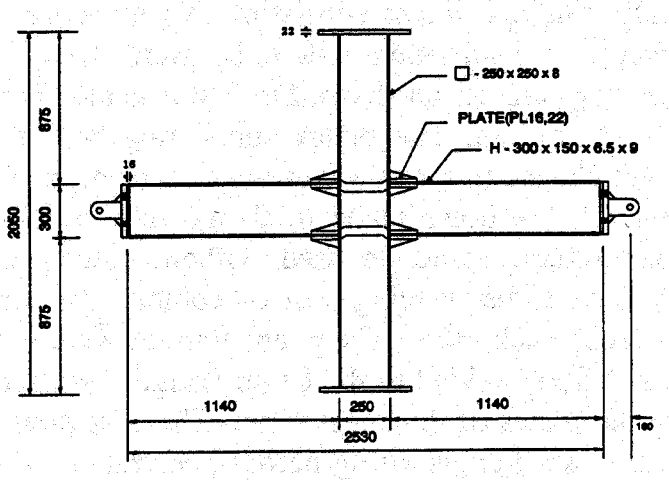

Fig. 4. Dimensions of cyclic test specimens (unit:mm)

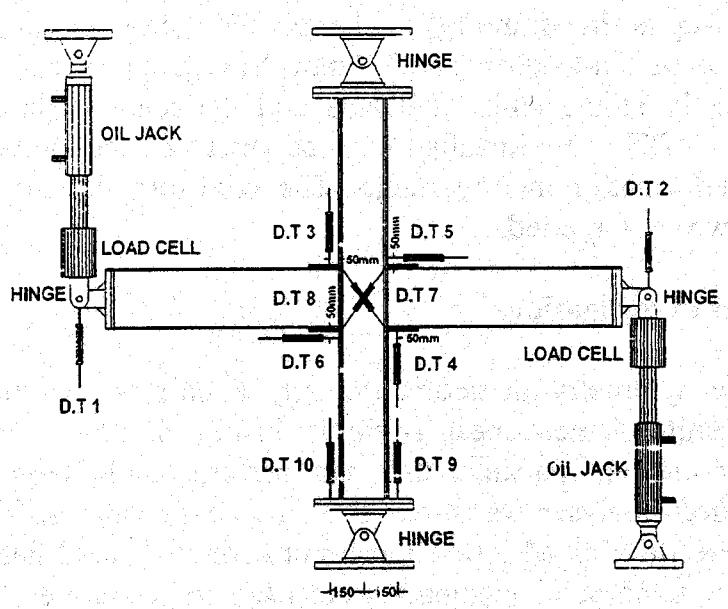

Fig. 5. Test set-up for cyclic loading

Table 1. Details of connection test specimens

Specimen	Bent Plate Size(mm)	T-Stiffener Size (mm)	Loading Type
M-PC16	16×40	None	Monotonic
M-PC22	22×40	None	Monotonic
M-PC28	28×40	None	Monotonic
C-PC22	22×40	None	Cyclic
C-PC28	28×40	None	Cyclic
PL16T100	16×40	100*×50×150×9	Cyclic
PL16T150	16×40	150*×50×150×9	Cyclic
PL22T100	22×40	100*×50×150×9	Cyclic
PL22T150	22×40	150*×50×150×9	Cyclic

Note: All Beam:H-300×150×6.5×9, All Column:⊠-250×250×8

* Dimensions at the face of column

or 100mm. The dimensions for monotonic and cyclic test specimens are shown in Fig. 3 and Fig. 4, respectively. The specimen details are listed in Table 1. All columns were cold-formed □ -250× 250× 8mm sections of SPSR400. All beams were hot-rolled H-300× 150× 6.5× 9mm sections

of SS400 (A36). The inside of tube column was filled with concrete of f'c=27.6N/mm^2 (4 psi).

The test set-up is shown in Fig. 5. The top and bottom is pin supported and the distance of pin-to-pin was 2375mm. Monotonic or cyclic load is applied separately at the ends of beams and the loading distance was 2850mm. The LVDTs were installed for load versus deflection curves and for the shear deformation measurements. The axial force for the concrete-filled column was not applied.

3. Analytical Investigations

Due to the symmetry in geometry, only a half of the model was analyzed and finite element mesh is shown in Fig. 6. ANSYS (ANSYS, 1996), a finite-element package that can perform both geometric and material nonlinear analyses was used. The columns, beams, stiffeners and bent plates were discretized into a mesh consisting of quadrilateral shell elements. Eight node solid elements were used for concrete. Two node contact elements were used at the face between concrete and steel tube columns. All material properties input were of the elastic-plastic nature without strain hardening. Material yielding is defined by the von Mises yielding function with isotropic material behavior. Suitable support and boundary conditions were specified in the analytical modeling to simulate the actual behavior of the test model.

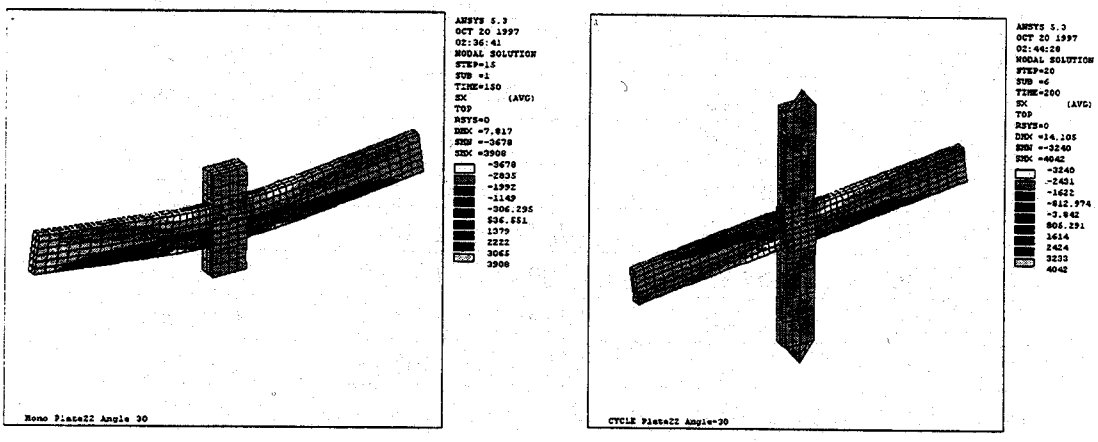

(a) Monotonic loading specimen M-PC22

(b) Cyclic loading specimen C-PC22

Fig. 6. Stress resultant at ultimate load

Fig. 6 shows the stress resultants for monotonic and cyclic specimen at the maximum load, respectively. It can be seen that plastic hinges are formed at the end of stiffened plate of monotonic specimen. Load-deflection relationships under static loading were obtained by using the finite-element method and compared with those obtained from the experiments as plotted in Fig. 7 and Fig. 8 for specimen M-PC22 and C-PC22, respectively. The close agreement between the test and analysis results shows that the finite element method can be used to predict the behavior of the connections accurately.

4. Experimental Results

Monotonic test specimens were tested on the universal testing machine. Specimens were simply supported at both end of beam and loads were applied at the center of column. Cyclic tests were conducted using two oil jacks with same pressure until failure occurred. The recorded beam-end displacements of each specimen can be interpreted as the total deformations consisting of column rotation, deformations of the bent plates and T-stiffeners, and the beam rotation. Table 2 gives the tensile coupon strength of the flange and the plates for each specimen

Table 2. Tensile coupon test results

Sections (1)	F_y(MPa) (2)	F_u(MPa) (3)	F_y/F_u (4)	Elongation(%) (5)
□ -250× 250× 8	356.7	443.9	0.8	32
H-300× 150× 6.5× 9 Flange	298.9	426.3	0.7	31
PL 9mm	300.8	418.4	0.72	33
PL 16mm	267.5	457.7	0.58	32
PL 22mm	293.0	527.2	0.56	34
PL 28mm	266.1	515.5	0.52	34

Fig. 7 shows the load versus displacement relationship for monotonic loads. P_p represent the load due to the full plastic moment of beam at the end of T-stiffener rather than the column face. Specimen M-PC16 shows the non-linear behavior from the start of loading because the strength ratio of bent plate to the full plastic moment capacity was about 55%. After the large rotation it show the sufficient strength. The local buckling at the beam flange was observed and finally the bent plates were cut and lead to

failure. The result represents that the flange of column is effective to increase the rotation capacity of beam. For the specimens, M-PC22 and M-PC28, the beams respond elastically until the load was slightly below that required to reach the yield stress of 298.9 MPa. Although the local buckling of the top flange outside of stiffener developed, the connection parts were within the elastic range. The load was terminated after pronounced ductility has been observed. The maximum loads applied for M-PC22 and M-PC28 were about 167kN and 158kN, respectively. The numerical result from finite element modeling is plotted in Fig. 7 for specimen M-PC22. The close agreement between the results shows that the finite element method can be used to predict the behavior of the connections accurately. Similar results were obtained on the other specimens tested.

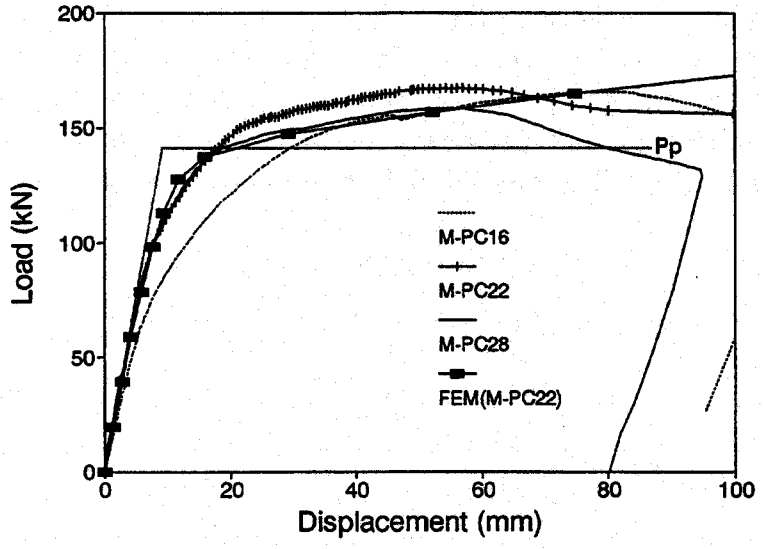

Fig. 7. Load versus displacement relationships for monotonic loads

The hysteretic loops of load versus beam deflection are shown in Fig. 8. There was no big difference in the loop shapes between specimen C-PC22 and C-PC28. It can be seen that the maximum load of cyclic load (C-PC22, C-PC28) was much lower than that of monotonic load (M-PC22, M-PC28) because the failure modes were different. At the end of second cycle, fracture of welding between bent plates and column holes were noted. During the third cycle, punching failure between the column holes and bent plates by the fracture of fillet welding were occurred. The pronounced local buckling in the beam was not obtained because of the premature fracture of welding. However, the specimen maintained load-

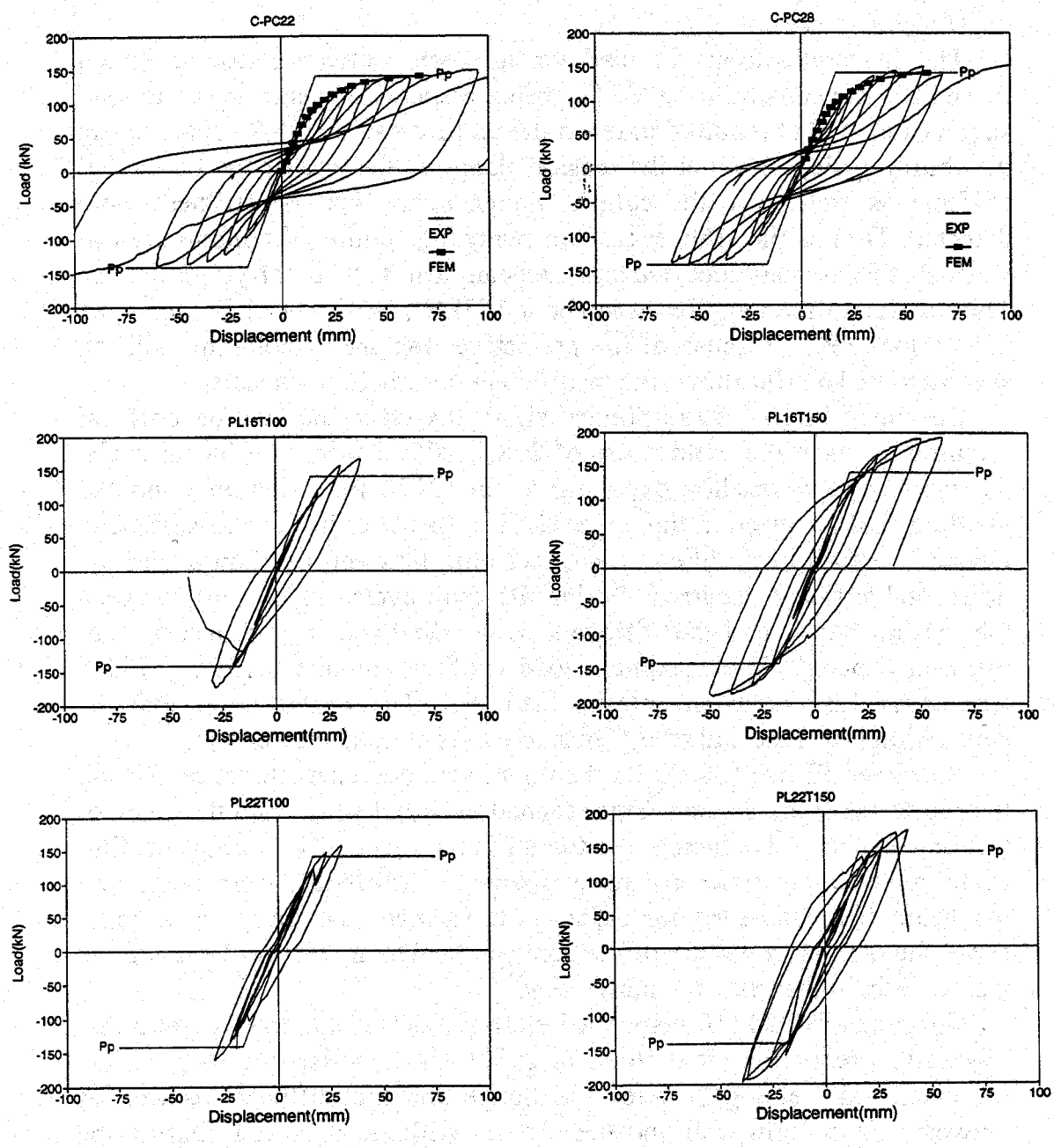

Fig. 8. Load versus displacement relationships for cyclic load

carrying capacity even when welding fracture occurred because of the bearing strength of concrete in tube column. Pinching behaviors were obtained after large deformation because of the slippage of bent plate in concrete as commonly shown in concrete connections. The ultimate load was slightly higher than the plastic capacity of the beam. Numerical results from finite element analysis are also plotted for the monotonic

loading. Close agreement is observed between finite element values and the skeleton curves of test.

The hysteretic loops of load versus beam deflection for specimen PL16T100 are shown in Fig. 8. The beam responded elastically up to load slightly below that required to reach the yield stress of 298.9 MPa. During the fourth cycle, cracks at the tension flange at the end of the horizontal stiffener as well as at the column flange at the vertical stiffness were detected. During the fifth cycle, the punching failure of column wall at vertical stiffness was occurred and the beam lost its load-carrying capacity. The maximum load applied was about 173kN, which was 1.23 times the plastic load (P_p). Because of the premature fracture of column wall, the specimen PL16T100 shows the insufficient deformation capacity.

Specimen PL16T150 responded elastically up to the load beyond that required to reach the yield stress of 298.9 MPa. During the fourth cycle, the beam flange reached the yield strain (2132 micro strain), and the yielding first occurred at the upper tension flange at horizontal stiffeners. During the fifth cycle, the crack of welding between the flange and the horizontal stiffness occurred. During the sixth cycle, all welding between the tension flange and the stiffeners were failed and the beam lost load-carrying capacity. The maximum load applied was about 193kN, which was about 1.37 times the plastic load (P_p). The results show that the connection is ductile and results in stable hysteretic characteristics.

Specimen PL22T100 shows the poor hysteretic characteristics. During the fourth cycle, the beam flange reached the yield stress, and the crack of welding between the flange and the stiffeners occurred. During the fifth cycle, all welding between tension flange and stiffeners were failed and the beam lost load-carrying capacity. It seemed that the poor welding cause the premature failure of the connection. The maximum load applied was slightly higher than the plastic load.

Specimen PL22T150 responded elastically up to the load beyond that required to reach the yield stress of 298.9 MPa. During the fourth cycle the cracks of welding between the flange and the stiffeners as well as between the column wall and the vertical stiffness occurred. During the fifth cycle, local buckling of compression flange occurred and loading hinge at right side was broken. The maximum load applied was about 198kN, which was 1.4 times the plastic load (P_p). The connection was expected the stable hysteretic loops, however, it lost load-carrying capacity due to the failure of loading hinge.

All specimens carried loads well above the plastic load of the beam. Specimens for monotonic load exhibit sufficient strength, stiffness, and deformation capacity. Specimens, C-P22 and C-P28 maintained stable characteristics even though they showed pinching behavior. If stiffeners

were designed and constructed properly, PL16T100 and PL22T100 would exhibit enough capacity to absorb and dissipate energy. However, specimens for cyclic loading in which a crack of a welding was initiated failed quite abruptly and showed insufficient deformation capacity. Welding procedures as well as workmanship are critical to the performance of the connection. Welding location for vertical stiffness was the end of round corner of cold-formed tube section. For the detail of cold-formed section, tensile forces of vertical stiffness are transferred to the web of column through shear stress while for the built-up section the forces of stiffeners are transferred to the web directly. Because of localized yielding due to cold forming, the tube sections include larger residual stress than the hot rolled sections. Welding at the end of round corner could cause the premature shear failure of column wall. Cold-formed round-corner column should be used carefully to avoid shear failure. Cold-formed section should be used carefully for the general application even in moderate seismic environment unless adequate plastic deformations are obtained.

5. Conclusions

A series of investigations, both analytically and experimentally has been carried out to study the effect of T-stiffeners on the behavior of box-column to H-beam connections. The analytical results showed good agreement with the test results. All nine specimens attained more than the plastic load of beam. Except specimens PL16T100 and PL22T100 with narrower T-stiffeners, all specimen exhibit sufficient deformation capacity. Bent plates without T-stiffeners may be good enough to resist seismic loading in moderate seismic zone. Cold-formed tube sections should be used carefully to avoid the welding fracture at the round corners of section. Wider T-stiffeners in cold-formed boxes are recommended than in the built-up boxes.

6. Acknowledgments

The investigation presented in this paper is part of research on Concrete-filled Column Connections being carried out in the STructure RESearch Station (STRESS). The writer gratefully acknowledge the support of STRESS.

7. References

ANSYS, (1996) Computer Program for the Static and Dynamic Finite

Element Analysis of Structure, ANSYS Inc., Version 5.3.

Shin, K.J., (1996) Behavior of Concrete-filled Column Connections using Plates, advanced STructure RESearch Station (STRESS) Report, Hanyang University.

Lee, S.L. and Shanmugam, N.E., (1993) Use of External T-stiffeners in Box-column to Beam Connections, Journal of Construction Steel Research, Vol. 26, 77-98.

Groux, Y.M. and Picard, A. (1977) Rigid Framing Connections for Tubular Column, Canadian Journal of Civil Engineering, Vol. 4, 143-144.

Dawe, J.L. and Groundin, G.Y., (1990) W-shape beam to RHS Column Connections, Canadian Journal of Civil Engineering, Vol. 17, 788-797.

Tsai, K.C., Wu, S. and Popov, E.P., (1995) Experimental Performance of Seismic Steel Beam-Column Moment Joints, Journal of Structural Engineering, ASCE, Vol. 121, No.6, 925-931.

Workshop on Structural Design Issues for Moderate Seismic Zones
February 24-25,1998, Urbana, Illinois

INELASTIC BEHAVIOR OF STEEL GIRDER CONNECTIONS TO CONCRETE-FILLED STEEL TUBE COLUMNS

S. P. SCHNEIDER, Associate Professor, Department of Civil Engineering,
University of Illinois at Urbana-Champaign, Urbana, IL, 61801, USA

ABSTRACT

Six large-scale connections were tested to failure using the quasi-static test method. All details consisted of a connection-stub which was to be shop fabricated and field bolted or welded in a less critical region for construction. Experimental results indicate that the inelastic connection behavior was very dependent on the type of connection detail. Connections welded to the skin of the tube created large distortions of the tube wall, and were susceptible to weld, flange or tube wall fracture. External diaphragm and continuous web details exhibited more favorable inelastic behavior, but the flexural strength of these connections began to deteriorate relatively early in the imposed deformation history. Deformed bars welded to the girder flange and embedded into the concrete core exhibited promising ductility with large flexural strength. Continuing the flanges through the composite column showed adequate strength, however due to excessive slipping this connection did not dissipate significant inelastic dynamic energy. Continuing the girder section through the composite column appeared to be the most effective detail to achieve the ideal rigid connection condition.

KEY WORDS: Concrete-filled steel tube columns, connections, large-scale tests.

1. INTRODUCTION

Concrete-filled steel tube (*CFT*) columns combine the advantages of ductility generally associated with steel structures with the stiffness of concrete components. The advantages of the concrete-filled steel tube column over other composite systems includes: the steel tube provides formwork for the concrete, the concrete

prolongs local buckling of the steel tube wall, the tube provides excessive concrete spalling, and composite columns add significant stiffness to a frame compared to more traditional steel frame construction. While many advantages exist, the use of *CFTs* in building construction has been limited due, in part, to a lack of construction experience and to the complexity of connection detailing. This paper summarizes part of an experimental program to study a variety of details to connect a steel girder to a circular *CFT* column.

Test data exists on a variety of connections details. Details that connect the girder to the steel tube only include: welding the girder directly to the skin of the steel tube (Valbert 1968), using web angles or shear tabs to connect the girder to the column (Shakir 1992; Bridge 1992), providing external or internal diaphragms (Kato *et.al.* 1992; Morino *et.al.* 1992), and variations of these details (Ansourian 1976). Conclusions from these studies suggest that connections loading the skin of the steel tube only can cause excessive deformation demands on the tube wall and connection components. Connections that attempted to improve this behavior include: through bolting girder end-plates (Prion*et.al.* 1992, Kanatani *et.al.* 1987), and continuing the structural steel shape through the column (Azizinamini*et.al.* 1992). Comparison of test data suggests that embedding connection components into the concrete core alleviates high shear demand on the tube wall, which may improve the seismic performance of the connection. The object of the research was to investigate the inelastic flexural behavior for a wide-range of connection details.

Six large-scale connections were tested in this research program and are shown in Fig. 1. Because of the difficulty in connection detailing, only circular tube columns were considered in this study. In general, the type of connection detail needed for a frame may depend on the relative size of the column and the girder at the joint. For example, the simple welded *Type I* connection may be more suitable for large diameter pipes, or perhaps thick tube walls, while the diaphragm *Type II* detail may be more appropriate for small diameter tubes. However, to compare the inelastic behavior of all connection details, the steel tube and the girder were kept constant for this study. Each tested connection consisted of a *356 mm* diameter pipe with a *6.4 mm* wall thickness, and a *W14x38* for the girder. The yield strength of the pipe and the girder was *320 MPa*, with an approximate concrete strength of *35 MPa*.

The primary interest of this research program was to investigate connections that develop the full flexural strength of the connected girder. To accomplish this, it was important to detail connections to just develop the plastic bending strength of the girder, as might be done in practice. Therefore, all of these connections were intended to just develop M_p of the girder at the face of the *CFT* column. Since

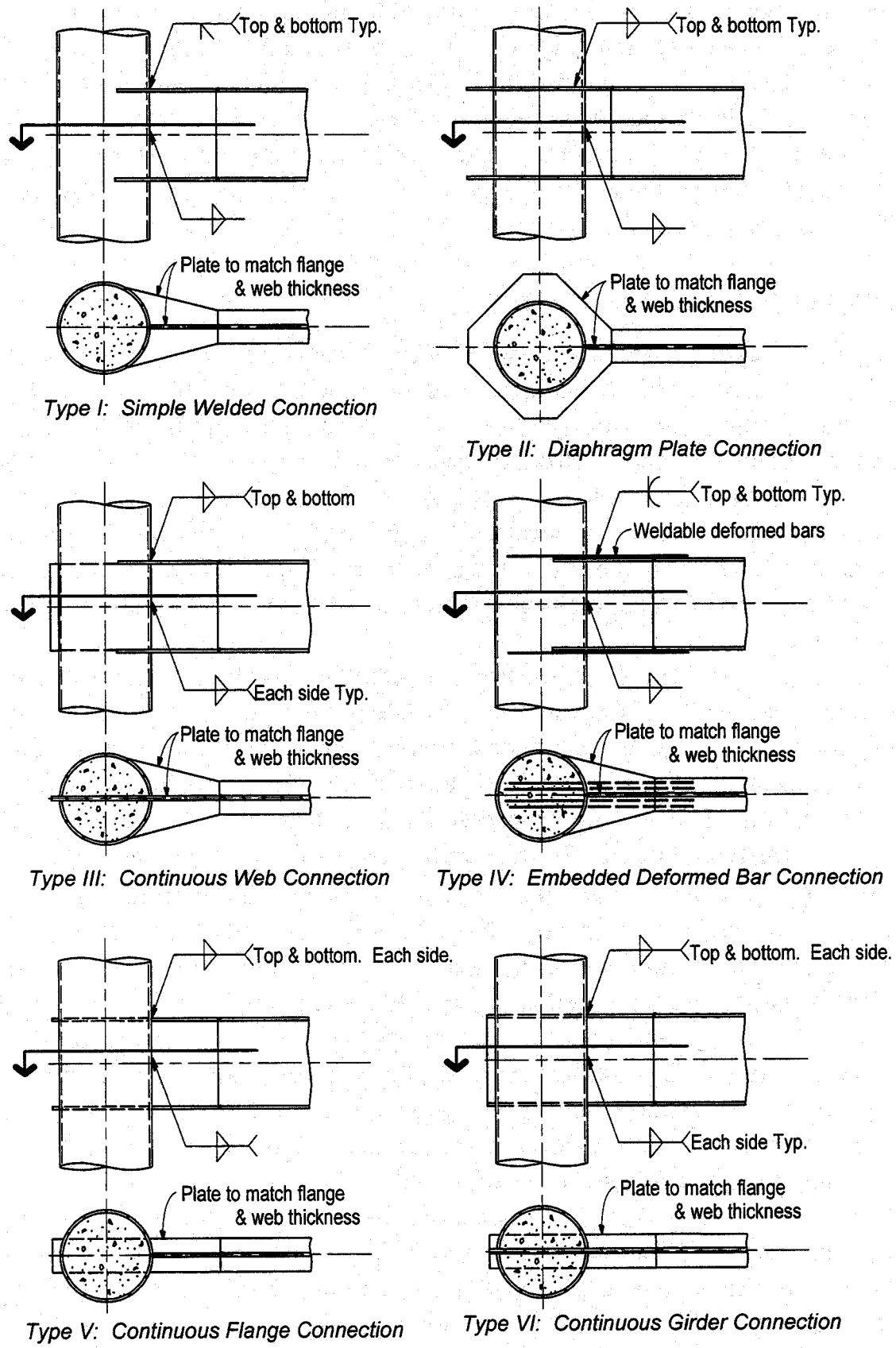

Figure 1. Connection Details

connection behavior was the primary interest, and not joint or panel zone behavior, the girder connected to only one side of the *CFT* column was sufficient. Consequently, a tube column and single girder specimen was tested, and cyclic deformations were imposed on the tip of the cantilever at a distance of *2.75m* from the face of the *CFT* column. The cyclic deformation history followed the recommendations provided by the *ATC-24 Guidelines for Cyclic Seismic Testing of Components* (ATC-24).

2. EXPERIMENTAL INVESTIGATION

The inelastic cyclic moment-rotation (M-θ) behavior for each connection is shown in Fig. 2. The reported normalized moment is the moment measured at the face of the *CFT* column divided by the plastic bending strength of the girder, M_p, computed using the actual strength and geometric properties of the *W14* section. The rotation was measured by a series of displacement transducers distributed along the girder depth with an initial gauge length being the distance between the column centerline and the end of the connection stub. Figs. 3 and 4 show the moment envelope and the measured effective stiffness, respectively, for each tested connection.

For the simple *Type I* connection, the girder was welded directly to the skin of the steel tube wall. Consequently, the steel tube was subjected to high local distortions adjacent to the connected region. Fracture initiated in the connection stub at a rotation of *1.25%*, and propagated into the tube wall by approximately *2.75%* rotation. This tearing propagate from the tips of the flange toward the web. Only one flange fractured, the tube wall separated from the concrete core for the other flange as it was subjected to tension. This resulted in an unsymmetric M-θ behavior and pinching of the hysteretic curves. Degradation in flexural strength began once the flange fractured, and continued upon subsequent deformation cycles. This fracture precipitated high shear demand on the web plate, which led to fracture of the weld between the web and the pipe wall. Consequently, the girder lost all of its gravity-load-resisting capacity shortly after flange failure. The stiffness of this connection was *85%* of the ideal rigid connection condition. Further, this connection exhibited the earliest decay in the effective stiffness, clearly due to the large distortions of the tube wall.

The external diaphragms of connection *Type II* were intended to alleviate the severe distortion of the steel tube skin. These diaphragms improved the cyclic behavior of the simple connection significantly. Each diaphragm fractured at approximately *2.0%* rotation. Upon subsequent imposed deformation cycles, the

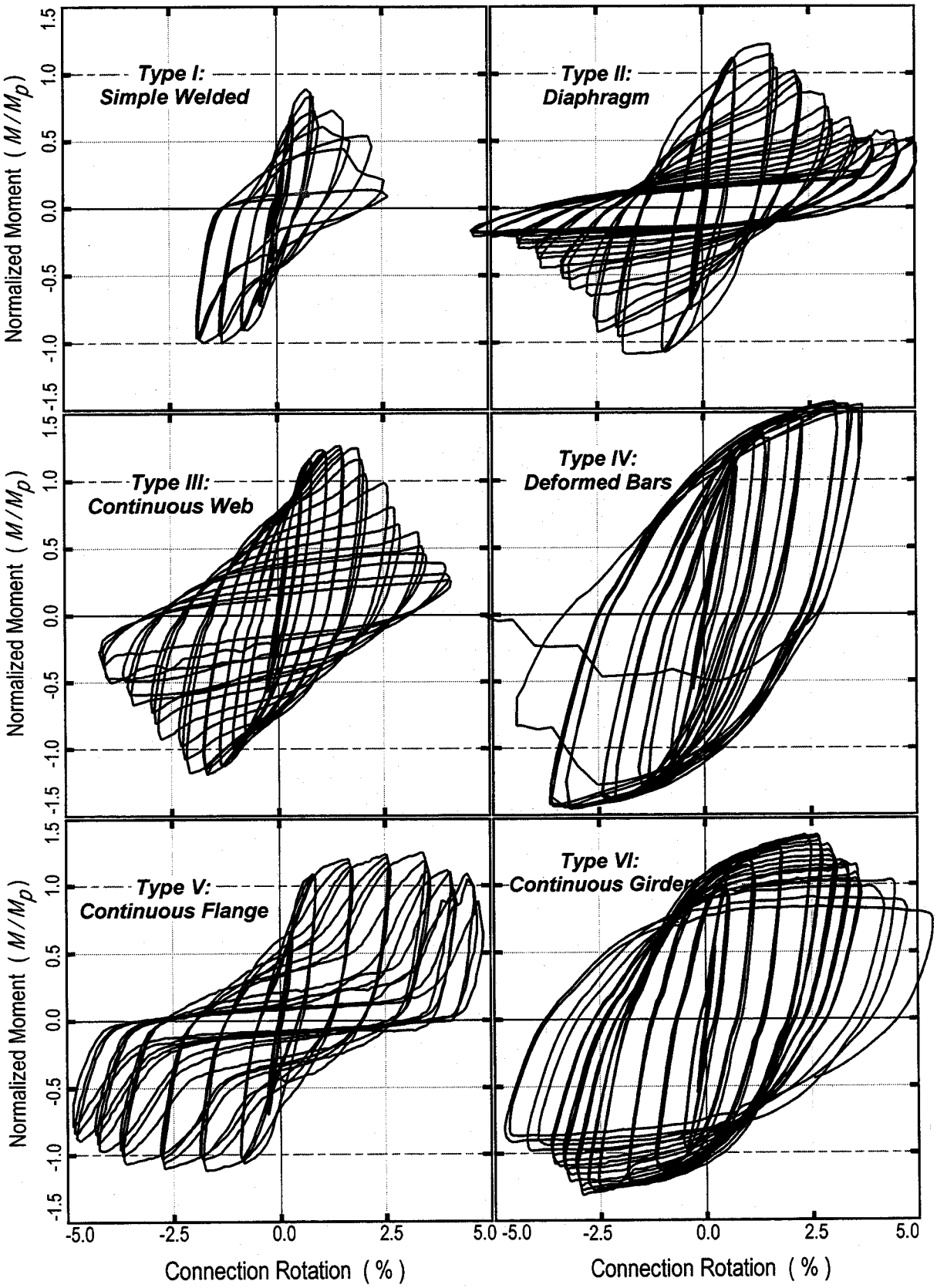

Figure 2. Moment-Rotation Behavior for Tested Connections

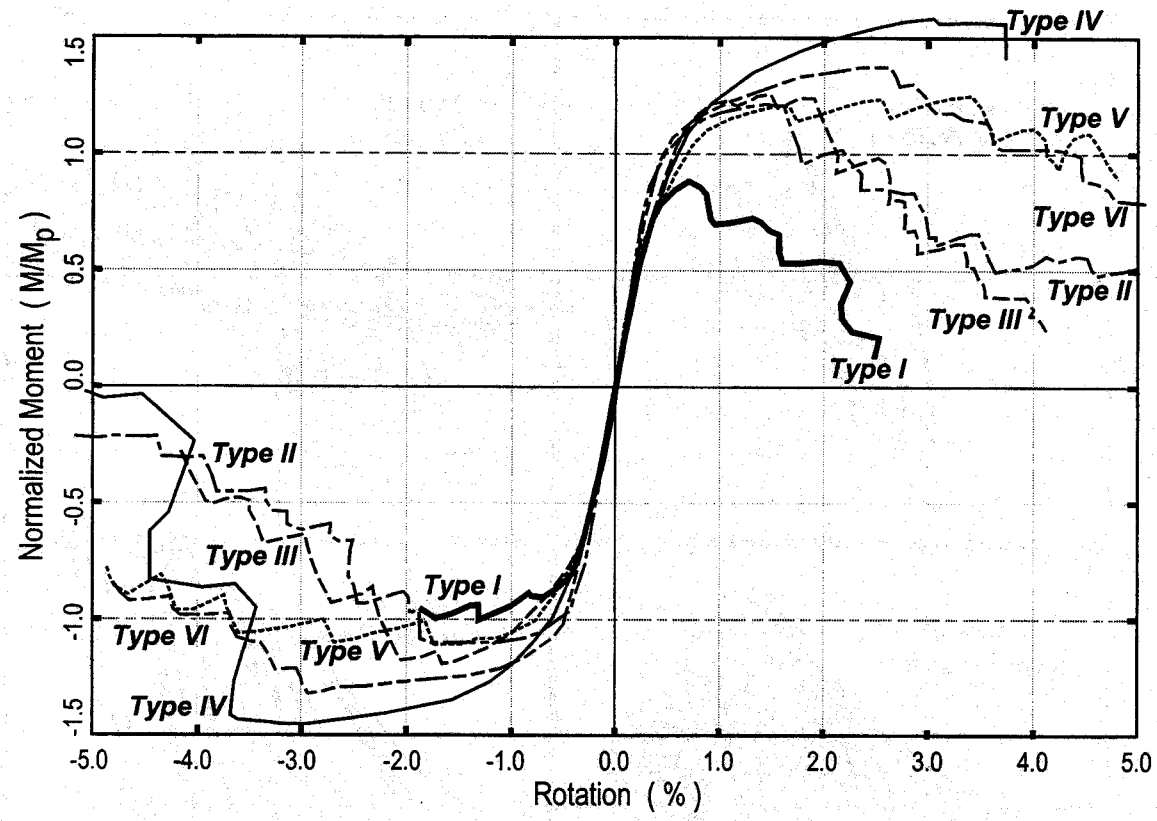

Figure 3. Moment-Rotation Envelope Curves for Tested Specimens

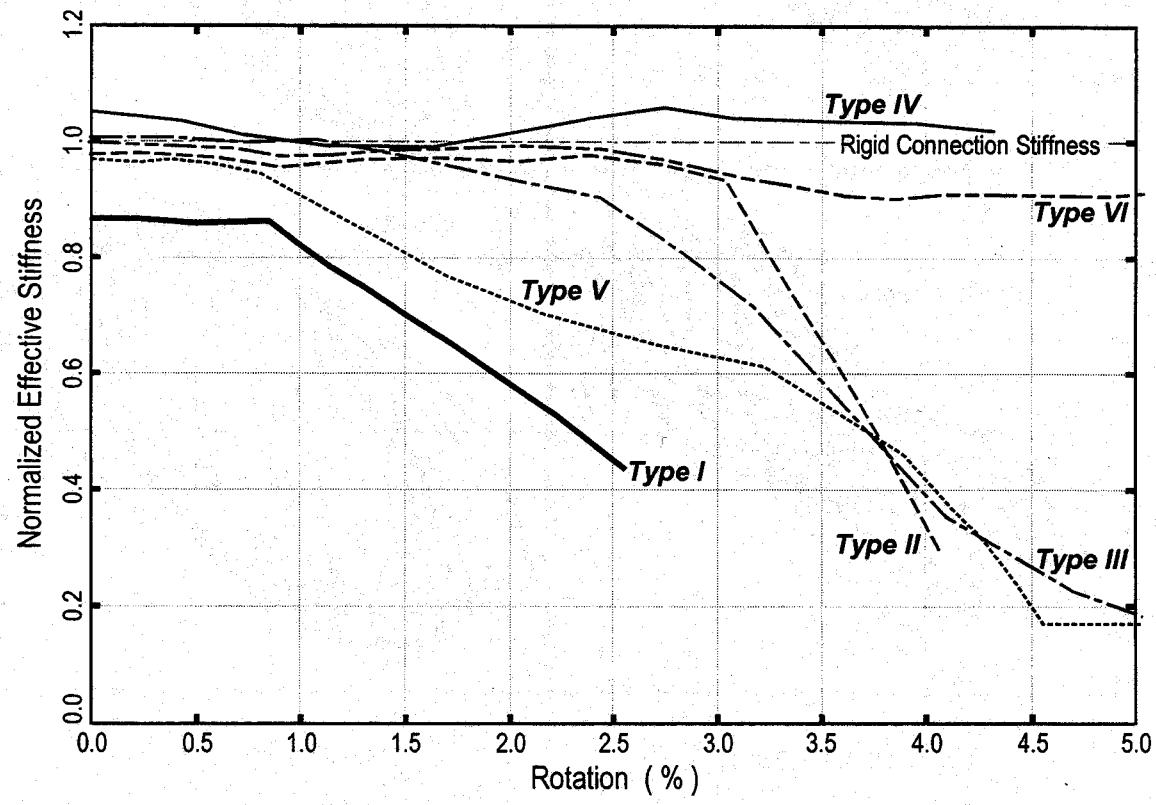

Figure 4. Variation of the Effective Stiffness

fracture propagated in each diaphragm, eventually tearing the tube wall at a rotation of *3.5%*. Deterioration of the *M-θ* behavior occurred at the onset of diaphragm fracture. At large cyclic deformations, the diaphragm buckled and the tube wall fractured along the depth of the girder. External diaphragm plates also exhibited reasonably stiff behavior, with relatively little deterioration before *3.0%* total rotation.

The intent of the continuous web *Type III* detail was to improve the flexure and the shear behavior of the simple *Type I* connection. However, significant web tearing was still observed once the flange fractured. Similar to the simple connection, the flange fracture exacerbated the high strain demands on the extreme fiber of the web. Because of the embrittlement of the web in the heat affected zone, tearing initiated close to the fillet weld that attached the web to the pipe wall. Fracture initiated at approximately *2.0%* rotation, creating a *20%* decrease in the peak flexural strength by the end of the imposed deformation cycles. Eventually, this fracture propagated from each flange toward the center of the web. A significant portion of the web was fractured by approximately *2.5%* total rotation, resulting in diminished hysteretic performance of the connection for large imposed rotations. The effective stiffness deterioration of the connection detail was reasonably gradual beginning at approximately *1.5%* total rotation.

Connection *Type IV* was identical to connection *Type I*, except four *20 mm* diameter (F_y=*420 MPa*) weldable deformed bars were embedded in the concrete core through holes drilled in the steel tube wall. Each deformed bar was then welded to the girder flange, and the weld was sufficient to develop *50%* more bar force than the minimum required weld. Embedment lengths were sufficient to develop the deformed bar under tested conditions. The *M-θ* behavior of the detail was a significant improvement compared to connection *Type I*. Initial wall tearing was observed at *3.0%* total rotation, however, this tearing was located in the tube wall between the openings for the deformed bars. The minor wall tearing did not affect the subsequent inelastic performance of the connection. Local flange buckling was also observed at a *3.0%* total rotation, which occurred in the girder beyond the connection region. This suggests that the connection was strong enough to initiate significant yield in the girder flange. Failure of the connection was caused by fracture of the deformed bars at approximately *3.75%* total rotation. Three of the four bars failed by tension rupture, while one bar pulled out of the concrete core. No significant stiffness or strength loss was observed prior to the fracture of the deformed bars. Each deformed bar that failed in tension ruptured between the end of the tube wall and the first weld location attaching the bar to the girder flange. The effective stiffness of this connection ranged between *98%* and

106% of the ideal rigid connection conditions, and did not appear to deteriorate over the range of imposed deformations. This increased connection stiffness was likely due to the added stiffness of the deformed bars on the top of each flange.

The *Type V* connection detail was tested to study the effect of continuing only the flanges through the *CFT* column. Flange plates were welded to the tube wall on each side of the column to transfer girder flange forces. The resistance was to have been induced by bearing of the steel tube against the concrete core, provided the continuity flange plate weld remained intact with the steel tube skin. No attempt was made to enhance the bond between the embedded flange plate and the concrete core. The lack of bond impacted the hysteretic performance of this connection significantly compared to other connection types. Both flange welds on the girder side of the column connection fractured at approximately *1.0%* rotation, and the flange plate welds on the opposite column side remained intact. This resulted in a tube wall fracture on the *CFT* face opposite the girder. Subsequent cycles only increased the tearing of the tube wall. As new deformation amplitudes were reached the connection resistance increased, but the resistance diminished upon subsequent same-amplitude cycles. This resulted in excessive pinching of the hysteretic behavior. The stiffness of this connection detail was larger than the simple welded *Type I* connection, however, stiffness deterioration was significant and began when the flange weld fracture was first observed.

Results of connection *Type VI* exhibited quite stable inelastic behavior. Local flange buckling was observed at approximately *2.75%* total rotation, and the web buckling was observed at about *3.0%* total rotation. Deterioration of the inelastic characteristics were observed after the onset of local web buckling. Failure of the connection was caused by fracture of the beam flange in the connection stub region. This flange tearing eventually propagated into the web. Although the flexural strength decreased approximately *30%* compared to the peak values, the hysteretic behavior remained stable even at large rotations. No crushing of the concrete was observed, and the tube wall showed no apparent signs of local distress. The effective stiffness remained equivalent to that of the ideal rigid connection condition throughout the imposed deformation history.

3. CONCLUSIONS

In general, inelastic connection behavior improved significantly when a larger portion of the girder force was transferred to the concrete core. However, the inelastic performance depended significantly on the connection detail. Some conclusions from this study are worth noting:

1. Connection *Type I* could not develop the plastic bending strength of the girder, while the flange, the weld, and the tube wall were susceptible to fracture. This connection lost almost all of its flexural strength at moderate rotations, and because of the high ductility demand on the web it subsequently lost its ability to resist gravity loads. This connection should not be used in moment-resisting frames to be constructed in regions of high seismic risk.
2. Connection *Type II* was able to develop the plastic bending strength, however, the inelastic properties deteriorated rapidly at the onset of diaphragm fracture. If the diaphragm is designed properly for the shear flow, this connection may alleviate some of the tube wall tearing observed in connection *Type I* behavior, and may extend the shear capacity of the connection. This connection, with modification, might be used in regions of seismic risk.
3. Extending the web through the *CFT* column, as in connection *Type III* improved the inelastic performance of the simple connection. However, the *Type III* connection still experiences significant web tearing and an eventual deterioration of the gravity-load-resisting capacity. Therefore, it appears necessary to prevent the flange or tube wall fracture to prevent excessive damage on the shear tab. Partially embedded shear tabs may prevent a complete loss in the gravity-load resistance. The tested detail may be more appropriate for braced connections.
4. Weldable deformed bars transferred much of the flange stresses into the concrete core. This connection *Type IV* exhibited considerable improvement compared to the simple *Type I* connection detail, and has the potential to be used in seismic regions. However, the quality of the installation of the deformed bars is critical.
5. Continuing the flange plates, as tested by the connection *Type V* detail, did not produce satisfactory inelastic cyclic behavior. The inability of the weld to transfer flange forces to bearing stresses on the concrete core on either side of the column resulting in large deformations with little resistance unless a new deformation amplitude was imposed. This produced significantly pinched hysteretic behavior. This connection detail should be modified before it can be used in frames constructed in seismic regions.
6. The through *CFT* column *Type VI* connection detail exhibited favorable hysteretic behavior. This appeared to be the most effective method to develop the plastic bending strength of the steel girder, and was the closest to representing ideal rigid connection conditions. While there appeared to be a *30%* decrease in flexural strength, the subsequent flexural resistance was equivalent to the plastic bending strength of the girder. Further, the cyclic behavior remained stable even at very large inelastic rotations.

4. ACKNOWLEDGMENTS

Results in this paper are based upon research funded by the National Science Foundation under Grant *NSF CMS 93-00682* with Dr S.C. Liu as the program director. Support for this work is gratefully acknowledge. Opinions expressed in this paper are those of the author, and do not necessarily reflect those of NSF.

5. REFERENCES

ATC-24 (1992). "Guidelines of Cyclic Seismic Testing on Components for Steel Structures." *Applied Technology Council*. Redwood City, CA.

Ansourian, P. (1976). "Connections to Concrete-Filled Tube Columns." *International Association of Bridge and Structural Engineers*, 36-I, pp. 1-22.

Aziznamini, A. and B. Prakash (1992). "A Tentative Design Guidelines for a New Steel Beam Connection Detail to Composite Tube Columns." *AISC Engineering Journal*, 3rd Quarter, pp. 108-115.

Bridge, R. and J. Webb (1992). "Thin Walled Circular Concrete-Filled Steel Tubular Columns." *Composite Construction of Steel and Concrete II, ASCE*, pp. 634-649.

Kanatani, H., M. Tabuchi, T. Kamba, J. Hsiaolien and M. Ishikawa (1987). "A study on Concrete-Filled RHS Columns to H-Beam Connections Fabricated with HT Bolts in Rigid Frames." *Composite Construction of Steel and Concrete, ASCE*, pp. 614-635.

Kato, B., M. Kimura, H. Ohta and N. Mizutani (1992). "Connections of Beam Flange to Concrete-Filled Tubular Columns." *Composite Construction of Steel and Concrete II, ASCE*, pp.528-538.

Morino, S., J. Kawaguchi, C. Yasuzaki and S. Kanazawa (1992). "Behavior of Concrete-Filled Steel Tubular Three Dimensional Subassemblages." *Composite Construction of Steel and Concrete II, ASCE*, pp. 726-741.

Prion, H.G.L. and A.B. McLellan (1992). "Connecting Steel Beams to Concrete-Filled Steel Columns." *In Proceedings, ASCE Structures Congress on Composite Compression Members*, San Antonio, TX, pp. 918-921.

Shakir-Khalil, H. (1992). "Full-scale Tests on Composite Connections." *Composite Construction of Steel and Concrete II, ASCE*, pp. 539-554.

Valbert, G. (1968). "Essais d'Assemblages Soudes d'une Solive Sur un Poteau en Tube Rempli de Beton." *Construction Metallique*, 4 Dec., pp. 27-38. (in French).

Workshop on Structural Design Issues for Moderate Seismic Zones
February 24-25, 1998, Urbana, Illinois

MODELING AND PERFORMANCE EVALUATION OF STEEL FRAME BUILDINGS UNDER SEISMIC LOADS

C.-H. Wang[1], Y. K. Wen[2]
1) Graduate Research Assistant, University of Illinois at Urbana-Champaign, USA
2) Professor, University of Illinois at Urbana-Champaign, USA

Abstract
The recent Northridge and Hyogoken-Nanbu earthquakes revealed that the highly regarded ductile welded steel moment frame buildings for seismic forces are vulnerable to brittle connection fracture failures. The performance of a large number of such structures in the building stock against future earthquakes has become a legitimate concern to the profession and needs to be investigated. For this purpose, a 3-D dynamic structural analysis method is developed which can account for biaxial and torsional effects of inelastic, degrading structures, brittle connection fracture, and member failure. Numerical examples and results are given.

Key words: Hysteresis model, Biaxial interaction, Reliability, Redundancy.

1 Introduction

The welded steel moment frame (WSMF) buildings had long been regarded as the best system against lateral loads such as those due to earthquakes because of its large ductility capacity. In the 1994 Northridge earthquake and the 1995 Hyogoken-Nanbu earthquake, however, there were many connection brittle fracture failures. The test results of steel connections in the recent SAC program in the US have verified the field ob-

servations and also shown a large variability in the load carrying capacity of these connections.

Member failure or connection fracture may alter the dynamic properties of structures such as vibration periods and mode shapes. Furthermore, torsional motion may be significantly increased so that structural response may be considerably amplified. Therefore, a dynamic structural analysis that can account for such effects is necessary to fully understand structural behavior under seismic loads. Currently available computer programs such as DRAIN-2DX and IDARC, however, are primarily for analysis of plane frames, therefore can not be used for study of torsional effect and biaxial interaction. Also, new models are needed for brittle connection fracture.

A methodology for inelastic, dynamic three-dimensional analysis of multistory building structures is presented herein. This model can account for biaxial and torsional response, pinching and connection fracture, and member failure of inelastic, degrading structures. Therefore it can be used to investigate the adequacy of building performance under future earthquakes.

2 Smooth hysteresis model for restoring moments

In inelastic dynamic structural analysis, restoring force models are needed which can account for various degrees of non-linearity and yet are efficient in computation. A smooth hysteresis model proposed by Wen (1980), and Park, Wen and Ang (1986) can be used for this purpose.

For a single degree of freedom, orthotropic system with different stiffness in the structural principal directions, the restoring moments can be expressed as

$$\begin{cases} H_x = \alpha k_x h_x + (1-\alpha)\ k_x z_x \\ H_y = \alpha k_y h_y + (1-\alpha) k_y \dfrac{\Delta_y}{\Delta_x} z_y \end{cases} \tag{1}$$

in which α is the post-to-pre-yielding stiffness ratio; k_x and k_y are the stiffness along X- and Y-axes, respectively; h_x, h_y and z_x, z_y are the elastic and hysteretic displacements, respectively; Δ_x and Δ_y are the yield rotations with respect to X- and Y-axes; z_x and z_y satisfy the following coupled differential equations:

$$\begin{cases} \dot{z}_x = \frac{1}{\eta}\{A\dot{h}_x - \nu[\beta(|\dot{h}_x z_x|z_x + \frac{\Delta_x}{\Delta_y}|\dot{h}_y z_y|z_x) + \gamma(\dot{h}_x z_x^2 + \frac{\Delta_x}{\Delta_y}\dot{h}_y z_x z_y)]\} \\ \dot{z}_y = \frac{1}{\eta}\{A\frac{\Delta_x}{\Delta_y}\dot{h}_y - \nu[\beta(\frac{\Delta_x}{\Delta_y}|\dot{h}_y z_y|z_y + |\dot{h}_x z_x|z_y) + \gamma(\frac{\Delta_x}{\Delta_y}\dot{h}_y z_y^2 + \dot{h}_x z_x z_y)]\} \end{cases} \quad (2)$$

in which A, β and γ are parameters controlling the shape of hysteresis; η and ν are parameters controlling the pre-yielding stiffness and ultimate strength, respectively. For deteriorating systems the parameters A, η and ν vary with time characterizing the extent of structural damage. The above model is for restoring moments without fracture. Additional considerations for connections with fracture failure will be given in Section 5.

3 Equations of motion of asymmetric multistory buildings

A two-story steel building with mass eccentricity is shown in Figure 1. Although the building is symmetric, the formulation given below applies also to buildings with asymmetry. Each floor diaphragm, of mass M_i and moment of inertia I_i, is assumed to be rigid in its own plane but flexible out-of-plane, which is reasonable for the floor system. By this assumption, the movement of the diaphragm at each floor level can be characterized by 3 rigid-body degrees of freedom in its own plane: translation in the X and Y directions, plus a rotation about the vertical axis. In addition, because the floor diaphragms are flexible out-of-plane, the column ends are allowed to rotate with respect to X- and Y-axes.

It is assumed that inertial resistance to rotation at column ends can be neglected; therefore, in dynamic analysis the rotational degrees of freedom of the columns can be eliminated by static condensation. After performing static condensation, the equations of motion, excluding damping term, can be expressed in matrix form

$$M\ddot{u}_a + T_s S = -M\ddot{u}_g \quad (3)$$

in which M is the lumped mass matrix including the moment of inertia of translation and rotation of diaphragms; $\ddot{u}_a$ is the relative acceleration vector of the mass center of diaphragms with respect to the ground; $\ddot{u}_g$ is the vector of ground acceleration; S is the vector of column-end shears; the matrix T_s adds the column-end shears acting at a particular floor diaphragm, as well as the torsion induced by those shears.

4 Modeling of the asymmetric multistory buildings

The yielding of the buildings is assumed to being confined to discrete hinge regions, which is located at the member ends. For beams, because the bi-axial interaction effect is negligible, the hinge yielding is restricted to happen only with respect to one principal axis of the beam cross section. For columns, in order to take into account the biaxial interaction, each column end is able to form two hinges with respect to the two principal axes of the column cross section; therefore there may be up to four plastic hinges formed on one column.

The displacement vector u can be partitioned into two vectors, u_a consisting of all the degrees of freedom with inertia, and u_c consisting of those without inertia. The member-end rotations at joint j are the joint rotation minus the deformations of the connecting plastic hinges. Thus the member-end moments can be expressed as

$$\begin{Bmatrix} S \\ R \\ H \end{Bmatrix} = \begin{bmatrix} K_{SS} & K_{SC} \\ K_{RS} & K_{RC} \\ K_{CS} & K_{CC} \end{bmatrix} \begin{Bmatrix} u_a \\ u_c \end{Bmatrix} - \begin{bmatrix} K_{SH} \\ K_{RH} \\ K_{HH} \end{bmatrix} \{h - z\} \tag{4}$$

in which h is the vector of plastic hinge rotation, z is the vector of the hysteretic components of hinge rotations, S for column-end shears, R for member-end moments at ends without hinges, and H for member-end moments at ends with hinges. The member-end moments H should be equal to the hinge element moments; therefore

$$H = K_e h + K_z z \tag{5}$$

The vector z is determined by employing the smooth hysteresis model, written symbolically,

$$\dot{z} = g(\dot{h}, z) \tag{6}$$

Considering the fact that rotational masses are not present at joints, the joint rotational equilibrium may be expressed in terms of only the member-end moments; i.e.,

$$T_R \begin{Bmatrix} R \\ H \end{Bmatrix} = \{0\} \tag{7}$$

where the matrix T_R is for summing up the end moments at a particular joint.

Examining Eqs. (3)–(7), one can verify that the number of unknowns (which are u_a, u_c, h and z) equals the number of equations. Therefore the dynamic response of the building is completely described by these equations. Readers interested in the detailed solution scheme are referred to Wang and Wen (1997).

5 Behavior of brittle connection fracture

Since the biaxial interaction effects are small in beams, the uniaxial smooth hysteresis model is used. After beam fractures occur, however, the hysteresis loops usually are asymmetric. Therefore the restoring force model of Park, Wen and Ang (1986) is modified as follows

$$\dot{z} = \frac{\dot{u}_1}{\eta}\left\{A - \nu|z|^n\left[\beta \operatorname{sgn}(\dot{u}_1 z) + \gamma + \varphi(\operatorname{sgn}(z) + \operatorname{sgn}(\dot{u}_1))\right]\right\} \tag{8}$$

in which φ is an additional parameter to model asymmetric yielding behavior after beam fractures; the symbol sgn(·) stands for the signum function. To model the slip and pinching behavior after fracture the slip-lock element (Baber and Noori, 1985) is used. The slip rates of slip-lock elements are given as

$$\dot{u}_2 = f(z)\dot{z} \tag{9}$$

in which $\dot{u}_2$ is the vector of slip rates of slip-lock elements. The velocity of plastic hinge rotations, $\dot{u}$, is $\dot{u}_1 + \dot{u}_2$. Therefore

$$\dot{u}_1 = \dot{u} - f(z)\dot{z} \tag{10}$$

Substituting Eq. (10) into Eq. (5.1) and noting the fact that $\operatorname{sgn}(\dot{u}) = \operatorname{sgn}(\dot{u}_1) = \operatorname{sgn}(\dot{u}_2)$, $\dot{z}$ can be expressed as

$$\dot{z} = \frac{h(z)}{\eta}\left\{A - \nu|z|^n\left[\beta\,\mathrm{sgn}(\dot{u}z) + \gamma + \varphi(\mathrm{sgn}(\dot{u}) + \mathrm{sgn}(z))\right]\right\}\dot{u} \tag{11}$$

in which

$$h(z) = \frac{1}{1 + \frac{f(z)}{\eta}\left\{A - \nu|z|^n\left[\beta\,\mathrm{sgn}(\dot{u}z) + \gamma + \varphi(\mathrm{sgn}(\dot{u}) + \mathrm{sgn}(z))\right]\right\}} \tag{12}$$

is the so-called pinching function. f(z) controls the spread and severity of pinching and is given by

$$f(z) = \sqrt{\frac{2}{\pi}}\frac{a}{\sigma}\exp\left\{-\frac{1}{2}\left[\frac{\mathrm{sgn}(\dot{u})\frac{z}{z_u} - q}{\sigma}\right]^2\right\} \tag{13}$$

where a, q, σ are coefficients of the spread and severity of pinching, z_u is the ultimate value of z. Detailed discussion of those pinching parameters can be found in Baber and Noori(1985) and Foliente(1995).

Experimental results indicate that fracture mostly originated from the bottom side of beam flange (Kaufmann, et al, 1997). Furthermore, although extensive fracture sometimes propagated into beam web or even column flange and web, in many cases there remained some residual resistance at connections (SAC, 1995).

In this study, it is assumed that the occurrence of beam fracture is limited to the bottom side; i.e., the fracture occurs only when the beam segment is under positive moment. Results from SAC program indicate that the residual resisting moment after cracking is about 20–40% of the original strength. When the bending direction reverses, the crack is closed up and the fractured cross section regains 70–90% of its uncracked strength. As for columns, it is a reasonable assumption that once a column fracture occurs the damaged column has no resistance at all. In order to determine the occurrence of fracture, a damage index, proposed by Park, Ang and Wen (1984), which accounts for the effects of excessive displacement and cumulative damage, is used as a measure of the capacity against fracture failure.

For the analysis of structures with possible connection fracture failure, a threshold value of damage index is assigned to each structural member-end with plastic hinges. It is assumed that the fracture at a connection will occur at a particular time instant if the threshold value of the connection is exceeded. The residual resistance of the fractured connection to positive moment is then reduced to a fraction, e.g., 25% of the original strength. An example of the resultant hysteresis loops at fractured connections is shown in Figure 4.

6 Numerical studies

6.1 Effect of connection failure

Consider a two-story building as shown in Figure 1. The mass centers of floor slabs have an eccentricity of 2.5 ft and 3.75 ft in X- and Y-directions, respectively, with respect to the center of geometry. The first three vibration periods of the structure with rigid floor diaphragms are .396(Y-direction), .338 (X-direction), and .207 (torsion) seconds, while they are .616, .499 and .310 seconds, respectively, with a flexible diaphragm assumption.

A pair of earthquake records generated in Phase II of SAC project (SAC, 1997) for Los Angeles, California, is used as the ground motion; namely, LA27 (fault-normal) and LA28 (fault-parallel), shown in Figure 2.

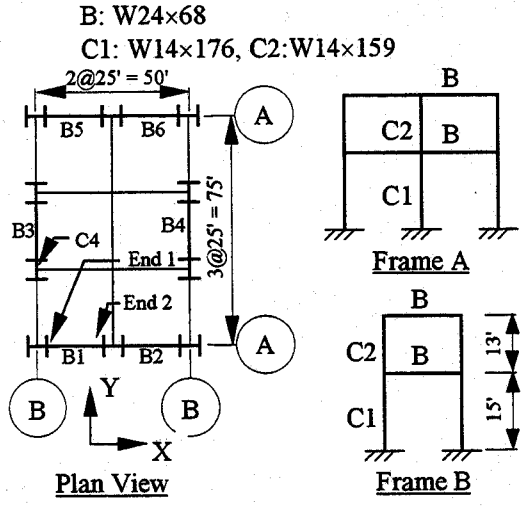

Figure 1. Example structure

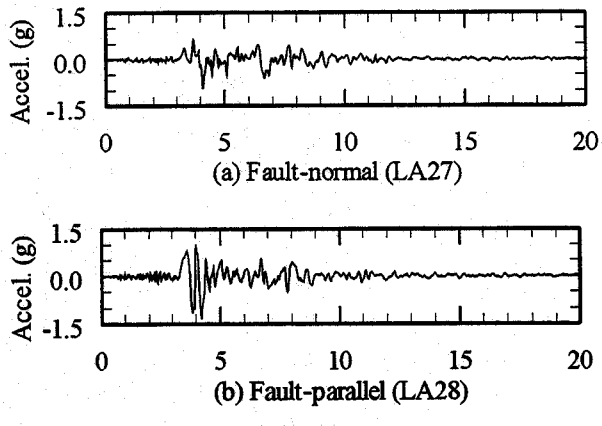

Figure 2. Time histories of a SAC-2 earthquake

The La27 and LA28 records are applied concurrently to the Y- and X-directions, respectively.

In the following computation, the damping ratios for the first two modes are assumed to be 2%; the rate of degradation for A, ν, and η are 0., .02, and .1, respectively. The P-Δ effect is taken into consideration. The residual strength of connections after cracking is assumed to be 30% of that before cracking on the cracked side and 90% on the uncracked side (SAC, 1996).

Six cases are investigated:

1. Floor diaphragms are rigid; structural members and connections are perfectly ductile.
2. Floor diaphragms are flexible; structural members and connections are perfectly ductile.
3. Same as in Case 2 except that beams 1–3 have a threshold value of damage capacity index of 0.1 for connection fractures, i.e., if the value is exceeded, connection fracture will occur.
4. Same assumptions as in Case 2 except beams 1–6 have a threshold value of damage capacity index of 0.1 for connection fractures.
5. Same assumptions as in Case 2 except beams 1 and 3 will fail completely once a damage index threshold value of 0.1 is reached.
6. Same assumptions as in Case 2 except that column 4 will fail completely once a damage index threshold value of 0.5 is reached.

Tables 1 and 2 list the maximum values of interested response quantities for the considered cases. Figure 3 shows the hysteresis loops for beam 1

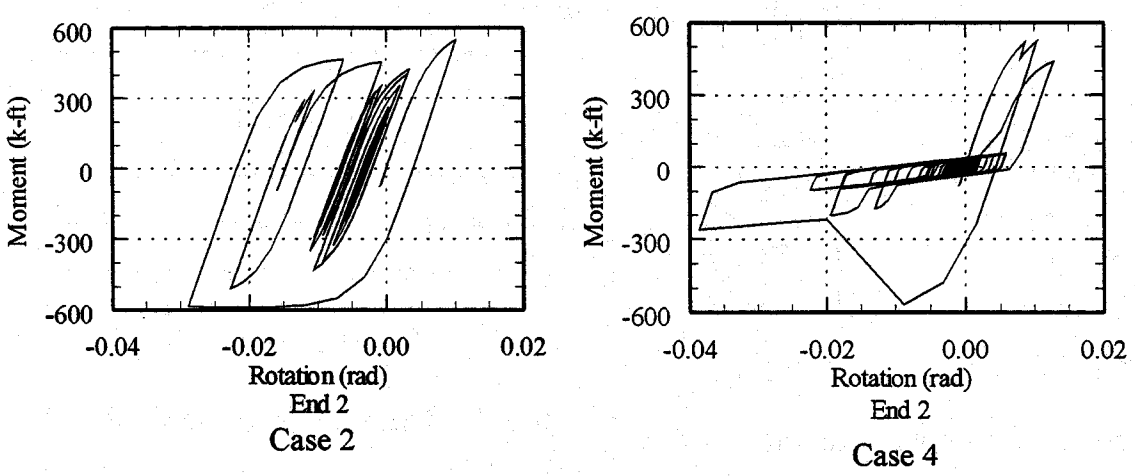

Figure 3. Hysteresis loops of beam 1

with and without fracture failure. Figure 4 shows the displacements of the 1st-floor mass center for cases 1 and 6. The effects of connection fracture, member failure, biaxial interaction and torsion are clearly shown in Tables 1 and 2 and Figures 3 and 4. The pinching and degradation of connection moment-rotation behavior compare favorably with test results (SAC, 1995).

Table 1. Maximum column drift ratios.

CASE	X (%)	Y (%)	D* (%)
1	3.012	1.125	3.106
2	4.664	4.023	4.936
3	4.645	4.560	4.806
4	4.907	4.807	5.089
5	4.929	5.186	5.483
6	4.664	5.831	6.019

* D denotes the maximum value of the absolute column drift ratios.

Table 2. Maximum displacements of 1st-floor mass center.

CASE	X (in)	Y (in)	R (rad), $\times 10^{-3}$
1	4.618	1.883	2.046
2	4.333	5.044	1.704
3	4.531	5.649	2.498
4	4.553	6.322	1.210
5	5.189	6.638	4.291
6	4.333	7.642	2.955

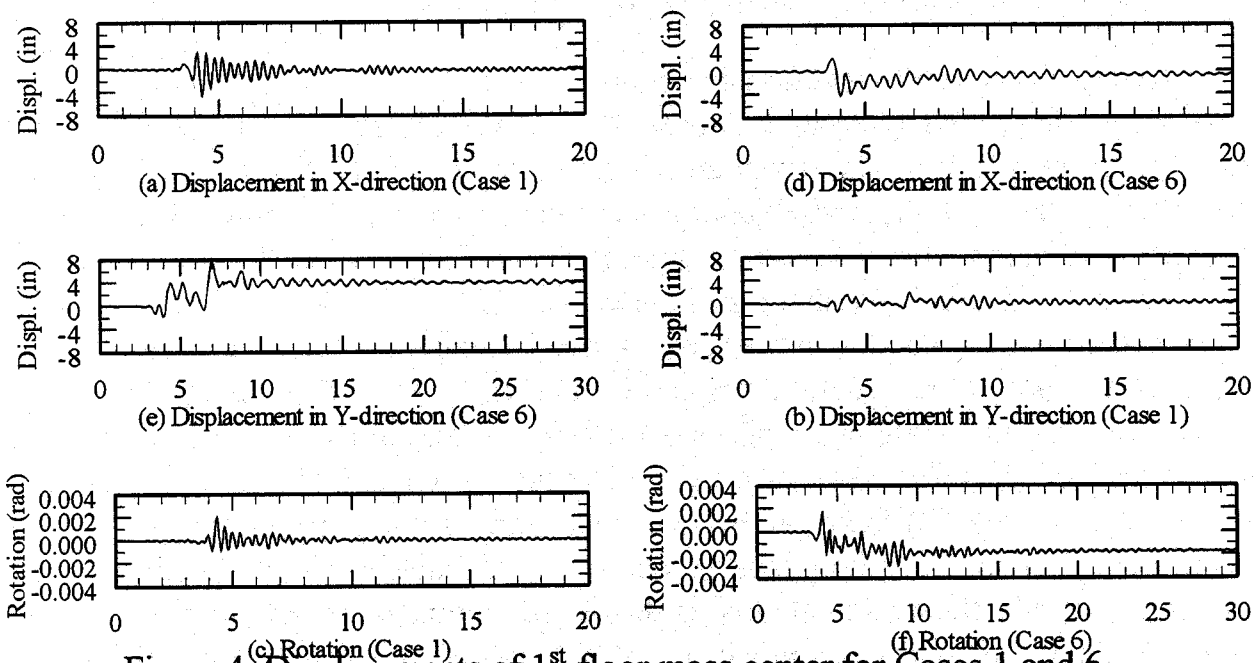

Figure 4. Displacements of 1st-floor mass center for Cases 1 and 6

Examining the results, the following can be inferred:

a. The flexible diaphragm assumption causes an increase in structural periods and, in this case, response amplification.
b. Comparing Case 2 to 3, as expected the torsion is significantly amplified by brittle fracture failure. However the displacements of floor mass centers in Case 3 increase only moderately, while the maximum column drift is even less than that in Case 2.
c. Comparison of Case 3 to 4 shows a somewhat unexpected result — the response with more fractured connections increases only moderately. This may be attributed to that (1) the fracturing of all 6 first-story beams are more symmetric compared to the fracturing of beams 1–3 only, (2) if fractured connections possess some residual strength, even as low as 30% of uncracked strength, it can have remarkable beneficial effects.
d. The comparison of Case 3 (or 4) and 5 again supports the finding in c. — total (unsymmetric) failures of beams 1–3 considerably amplify the response of the structure.
e. In Case 6, the response as well as permanent displacements increase drastically, confirming the expectation that any column failure can lead to serious consequences such as collapse.

6.2 Structural reliability and redundancy

The suites of ground motions in Phase II of SAC program are used as earthquake excitations. This program generated three suites of time histories corresponding to the probability of occurrence of 50%, 10% and 2% in 50 years. Each suite has 10 pairs of time histories. Each pair consists of a fault-normal and a fault-parallel time history.

In order to examine the influences of biaxial excitation and possible connection fracture on structural response, three cases are investigated: (1) Only fault-normal component of time histories is applied along the Y-direction, which is the weak direction, of buildings with ductile connections (no fracture); (2) fault-parallel and fault normal components are applied along X- and Y- directions respectively, of buildings with ductile connections; (3) fault-parallel and fault-normal components are applied along X- and Y-directions respectively, of buildings with possible connection fractures. Capacity against brittle joint failure is assumed to be random and randomly distributed through the building. To examine the effects of

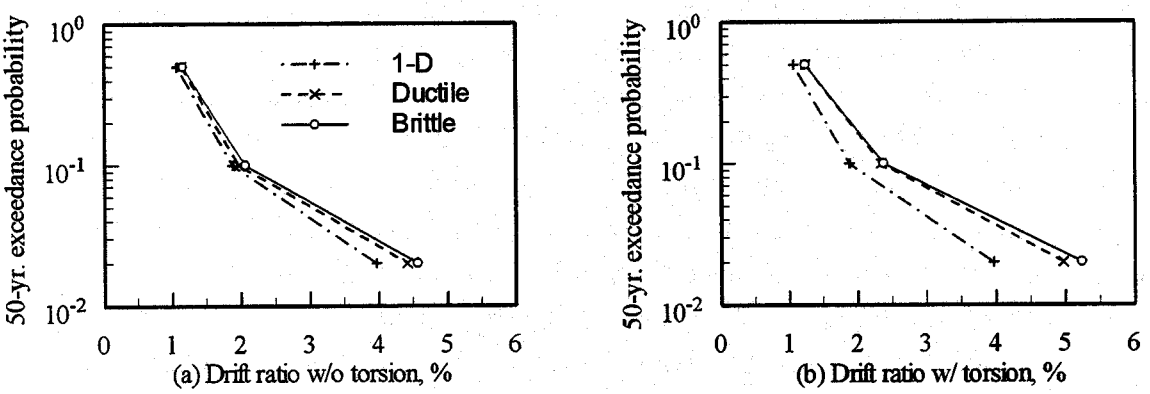

Figure 5. Maximum column drift ratio vs. 50-year probability of exceedance

torsional motion on structural response, the response of building without torsion was studied first. The median values of maximum column drift ratio without torsion at the three probability levels are shown in Figure 5(a). Figure 5(b) shows the results for buildings with torsion from mass eccentricity and unsymmetric connection fractures.

From Figure 5, it can be seen that: (1) when torsion is neglected, the differences among the results of the three cases are small at levels of 50% and 10% in 50 years. They become notable, however, at level of 2% in 50 years when biaxial excitation becomes important; (2) contrasting with the above observation, when torsion is included, the responses increase significantly at all probability levels. The effects of torsion and biaxial interaction, therefore, play an essential role in structural response; (3) the response amplification by connection fracture is only moderate compared to that by torsion and biaxial interaction, particularly at small probability levels. One contributing factor is that fractures may increase damping and shift the natural frequencies that may compensate the effect of the loss of strength after fracture.

7 Conclusions

The Northridge and Hyogoken-Nanbu earthquakes provided a severe test and showed the vulnerability of a large number of welded steel moment frame buildings. To investigate the safety and system performance of the structure, realistic modeling of the beam-to-column connection fracture and the out-of-plane flexibility of floor diaphragms are needed. For this purpose, a 3-D dynamic structural analysis model is developed which can account for biaxial and torsional effects, pinching and brittle connection

fracture, and member failure of inelastic, degrading structures. For verification, a 2×3 bay, 2-story steel building is analyzed using SAC-2 earthquake ground motions. It was found that the response behavior of WSMF buildings with connection fractures may only be moderately altered if the fracture occurs only in beams which have some residual strength after the fracture. Experimental results of the SAC project also showed that some fractured connections are still able to undergo many cycles of load reversal; therefore such connections may act as energy dissipators and limit the structural response. On the other hand, once connecting fracture results in complete structural member failures, in particular in columns, the response will increase drastically so that collapse may occur.

The reliability of the building with possible brittle connection failure against earthquakes of various levels of probability of occurrence in a 50-year time interval was also investigated. The results show that the effects of connection fracture on response are only moderate when torsional effects are not considered, whereas when such effects are properly considered, torsion and biaxial interaction significantly amplifies the response of structures at all probability levels. Therefore in design these effects deserve careful consideration to ensure safety and reliability.

8 References

Baber, T. T., and M. N. Noori (1985). Random Vibration of Degrading, Pinching Systems. *J. of Engng. Mech., ASCE* 111(8): 1010–1026.

Foliente, G. C. (1995). Hysteresis Modeling of Wood Joints and Structural Systems. *J. of Struct. Engng., ASCE* 121(6): 1013–1022.

Kaufmann, E. et al. (1997). Failure analysis of welded steel moment frames damaged in the Northridge earthquake. *NISTIR 5944, NIST.* Maryland: Gaithersburg.

Park, Y.J., A.H-S. Ang & Y.K. Wen (1984). Seismic damage analysis and damage-limiting design of R.C. buildings. *Civil engng studies, structural series no. 516.* U. of Illinois, Urbana-Champaign.

Park, Y.J., Y.K. Wen & A.H-S. Ang (1986). Random vibration of hysteretic systems under bi-directional ground motions. *Earthquake engineering and structural dynamics.* 14: 543–557.

SAC (1995). Technical report: case studies of steel moment frame building performance in the Northridge earthquake of January 17, 1994. SAC 95-07.

SAC (1996). Technical Report: Experimental Investigation of Beam-Column Subassemblages. SAC 96-01, Part 1.

SAC (1997). Develop Suites of Time Histories. Draft Report.

Wang, C.-H. and Y. K. Wen (1997). Redundancy of steel frame buildings under seismic loads. Paper no. 307, Proceedings of *ICOSSAR'97*, Kyoto, Japan, Nov. 24-28, 1997.

Wen, Y.K. (1980). Equivalent linearization for hysteretic system under random excitation. *J.Applied Mechanics, ASME.* 47: 150–154.

LIST OF PARTICIPANTS

Dan Abrams
1245 Newmark Laboratory
University of Illinois at Urbana-Champaign
205 N. Mathews
Urbana, IL 61801
Phone: (217) 333-0565
Fax: (217) 333-3821
d-abrams@uiuc.edu

Shirley Dyke
Department of Civil Engineering
Washington University in St. Louis
1 Brookings Drive
Campus Box 1130
St. Louis, MO 63130
Phone: (314) 935-5695
Fax: (314) 935-4338
sdyke@cive.wustl.edu

Jamshid Ghaboussi
3118 Newmark Laboratory
University of Illinois at Urbana-Champaign
205 N. Mathews
Urbana, IL 61801
Phone: (217) 333-6939
Fax: (217) 333-9464
Jghabous@uiuc.edu

Phillip L. Gould
Department of Civil Engineering
Washington University in St. Louis
1 Brookings Drive
Campus Box 1130
St. Louis, MO 63130-4899
Phone: (314) 935-6303
Fax: (314) 935-4338
pgoul@seas.wustl.edu

Sang Whan Han
Dept. of Architectural Engineering,
Hanyang University
Seoul 133-791, Korea
Phone: +82-2-290-1715
Fax: +82-2-291-1716
swhan@email.hanyang.ac.kr

Thomas G. Harmon
211 Urbauer Hall
Department of Civil Engineering
Washington University in St. Louis
1 Brookings Drive
St. Louis, MO 63130
Phone: (314) 935-4536
Fax: (314)935-4338
tharm@seas.wustl.edu

Neil M. Hawkins
2129e Newmark Laboratory
University of Illinois at
Urbana-Champaign
205 N. Mathews
Urbana, IL 61801
Phone: (217) 333-3815
Fax: (217) 333-9464
nmhawkin@uiuc.edu

Li Hyung Lee
Dept. of Architectural Engineering
Hanyang University
Seoul, Korea
Phone: 82-2-290-0547
Fax: 82-2-290-0548
llh@stress.hanyang.ac.kr

Jeong-Ho Moon
Dept. of Architectural Engineering
Hannam University
Daejon, Korea 306-791
Phone: 82-042-629-7554
Fax: (same as above)
mnjh@eve.hannam.ac.kr

Stephen P. Schneider
3106 Newmark Laboratory
University of Illinois at Urbana-Champaign
205 N. Mathews
Urbana, IL 61801
Phone: (217) 333-8691
Fax: (217) 333-9464
spschnei@uiuc.edu

Soo-Yeon Seo
3148 Newmark Laboratory
University of Illinois at Urbana-Champaign
205 N. Mathews
Urbana, IL 61801
Phone: (217) 333-4311
Fax: (same as above)
sooseo@uiuc.edu

Kyung-Jae Shin
Dept. of Architectural Engineering
Hannam University
Daejon, Korea 306-791
Phone: 82-42-629-7396
Fax: 82-42-672-2621
shin@eve.hannam.ac.kr

Yuri Totoev
Department of Civil Engineering
The University of Newcastle
University Drive
Callaghan, NSW, 2308, Australia
Phone: +61-2-49215290
Fax: +61-2-49216991
ceyuri@civeng.newcastle.edu.au

Y.K. Wen
3129e Newmark Laboratory
University of Illinois at
Urbana-Champaign
205 N. Mathews
Urbana, IL 61801
Phone: (217) 333-1328
Fax: (217) 333-9464
y-wen@uiuc.edu

Waon-Ho Yi
Dept. of Architectural Engineering
Kwang Woon University
Seoul, Korea
Phone: +82-2-917-3578 or
+82-2-940-5195
Fax: +82-2-940-5191
whyi@daisy.kwangwoon.ac.kr

University of Illinois
at Urbana-Champaign

**Department of
Civil Engineering**

217 333-8038
217 333-9464 *fax*

STRESS-MAE CENTER WORKSHOP
URBANA, IL
TUESDAY, FEBRUARY 24 – WEDNESDAY, FEBRUARY 25

Location: Room 329 Grainger Engineering Library

PROGRAM

Tuesday

1:00 p.m.	Welcoming Remarks *Professor David E. Daniel*, Head, Civil Engineering, UIUC
1:15 p.m.	Introduction of STRESS Center *Dr. Li Hyung Lee*, Director, STRESS Center
1:45 p.m.	Introduction of MAE Center *Dr. Daniel P. Abrams*, Director, UIUC, MAE Center
2:15 p.m.	Behavior of Concrete-Filed Box Column to H-Beam Connections *Dr. Kyung Jae Shin*, STRESS Center
2:50 - 3:05 p.m.	Break
3:05 p.m.	Steel Beam Connections to Concrete Filled Steel Tubes *Dr. Stephen P. Schneider*, UIUC, MAE Center
3:40 p.m.	Spreading Beam Plastic Hinging Zone For Ductile Behavior of High-Strength RC Beam Column Joints Using Vertically-Anchored Intermediate Reinforcements *Dr. Waon Ho Yi*, STRESS Center
4:15 p.m.	Developments in the Use of Semi-Active Control for Earthquake Hazard Mitigation. *Dr. Shirley J. Dyke*, WUSTL, MAE Center
4:35 p.m.	Concrete Columns Confined with Carbon Composites *Dr. Tom Harmon*, WUSTL, MAE Center
5:05 p.m.	Adjourn
6:30 p.m.	Dinner, Kennedy's Restaurant Sunnycrest Center, Urbana

MAILING ADDRESS: NEWMARK CIVIL ENGINEERING LABORATORY MC-250 · 205 NORTH MATHEWS AVENUE · URBANA, ILLINOIS 61801-2352

STRESS-MAE CENTER WORKSHOP
URBANA, IL

PROGRAM

Wednesday

8:00 a.m.	The Effects of Hysteretic Models on Strength Reduction Factors *Dr. Sang Whan Han*, STRESS Center
8:35 a.m.	Modeling and Reliability of Steel Frame Buildings with Brittle Joint Fractures *Professor Y.K. Wen and C.H. Wang,* UIUC, MAE Center
9:10 a.m.	Computational Methodology and Design Equation for Ultimate Stress of Unbonded Tendon *Dr. Jeong Ho Moon*, STRESS Center
9:45 – 10:00 a.m.	Break
10:00 a.m.	Effect of Prior Earthquake Damage on the Response of Simple Structures to Future Earthquakes *Dr. Mark A. Aschheim*, UIUC, MAE Center
10:35 a.m.	Limit Drift and Energy Dissipation Ratios of Shear Walls Based on Structural Testing *Dr. Soo-Yeon Seo*, STRESS Center
11:10	Seismic Analysis and Evaluation of Long Span Bridge *Dr. Jamsid Ghaboussi*, UIUC, MAE Center
12:00	Adjourn
12:15	Lunch – Illini Union